EFFECT OF WIRELESS COMMUNICATION TO TUNNELING GIANT MAGNETO-RESISTIVE (TGMR) READER IN HEAD GIMBAL ASSEMBLY PROCESS

DUTHARUTHAI NA POMBEJARA

A THESIS SUBMITTED IN PARTIAL FULFILLMENT
OF THE REQUIREMENT FOR THE DEGREE OF
MASTER OF ENGINEERING IN DATA STORAGE TECHNOLOGY
INTERNATIONAL COLLEGE
KING MONGKUT'S INSTITUTE OF TECHNOLOGY LADKRABANG
2016

KMITL-2016-IC-M-005-004

APPROVAL SHEET

หัวข้อวิทยานิพนธ์	ผลกระทบของการสื่อสารไร้สายต่อหัวอ่านแบบทันนัลลิ่งแมกนิโตรีสิสทีฟ (TGMR) ในขั้นตอนการประกอบชิ้นส่วนเฮดกิมบอล (HGA)
นักศึกษา	นางสาวดุจหฤทัย ณ ป้อมเพ็ชร
รหัสประจำตัว	54600706
ปริญญา	วิศวกรรมศาสตรมหาบัณฑิต
สาขาวิชา	เทคโนโลยีการบันทึกข้อมูล
พ.ศ.	2559

อาจารย์ที่ปรึกษาวิทยานิพนธ์ ผศ.ดร.ชัยยันต์ เจตนาเสน

บทคัดย่อ

ในปัจจุบันเทคโนโลยีการบันทึกเชิงแม่เหล็กใช้หัวอ่านแบบ TGMR ซึ่งถูกพัฒนาให้มีการอ่านข้อมูลด้วยความเร็วและใช้พื้นที่ในการบันทึกข้อมูลที่มีประสิทธิภาพสูงขึ้นมาก ในกระบวนการผลิตขั้นสูงมีการใช้เครื่องมือการผลิตแบบอัตโนมัติ อุปกรณ์การสื่อสารแบบไร้สายจึงถูกนำมาใช้มากขึ้นเพื่อเพิ่มประสิทธิภาพในการผลิต แต่อย่างไรก็ตามสนามแม่เหล็กไฟฟ้าจากอุปกรณ์การสื่อสารแบบไร้สายอาจเป็นอันตรายและสามารถทำลายชิ้นงานที่มีความอ่อนไหวต่อพลังงานได้ เช่น หัวอ่านแบบ TGMR ในกระบวนการประกอบหัวอ่าน การค้นคว้าวิจัยนี้จะทำการสำรวจการรบกวนของสนามแม่เหล็กไฟฟ้าจากอุปกรณ์การสื่อสารแบบไร้สาย โดยใช้เครื่องมือวัดสนามแม่เหล็กไฟฟ้า CTM048 พร้อมกับเสาอากาศแบบมีทิศทางเป็นระบบการวัด และใช้เครื่องมือวัด Agilent 34410A ในการวัดแรงดันไฟฟ้าและการเปลี่ยนแปลงอุณหภูมิ ของหัวอ่าน TGMR ขณะที่อยู่ในพื้นที่การกระกอบเฮดกิมบอลและมีการสื่อสารแบบไร้สาย ค่าสัมประสิทธิ์ความแตกต่างอุณหภูมิในโครงสร้างเซนเซอร์ความต้านทานจะนำไปเทียบเคียงกับอุณหภูมิของหัวอ่าน TGMR แรงดันไฟฟ้าของ TGMR จะถูกนำไปคำนวณเป็นค่ากำลังไฟฟ้า โดยค่าทั้งสองจะถูกเปรียบเทียบกับค่าขีดจำกัดความเสียหายของหัวอ่านและสรุปเป็นแบบจำลองการคาดหมาย ท้ายที่สุดมีการยืนยันโดยใช้ตัวอย่างหัวอ่านจริงทำการทดสอบผลกระทบต่อประสิทธิภาพทางไฟฟ้าต่อ TGMR ทั้งก่อนและหลังกระบวนการประกอบหัวอ่านด้วยเครื่องทดสอบ Quasi Static.

Thesis	Effect of Wireless Communication to Tunneling Giant Magneto-Resistive (TGMR) Reader in Head Gimbal Assembly Process
Student	Ms. Dutharuthai Na Pombejara
Student ID.	54600706
Degree	Master of Engineering
Program	Data Storage Technology
Year	2016
Thesis Advisor	Asst.Prof.Dr.Chaiyan Jettanasen

ABSTRACT

TGMR is current technology of magnetic recording read sensor which dramatically improves readout amplitude, speed and recording areal density. In advanced manufacturing environment, automated tools are increasingly used and wireless communication device is aimed to be employed to enhance the operation efficiency. However, electromagnetic fields from wireless communication could harm the most energy sensitive devices, such as TGMR reader sensor, in head gimbal assembly process. This study surveys, therefore, electromagnetic interference from wireless communication devices using CTM048, EM Field Meter with CTS001 directional antenna and electromagnetic field module, then use Agilent 34410A to measure TGMR voltage and thermal change of TGMR head while assembling to be head gimbal, in the field of wireless communication. Build-in Differential-Ended Temperature Coefficient of Resistivity sensor is utilized for proximal TGMR temperature and calculation from TGMR voltage will give power which will be compared with TGMR failure threshold and summarized as prediction model. At the final part of this study, impact to electrical performance of real TGMR pre and post actions simulating HGA assembly process will be confirmed using Quasi-static Tester.

ACKNOWLEDGEMENT

This thesis would not be accomplished if it was without the guidance and the support of several persons who contributed and extended their appreciated assistance in the completion of this research.

First, I would like to sincerely thank for scholarship, financial, equipment and technical expertise support under the collaboration development of Seagate Technology (Thailand) Ltd., National Electronics and Computer Technology Center (NECTEC) and National Science and Technology Development Agency (NSTDA) and last but not least College of Advance Manufacturing Innovation King Mongkut's Institute of Technology Ladkrabang.

My sincere appreciation is express to my Seagate colleagues and management for enthusiastic supporting to my study to accomplish this collaboration development.

I am really grateful entire teaching staff in the College of Advance Manufacturing Innovation program that enlightened me and made me enjoy every single seconds of learning in the classes. I promise to apply the knowledge that I have acquired as the most valuable assets.

I express my greatest appreciation to authors of all studies in the past for their hard working and kind publishing valuable literatures which I can build-on my research.

I am utmost gratitude to my advisor Asst.Prof.Dr.Chaiyan Jettanasen, who provided valuable advices , always encouraged, gave time and chances to help me go over all the obstacles in the completion this research.

Finally, I would like to express my deepest appreciation and sincere gratitude to family and my friends for their love, moral support, and encouraging for the entire of my study.

Dutharuthai Na Pombejara

CONTENTS

CONTENTS (Continue)

LIST OF FIGURES

LIST OF FIGURES (Continue)

LIST OF FIGURES (Continue)

LIST OF FIGURES (Continue)

LIST OF FIGURES (Continue)

LIST OF FIGURES (Continue)

LIST OF FIGURES (Continue)

LIST OF TABLES

CHAPTER 1

INTRODUCTION

1.1 Background and Problem Statement

Nowadays wireless communication has been integrated to every activity owing to its convenience. The use of devices generating electromagnetic wave can produce interference that may cause undesirable effects to sensitive equipment or sensitive devices in nearby areas. In hard disk drive manufacturing, there is a special component that is very sensitive to external energy such as electrostatic discharge (ESD), magnetic field, and electromagnetic interference (EMI). The component is known as hard disk drive reader head or reader sensor. The reader sensor technology had been developed for decades, to accomplish higher areal density and better signal-to-noise ratio, such evolution from AMR (Anisotropic Magnetoresistance), GMR (Giant Magnetoresistance) and TGMR (Tunneling Giant Magnetoresistance) respectively. More the reader sensor is small more it is sensitive to external energy.

Some researches proved that Electromagnetic Interference (EMI) affected to magnetic recording read head, but none of them studied on real TGMR read head yet. Previous studies on EMI effect from wireless communication were done on 5 Gb/in^2 PtMn GMR sensors [1-3], while current technology is up over 500 Gb/in^2 sensor. A study mentioned about TGMR head, but no technical discussion or end result of TGMR sensor impact were presented in the paper [4]. Newer studies had simulated TGMR sensor impact in stand-alone stage. The consideration of connection to slider body, trace-gimbal assembly (TGA), suspension or other assembly was excluded from the simulation scope [5-6]. A study concluded that magnetic heads in

production could be exposed to electrical overstress exposure of different types due to the ultra-sensitive nature of magnetic heads [7]. Also, studies of the effect of EMI on TGMR head in dynamic Tester [13] and GMR head in spin-stand tester [14] have not explained how reader sensors response to the EMI yet.

In this study, we would like to provide methodology to understand how TGMR responses to the inference from wireless communication in terms of voltage dropped and temperature change on actual TGMR. Then the electrical performance of real TGMR on HGAs will be compared. It is to confirm for making decision if the electromagnetic fields from wireless communication devices to be used in the manufacturing process area will harm the most energy sensitive devices, such as Tunneling Giant Magneto-Resistive (TGMR) recording reader sensor, in assembly process.

1.2 Objective

To find out what kind of wireless communication devices has significant electromagnetic interference (EMI), in form of electric field, and knows the most influence direction of each wireless communication device to its field strength.

To observe actual voltage dropped and estimate temperature of TGMR while being exposed to the field of wireless communication device. Then, compare actual measurement result with TGMR damage threshold.

To confirm actual effect to electrical performance of TGMR in HGA assembly process while being exposed to the field of wireless communication device.

To provide guideline of methodology to assess risk from wireless communication device, as well as suggestion of controlling its effect to TGMR heads in HGA assembly process.

1.3 Scope and limitation of work

This study is limited to one particular design of TGMR and HGA and its assembly process. Wireless communication devices in this study are selected from most likely being used during the study period of time, and it is only one sample per type.

This study has not included effect from all frequencies of wireless communication devices used. For example, 5GHz WiFi devices has not been included in this study due to it is not typically used in large factory areas like hard disk drive manufacturing, as in general, the higher the frequency of a wireless signal, the shorter its range. Thus, 2.4GHz networks have been selected because they cover a substantially larger range than 5GHz wireless networks.

To avoid damage of tooling and equipment used in this study. There is limitation of the distance set up in real HGA processes, which could not allow wireless communication device come closer than 100 mm to the TGMR due to obstruction of the automate tooling.

1.4 Expected Benefit

As the technology has never been stopped developing, the knowledge from this research would help understanding how to assess risk from wireless communication devise and decision for proper control condition. Over-killing control may obstruct opportunities to improve process efficiency or cost concern. Loosen control may lead to quality problem, failure of component, yield and profit lost. Optimum selection and control of using wireless communication devices in the manufacturing environment will benefit to process efficiency, quality, time to market and cost of the products.

1.5 Literature Review

A.Wallash and D. Smith studied EMI effect to GMR head connecting with dipole and loop antennas [1]. KeyTek MiniZap set up at 3 kV maximum with MZT-12-H-Field attachment was EMI source. Twenty spin-valve GMR sensors with an IrMn exchange layer were used and measured GMR Resistance as affected in this study. It found magnetic failure and melting failure from all types of antenna (5 and 10 inches dipole and 2.5 x 3 inches loop). Failure threshold depends on antenna length and distance from EMI source. In this paper, there was no study on TMR head, and no study on head without antenna.

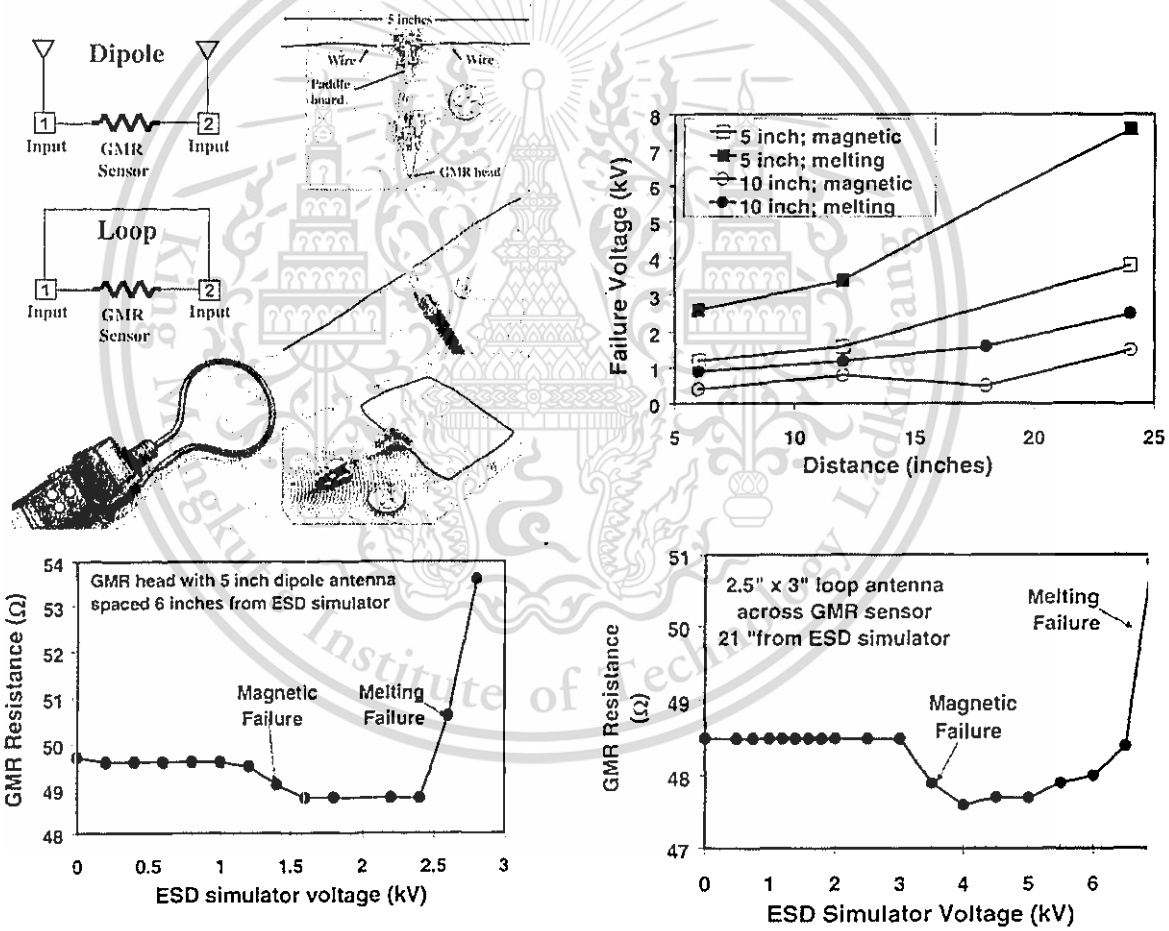

Figure 1.1 Experiment setup and result of EMI effect to GMR head connecting with dipole and loop antennas [1]

C.F. Lam, D. Martinez's study [2] was different from Wallash and Smith's. They used Ground SST Tweezers to create spark from Keytek Mini-Zap DUT, Standalone (without antenna) versus attached with 8-inch loop. KPIV measured with EM-eye meter, same Lecroy but Shielded CT-1. KPOV measured with QST GMR Resistance and Amplitude. The result showed that, stand-alone wire or FOS or TSA HGA was not susceptible to EMI damage. It was demonstrated even at 16 kV MiniZap sparks and at 0.5 inch distance away. HGA is susceptible to EMI damage only when wire is attached to the GMR electrodes. The study did not include TMR sensor.

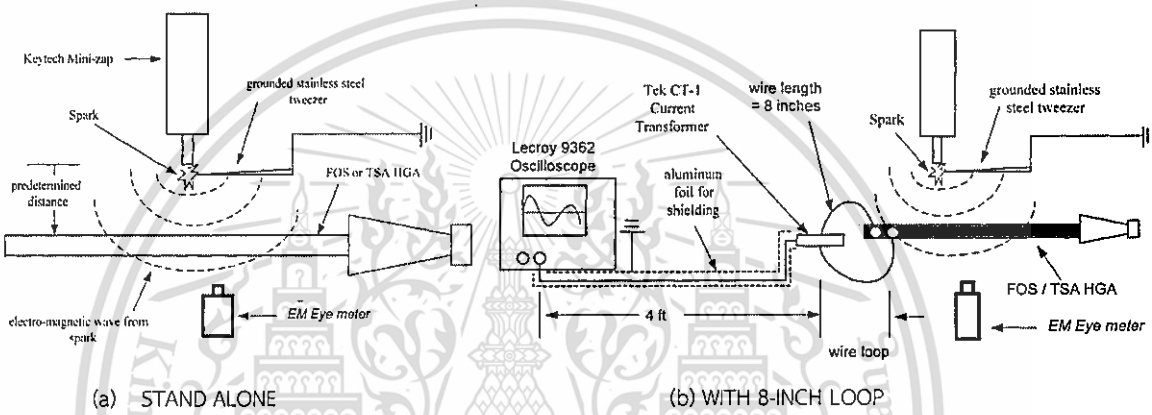

Figure 1.2 Experiment setup of ESD sensitivity study of GMR recording heads with a flex-on-suspension head-gimbal assembly [2]

Distance from HGA	MiniZap spark V (kV)	EM-Field strength (V/m)	EMI-damage			
			STAND ALONE		WITH 8-INCH LOOP	
			FOS-HGA	Wire-HGA	FOS-HGA	Wire-HGA
3 ft.	16	0.4	no	no	no	no
2 ft.	16	0.5	no	no	no	no
1 ft.	16	0.6	no	no	no	no
6 inch	16	1.1	no	no	no	no
3 inch	16	1.9	no	no	no	no
2 inch	16	3.2	no	no	yes	no
1 inch	16	4.6	no	no	yes	yes
0.5 inch	16	> 5.0	no	no	yes	yes

Figure 1.3 Experiment result of ESD sensitivity study of GMR recording heads with a flex-on-suspension head-gimbal assembly [2]

V. Kraz, A.Wallash studied the Effect of EMI from Cell Phone on GMR Recording Heads and Test Equipment [3]. Study cell phone in 800 MHz range with 5 GB/in^2 PtMn GMR sensor only. Three types of cell phones (AMPS, TDMA and CDMA) did not cause magnetic or resistance change damage to the GMR heads. ESC sources such as plastic bag more likely to be the threat of reader damaged.

Measurement Equipment	LeCroy oscilloscope model 9362
	HP (Agilent) Spectrum Analyzer model HP8595A
	Credence Technologies' EMI/ESD Diagnostic Kit CTK053 with CTS001 calibrated broadband active antenna
	Credence Technologies' EM Aware ESD Event monitor CTC034 with local and remote antenna CTC113
RF Emission Sources	Motorola 845 MHz CDMA phone
	Nokia 6162 800 MHz TDMA phone
	Motorola 830MHz AMPS phone
ESD sources	Bag of SMA RF connectors
	Plastic tube with two metal cylinders
	Barbecue lighter
GMR Test Equipment	QST Tester model Integral Solution International 2001 (Resistance and amplitude measure)
GMR Heads	5 Gb/in^2 PtMn GMR heads used in this study 30 V_{HMB} magnetic failure level

Figure 1.4 Experiment setup of the effect of EMI from cell phone on GMR recording heads and test equipment [3]

Test Setup GMR HGA	Mobile Phone	ESD Source
Without antenna	All models: No damaged	All types: No damaged
With 11 cm monopole antenna	All models: No damaged	All types: No damaged
With 30 cm monopole antenna	All models: No damaged	Plastic Bag w/connectors : Fatal damage (open)
With single loop antenna 6" diameter	All models: No damaged	Plastic bag w/cylinder Fatal damage (open)
With double loop antenna 2.75" diameter	All models: No damaged	Plastic Bag w/connectors : Fatal damage (open)
Mounted in QST	All models: No damaged	All types: No damaged
Mount on Guzik Tester	All models: No damaged	All types: No damaged

Figure 1.5 Experiment result of the effect of EMI from cell phone on GMR recording heads and test equipment [3]

S. Natori, T. Wada, et all studied a relatively simple method for comprehending the basic characteristics of EMI using CT1, Digital oscilloscope and Fast Fourier Transform Software [4]. The magnitude and frequency components of the waveforms are dependent on their generation sources. The difference between each type of sources is especially cleared by analyzing the each frequency component using FFT. The larger the spark voltage and the shorter the distance from source, the larger EMI peak power level. EMI radiation on GMR head was conducted under the following conditions: 1) GMR head was left in front of a noisy ionizer for 10 minutes. 2) A person holding metal tweezers was charged up to 1kV. The metal tweezers were then contacted to a metal plate. 3) A CPM was charged up to ± 4kV. The CMP then was made contact with metal wires. 4) EMI radiation from lighter. Irradiation condition 1) to 3) was performed 10 times at a distance of 10 cm from the GMR head.

The electric and magnetic characteristics of the GMR heads were compared using a QST before and after the irradiations condition 1) to 4). No changes were seen on the characteristics of the GMR heads for each condition. They had not mentioned about experiment on TMR head

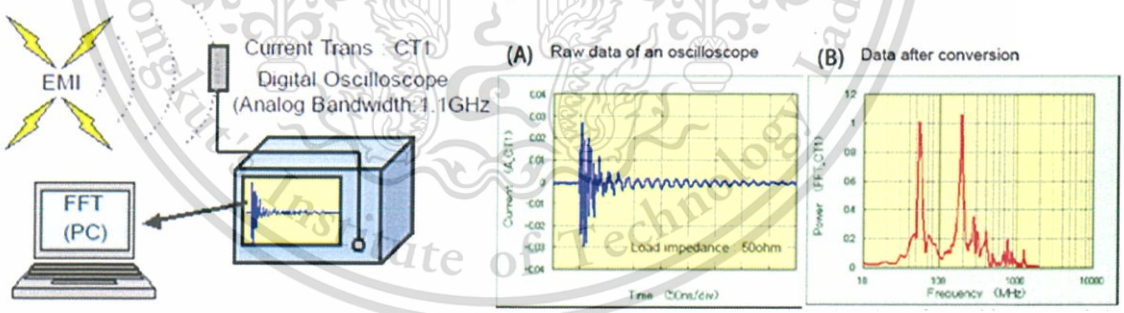

Figure 1.6 Experiment setup of study of EMI phenomena for GMR/TMR head. EMI waveform and frequency analysis [4]

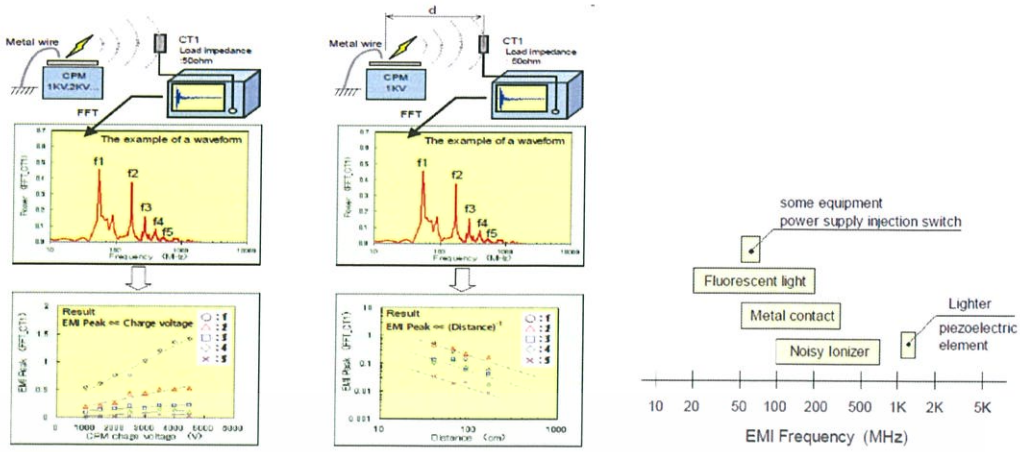

Figure 1.7 Experiment result of the study of EMI phenomena for GMR/TMR head. **(a)** voltage dependence of EMI peak power **(b)** distance dependence of EMI peak power **(c)** frequency band of EMI waveform. [4]

S.Kaengrang, A.Kaewrawang studied on the increasing temperature on stand-alone TuMR read sensor [5] with no connection to outside system, no detail of investigation on real TMR head showed radiated EMI in 2 conditions;

(a) EMI in the ranges of 30-1000 MHz, the electric field intensity is 10 V/m.

(b) Electric field intensity is varied between 1×10^{10} to 1×10^{14} V/m.

Simulation used commercial finite integral technique (FIT) software (CST STUDIO SUITETM 2010), the compare result with Blocking temperature (T_b) and the melting temperatures (T_m). Simulation showed that temperature distribution in stand-alone TuMR read sensor was affected by electric field intensity at 1×10^{13} V/m and above. Temperature of AFM and Al_2O_3 spacer layers were started to be higher than Tb (250) and Tm (2000).

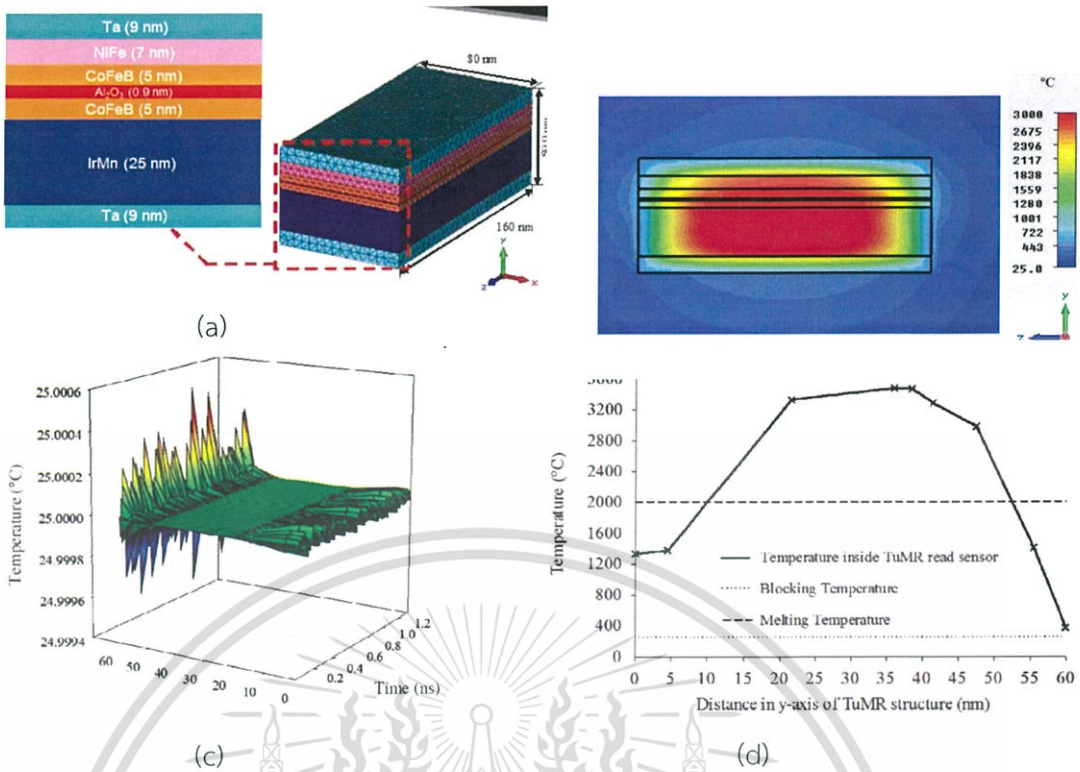

Figure 1.8.1 Simulation result of EMI inducing heat on TMR read sensor. **(a)** Structure of TuMR. **(b)** Temperature distribution inside TuMR read sensor (Electric field intensity is $1x10^{13}$ V/m) **(c)** Temperature inside TuMR read sensor at 1 GHz **(d)** Simulations if temperature in multilayer of TuMR with electric field intensity = $1x10^{13}$ V/m [5]

	Electric Field Intensity (V/m)				
Each Layers	$1x10^{10}$	$1x10^{11}$	$1x10^{12}$	$1x10^{13}$	$1x10^{14}$
Ta	25.00849	25.14288	38.49845	1372.753	135071.3
IrMn	25.01044	25.33849	58.06672	3328.722	330894.6
CoFeB	25.01054	25.353	59.47583	3470.831	344774.0
Al2O3	25.01064	25.3537	59.55105	3478.241	345527.5
CoFeB	25.01044	25.33449	59.47583	3286.379	326312.9
NiFe	25.01014	25.30408	54.58643	2982.384	295894.0
Ta	25.01014	25.1463	38.8147	1405.507	138131.1

Figure 1.8.2 Simulation result of temperature at each layers report to electric field intensity with 1 GHz [5].

S. Puapairoj, C. Sa-Ngiamsak studied effects of E-field and H-field on TMR head caused by discharge current during electrical connection [6]. The study measured current through gold wire bond with shielded CT-6 and Lecroy DDA125. Then, simulate E-field and H-field with software to compare with dielectric breakdown (threshold) of insulator and exchange coupling field (H_{ex}) of AFM. In this bonding process, radiated electric field plays a stronger role to TMR heads than the radiated magnetic field due to its oxide layer. Direction of the TMR heads during bonding process plays a role in the fields transmitted into the MR heads. E-Field and H-Field result only determined by simulation. There is not yet investigation on real TMR head as in this study.

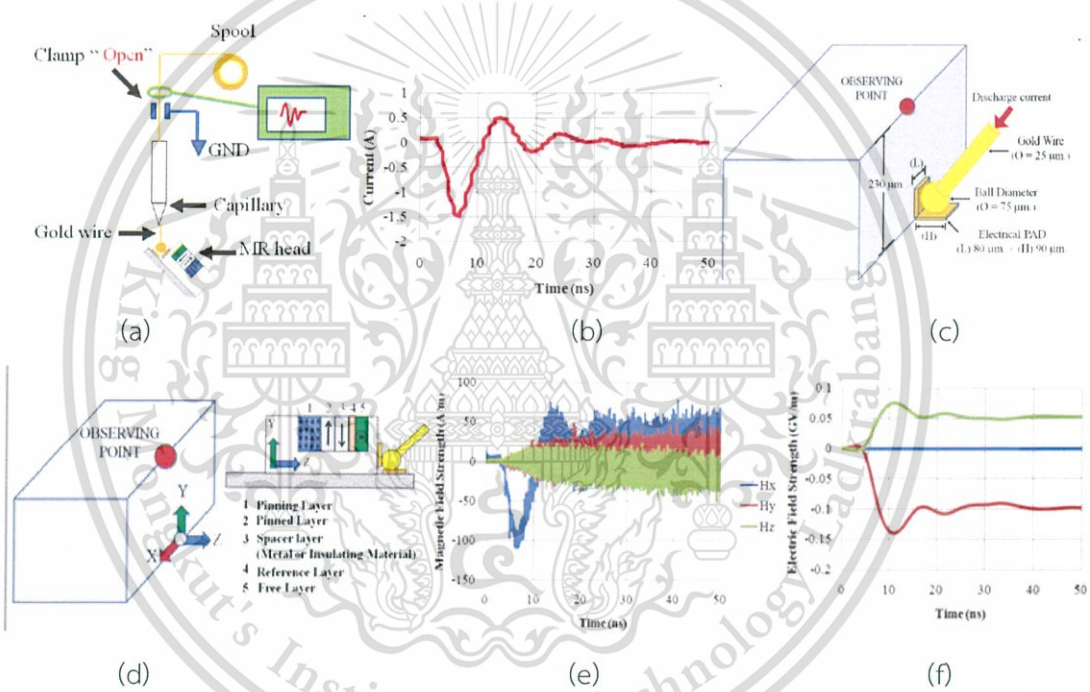

Figure 1.9 Experiment setup and result of effect of ESD and EMI on TMR head during bonding process of gold ball bonding machines. **(a)** position of measurement **(b)** current waveform **(c)** structure of gold wire, gold ball and electrical pad **(d)** direction of observation **(e)** magnetic field strength at MR heads **(f)** electric field strength of MR head [6].

V. Kraz, P. Tachamaneekorn, and D Napombejara, studied on EOS exposure of magnetic heads and assemblies in automated manufacturing [7]. The magnetic heads in production can be exposed to EOS exposure of different types. Several EOS sources are examined in the paper such as unreliable contact with ground, inductance in ground path, inductive and capacitive coupling and excessive ground current. Discussion on how the exposure would influence damage to the magnetic head suggests some issues to consider. They are voltage sensitivity of the head, current path, long-term exposure and latent damage concern. Due to the ultra-sensitive nature of magnetic recording head, damage threshold of component shall be defined, and then the measurement technique to quantify EOS exposure should be applied to compare and make decision that the tool can be qualified to handle or use based on amount of EOS exposure that the tool provides.

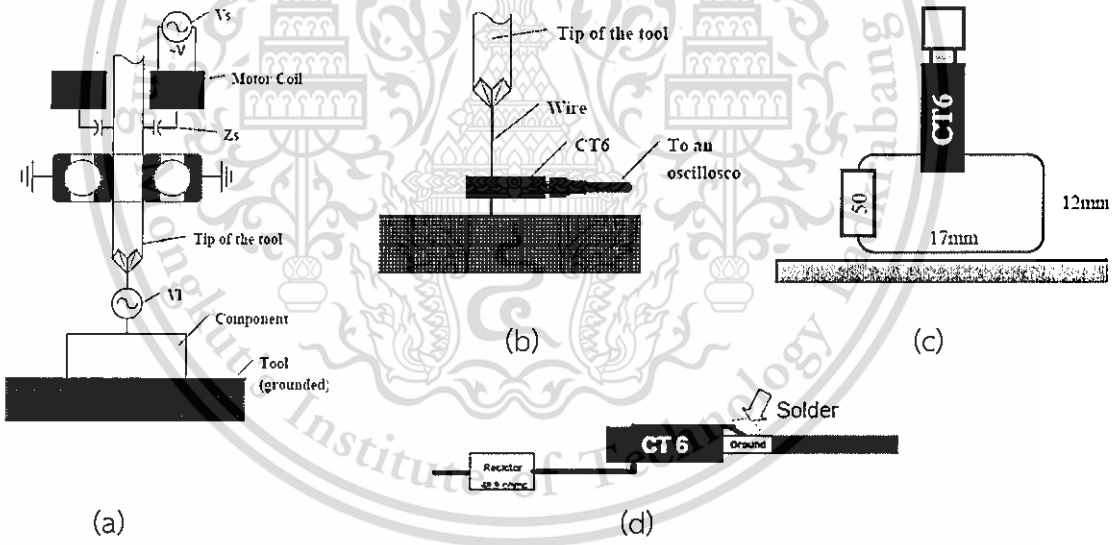

Figure 1.10 Example of EOS exposure measurement technique **(a)** generation of voltage in a tool via capacitance **(b)** current in gold ball bonding tool **(c)** current induced by transformer coupling in the tool **(d)** current exposure on direct contact with CT-6 probe. [7]

A Kruesubthaworn, R. Sivaratana, V. Ungvichianc, A. Siritaratiwat had studied the testing parameters of TMR heads affected by dynamic-tester induced EMI [13]. The result showed that power cable connector of robot propagated high density of EMI and induced to spindle motor at about 2212 V/m. However, this level of interference is not significant enough to make damage to TMR magnetic read head. By the way, this experiment cannot explain impact of EMI to magnetic read head in term of magnetic properties. So, A. Kruesubthaworn, A. Pratoomthip, A. Siritaratiwat, V. Ungvichian, studied anomalous magnetic responsiveness of giant magnetoresistive heads under specific electromagnetic interference frequencies using quasi-static tester [14] to indicate experiment result by varying frequency of EMI in the range of 500-550 MHz, 700-800 MHz and 900-1000 MHz, and also vary its polarization. Result in this experiment was found change of QST parameters while sweeping the EMI frequency. The maximum change of MR amplitude and hysteresis was 10.2% at 910 MHz and 8.37% at 935 MHz.

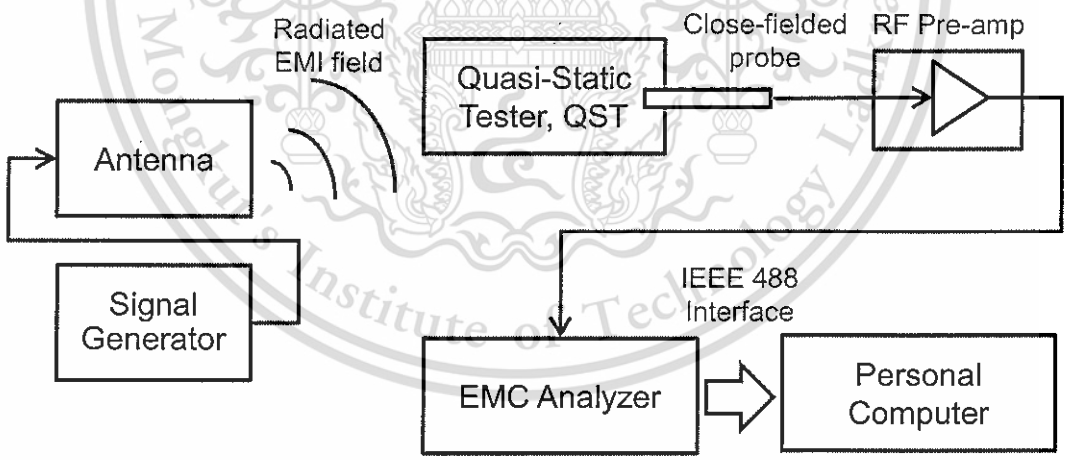

Figure 1.11 Experiment setup of anomalous magnetic responsiveness of GMR head under specific electromagnetic Interference frequencies using quasi-static tester [14]

C. Surawanitkun, A. Kaewrawang, et al studied magnetic instability in tunneling magnetoresistive heads due to temperature increase during electrostatic discharge" [36].

Three-dimension finite-element method was used to analyze the spatial and temporal profiles of the temperature during the discharge. The results from the three models show that, although the highest temperature occurs in the MgO barrier layer, the initial magnetic modification likely arises in the IrMn antiferromagnetic layer due to its low Néel temperature. They also found that the increase in temperature is proportional to the square of the ESD voltage.

The modeling using magnetic tunneling junction element in the head has a lateral size of 80 nm × 80 nm and a resistance of 2 $\Omega \cdot \mu m^2$ for the entire TMR head. The values of the electrical conductivity σ, density ρ, heat capacity cp, and thermal conductivity K of the various materials are given in Table I. These values are used for the thermal calculation using the heat conduction equation. The high current densities in the TMR junction Joule heating leads to a significant increase of the temperature inside TMR stack. For ESD failure analysis, the temperature damage is relevant to the discharge time durations of 40, 14, and 0.4 ns, for HBM, MM, and CDM, respectively. They also found that the maximum temperature T_{max} occurred shortly (sub-nanosecond) after the peak in the current transient, because the temperature increases during the current transient and saturates almost immediately. Similarly, after turning the current off the temperature in the structure decreases rapidly. The highest temperature occurs in the MgO barrier because it has the lowest electrical conductivity. Power dissipation within TMR stack is all concentrated in the MgO layer by the same reason. Furthermore, the temperature for MM is the highest because it experiences the highest discharge current, as it has the highest ESD capacitance.

In the TMR stack structure, T_N of IrMn is 417 °C and the T_C of NiFe, CoFe, and CoFeB are 570, 950, and 1040 °C, respectively. If no barrier breakdown occurs, the sequence of the magnetic degradation from HBM, MM, and CDM starts in the IrMn layer followed by the NiFe free layer, the CoFe and the CoFeB layer. The MM voltage (V_{MM}) of 1.5 V is already sufficient to cause a temperature rise exceeding T_N in AFM layer. The discharge of the charging voltage causes the peak current I_p of about 4.5 mA flowing through the TMR stack structure. The HBM voltage (V_{HBM}) of 8.7 V and the CDM voltage (V_{CDM}) of 1.7 V are the corresponding voltage giving a failure peak current I_p of about 4.5 mA and 4.9 mA, respectively.

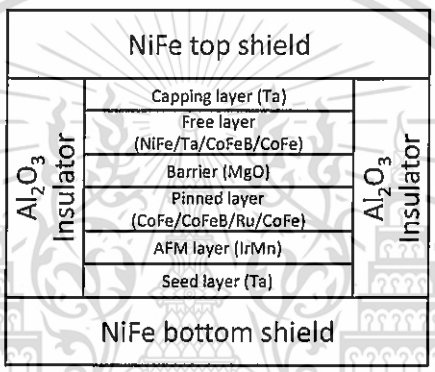

Figure 1.12 (a) Structure of TMR read head element in the composite thin-film magnetic head [36]

TABLE I : MATERIAL PROPERTIES USE IN 3-D FEM FOR THERMAL ANALYSIS

Material	σ $(\Omega\cdot m)^{-1}$	K (W/(m·K))	Cp (J/(kg·K))	ρ (kg/m^3)
Ta	6.5×10^{5}	58.0	153	16700
IrMn	6.8×10^{5}	35.6	409	10300
CoFe	5.85×10^{6}	20.0	423	8150
Ru	1.39×10^{7}	116.0	240	10960
CoFeB	5.85×10^{6}	88.0	405	9140
MgO	4.00×10^{2}	45.0	935	3580
NiFe	4.76×10^{6}	30.0	470	8440
Al_2O_3	1.00×10^{-12}	1.5	760	3960

TABLE II : VALUE OF CAPACITANCE, RESISTANCE, AND INDUCTANCE FOR HBM, MM AND CDM

ESD Model	C_{ESD} (pF)	R_{ESD} (Ω)	Ls (nH)
HBM	100	1500	8000
MM	200	-	500
CDM	5	-	20

Figure 1.12 (b) Simulation parameters of magnetic instability in TMR heads due to temperature increase during electrostatic discharge [36]

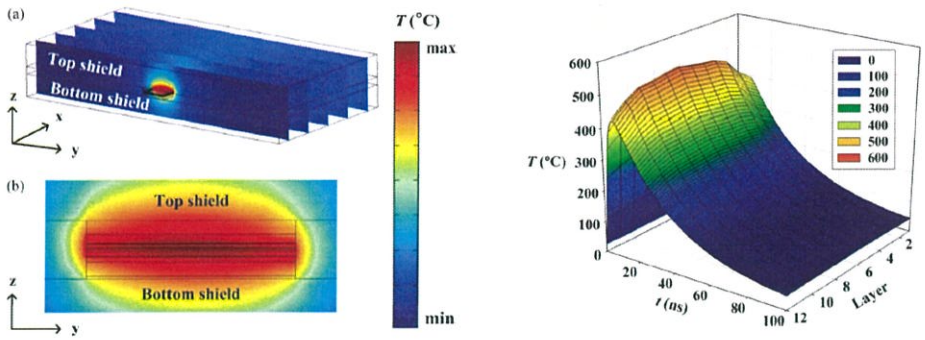

(a) (b)

Figure 1.13 Simulation result of temperature distribution. **(a)** Distribution of temperature during the discharge with 40, 14, 0.4 ns for HBM, MM and CDM, respectively at surround and inside of TMR **(b)** Temperature increases during the discharge at MM voltage of 1.5 V in the TMR head. [36]

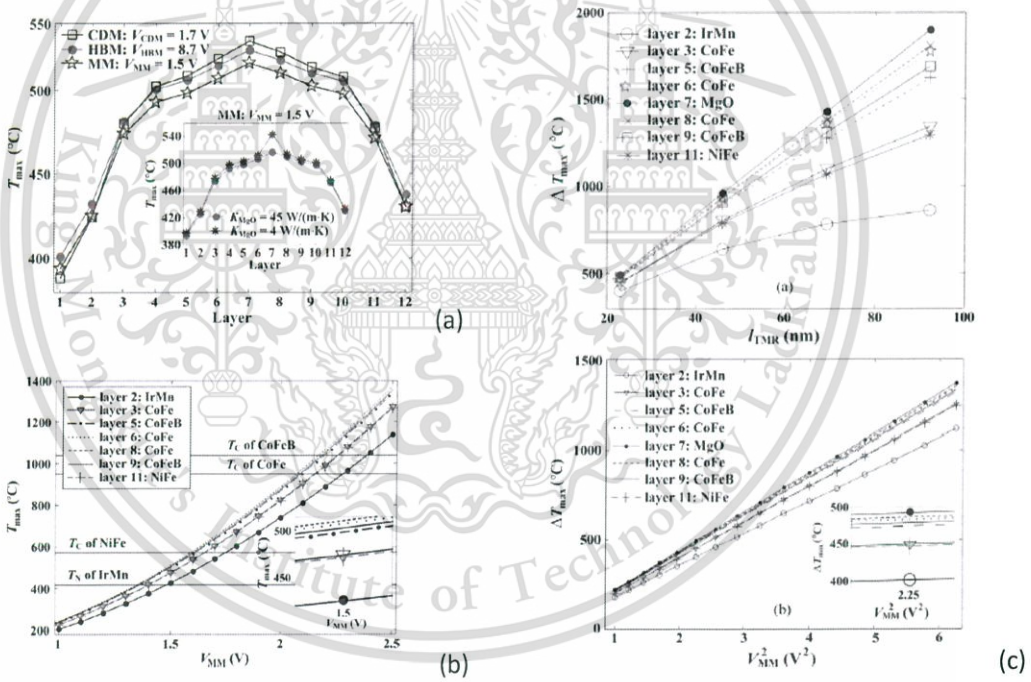

Figure 1.14 Simulation result of T_{max} and ΔT_{max} correlation to layer, V_{MM}, I_{TMR} and V^2_{MM} **(a)** T_{max} in the TMR junctions at V_{HBM} = 8.7 V, V_{MM} = 1.5 V, V_{CDM} = 1.7 V. The inset shows the T_{max} in TMR junctions at V_{MM} of 1.5 V for different K_{MgO} **(b)** T_{max} in the magnetic layers of TMR junctions for different V_{MM}. **(c)** ΔT_{max} in the magnetic layers of TMR junctions depending on the TMR thickness (I_{TMR}) and the V^2_{MM} [36]

K. Marongmued and C. Sa-Ngiamsak studied how does electrostatic discharge event not cause polarity flip in TMR read heads" [37]. 3-D FEM simulation was used to monitor the threshold ESD current causing soft failure and hard failure mechanisms in particular TMR structure. Temperature increment in free, oxide, pinned, pinning layers and electric field across the oxide barrier due to ESD current attack were monitored at the same time. The results reveal that the oxide breakdown at the insulator barrier requires lower amplitude of ESD current than the case of the magnetization reversal caused by the Joule heating at the interface FM/AFM. The oxide breakdown or hard failure for this particular TMR occurs at the ESD peak amplitude of 4 mA while the case of pinned layer reversal needs 6 mA. These indicate that the ESD current is not the cause of magnetization reversal in TMR read heads. ESD will induce the hard failure rather than soft failure on TMR head. This finding will benefit particularly for the production line to analyze the cause of TMR head failure; hence if polarity flips is found in TMR production process, then the ESD event is not the cause. The prime elements are heat and magnetic field disturbances simultaneously rather than ESD events. [37]

TABLE I : CRITICAL PARAMETERS		
Layer	Parameters	Critical Value
FM/AFM	Blocking Temperature (T_B)	170 °C
AFM	Neel Temperature (T_N)	420 °C
FM	Curie Temperature (T_C)	520 °C
AlOx	Electric Field Breakdown (E_B)	8.3 MV/cm

TABLE II : ELECTRICAL PARAMETERS OF SIGNIFICANT LAYERS			
Layer	Heat Capacity (J/kg·K)	Thermal Conductivity (W/(m·K))	Electrical Conductivity (S/m)
IrMn	316	35.6	6.80×10^5
CoFe	446	37	3.33×10^6
AlOx	900	27	500

(a)

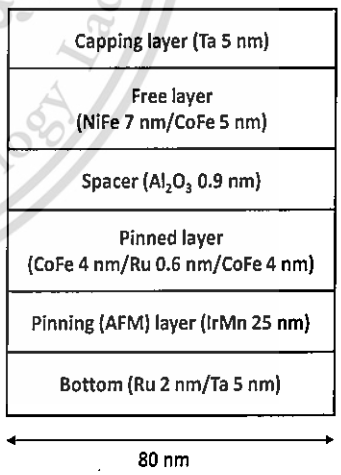

(b)

Figure 1.15 (a) Simulation parameters in the paper (b) Structure of TMR read head element [37].

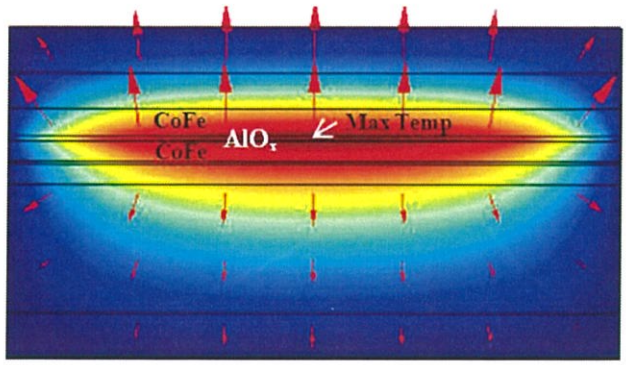

(a)

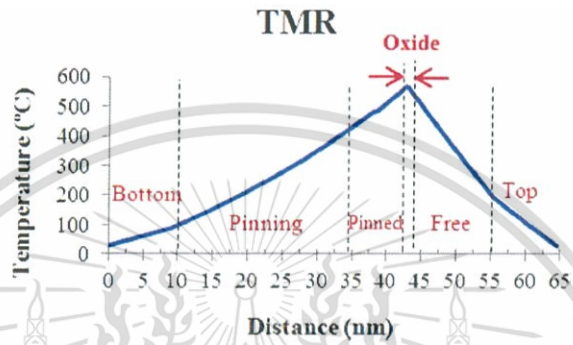

(b)

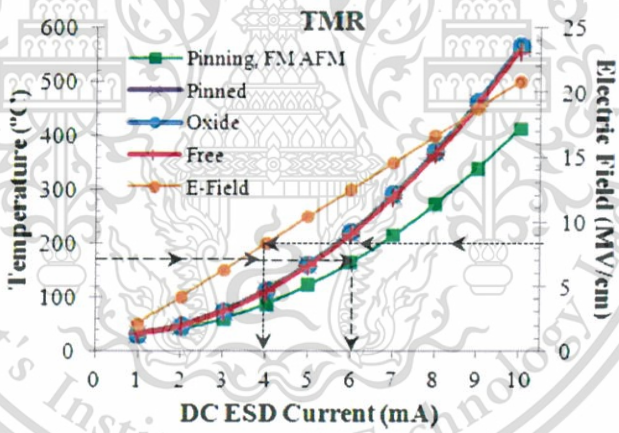

(c)

Figure 1.16 Simulation results in the paper [37]. **(a)** Temperature profile and heat flux of TMR sensor induced by ESD **(b)** Temperature distribution of a cross-section TMR zapped with ESD current of 10 mA peak amplitude **(c)** ESD threshold current at critical temperatures and electric field breakdown across an oxide layer [37]

All studies in this part are valuable to this thesis. They provide idea and reference of magnetic recording head, methodology, measurement technique, and analysis of result.

1.6 Thesis Structure

The structure of this thesis consists of 5 chapters.

Chapter 1 Introduction and literature review

Chapter 2 Theory

Chapter 3 Research methodology

Chapter 4 Experimental result and discussion

Chapter 5 Conclusions and suggestion

CHAPTER 2

THEORY

Wireless communication technologies are interesting to be used in hard disk drive manufacturing to improve process efficiency and reduce cost. But magnetic read sensor on head gimbal assembly is the most sensitive device to external energy. This study is to explore if using of wireless communication devices in HGA process will harm the latest version of magnetic read sensor or TGMR.

This chapter provides a review of related theories to the study which are, basis of wireless communication, electromagnetic and thermal theory, electromagnetic interference, basic hard disk drive assembly parts and process, magnetic read head technologies, recording head with difference-end temperature coefficient resistor (DETCR), failure mode of TGMR, and quasi-static test of TGMR.

2.1 Basis of wireless communication

Wireless communication is the transfer of information between two or more points that are not connected by an electrical conductor. The term of wireless communication was introduced in the 19th century and wireless communication technology has been developed over the subsequent years. It is one of the most important media of transmission of information from one device to other devices. In this technology, the information can be transmitted through the air without requiring any cable or wires or other electronic conductors, by using electromagnetic waves such as IR, RF, satellite and etc. Wireless communication consists of several types of technology such as Satellite Communication, Infrared Communication, Broadcast Radio, Microwave Communication, Wi-Fi, Bluetooth Technology and Mobile Communication Systems [15].

Advantages of Wireless Communication:

- Any data or information can be transmitted faster and with a high speed,
- Maintenance and installation is less costly for these networks,
- The internet can be accessed from anywhere wirelessly, and
- It is very helpful for workers, doctors working in remote areas as they can be in touch with medical centers.

Disadvantages of Wireless Communication:

- An unauthorized person can easily capture the wireless signals which spread through the air,
- It is very important to secure the wireless network so that the information cannot be misused by unauthorized users,
- Some of wireless communication devices use high power and generate electromagnetic interference.

Applications of Wireless Communication

Applications of wireless communication involve security systems, television remote control, Wi-Fi, cell phones, wireless power transfer, computer interface devices and various wireless communication based projects. There are typically large numbers of wireless communication devices which are in use within manufacturing and business facility because it can help improving operation efficiency such as operation cost, productivity, data recording and analysis, machine learning, decision making and quality improvement, and etc. Current wireless communication technologies make use of electromagnetic spectrum and sub-spectrum of radio wave and microwave band. So, it cannot completely avoid electromagnetic interference. Some businesses need to safeguard their operation from the effects of using wireless communication devices and its network. Topology of wireless communication networks are illustrated in table 2.1.

Table 2.1 Wireless Network Topology [15]

Network	Technology, Standard	Frequency	Approximate Range	Example Devices	Power
Peer-to-peer	2-way radio	150-470 MHz	1-30 Kilometers	Walkie-talkie, Ham radio, Public safety radio system	1-5 Watts
Wireless Personal Area Network (WPAN)	Bluetooth 802.15.1	2400 MHz, 5000 MHz	15 meters	Cordless phone Computer's peripheral devices	0.01-0.2 Watts
Wireless Local Area Network (WLAN)	IEEE 802.11a/b/g	2400 MHz, 5000 MHz	150 meters in-door 300 meters out-door	WiFi Router	0.1-0.5 Watts
Wireless Wide Area Network (WWAN)	CDMA, GSM, GPRS, Edge, iDEN	800, 900, 1700, 1800, 1900, 2100 MHz	5-50 kilometers	Cellular network Mobile phone	0.05-0.5 Watts

2.2 Electromagnetic and thermal theory

Electric and magnetic forces, gravity and the weak and strong forces are the five known forces of physics. Electromagnetism embraces both electricity and magnetism and is basic to everything involving electric matters and magnetic. The electromagnetic spectrum is widely broad from attometers (10^{-18}) to kilometers (10^{3}) wavelength. It includes natural, science and technology phenomena in our everyday experience. Figure 2.1 illustrates the electromagnetic spectrum with wavelength on a logarithmic scale from the shortest gamma rays to the longest radio waves. Wavelengths are expressed in metric units. The atmospheric opacity is shown at the top with the optical and radio windows in evidence. [17]

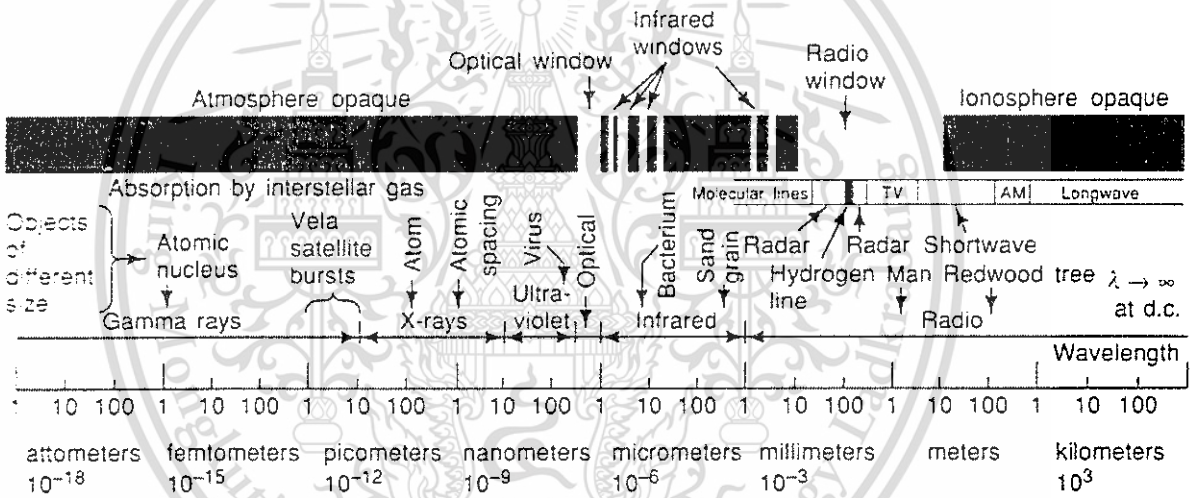

Figure 2.1 Electromagnetic spectrum [17]

Electric field ($\vec{E}$) and magnetic field ($\vec{B}$) are vector fields and in general have amplitudes and directions that vary with the three spatial coordinates such as in Cartesian coordinates x, y, z and the time coordinate t. The electric field is measured in volt per meter (V/m) and the magnetic field in Webbers (Wb) or Ampere per meter (A/m). The electric field ($\vec{E}$) and magnetic field ($\vec{B}$) are regards as fundamental in that they give the force ($\vec{F}$, newtons) on a charge (q, culombs) moving with velocity (v, m/s); that is, Laurentz force equation, [18]

$$\vec{F} = q(\vec{E} + v\vec{B}) \tag{2.1}$$

One of the basic law of electromagnetic phenomena is Faraday's law which states that a time-varying magnetic field generates an electric field. Let C is an arbitrary closed curve that forms the boundary of a non-moving surface S. The time rate of change of the total magnetic flux through the surface S is,

$$\partial(\int_s \vec{B} \bullet dS)/\partial t \tag{2.2}$$

According to Faraday's law, this time rate of change of total magnetic flux is equal to the negative value of the total voltage measurement around C, an arbitrary closed curve that forms the boundary of a non-moving surface S. The later quantity is given by,

$$-\oint_c \vec{E} \bullet dl \tag{2.3}$$

Hence, the mathematic statement of Faraday's law is,

$$\oint_c \vec{E} \bullet dl = -\frac{\partial}{\partial t}\int_s \vec{B} \bullet dS \tag{2.4}$$

As the structure of TGMR read sensor has electrical resistance, once it has voltage drop, current will flow through the sensor per Ohm's law ($V = IR$) . In other words, if a resistance is subjected to a voltage, or if it conducts a current, then it will always consume electrical power and we can superimpose these three quantities of power, voltage and current into a triangle called a Power Triangle with the power, $P = IV$, which would be dissipated as heat in the resistor at the top, with the current consumed and the voltage across it at the bottom ($P = V^2/R$ or $P = I^2R$). From Faraday's law, the voltage induction to TGMR in electromagnetic field can be described as $V = -d\phi/dt$, while V is induction voltage (volts), ϕ is magnetic flux (Wb) and t is time in seconds [17]. The heat equation can be expressed as,

$$Q = \frac{1}{\sigma}|J|^2 = \sigma|\nabla V|^2 \tag{2.5}$$

While Q is joule heat induced by current pulse (J/s or W), σ is electrical conductivity of the resistor (S/m), J is current intensity (A/m^2), which is equal to $\sigma\bar{E}$ or $-\sigma\nabla V$, V is Voltage (volts). [20]

The change of Joule heating makes change to the temperature of the resistor according to the heat transfer equation,

$$Q = \rho C \frac{\partial T}{\partial t} - \nabla \bullet (k \nabla T) \tag{2.6}$$

When ρ is density of the material (kg/m^2), T is temperature ($^{\circ}$C), C is heat capacity (kJ/K/kg), k is thermal conductivity of the material (W/K/m). [20]

From the equation above, if the material has high density, high thermal capacity but low thermal conductivity, the material supposes to get higher temperature.

The Néel temperature or magnetic ordering temperature (T_N) is the temperature above the point that an antiferromagnetic material becomes paramagnetic. Meaning that, the thermal energy becomes large enough to destroy the macroscopic magnetic ordering within the material. Heat is able to be transferred by electromagnetic wave. The relation of energy and frequency can be explained by Plank's law,

$$E = hf \tag{2.7}$$

When E is energy (J), h is Plank's constant equal to 6.626070040(81)×10^{-34} (Js), f is frequency (Hz)

To select the sensor to measure temperature of TGMR, beside the proximity of the sensor to TGMR, the material thermal properties should not have much difference to ensure that temperature at the sensor is similar to at DUT. As Kirchoff's identity states that, at thermal equilibrium, absorptivity (α) is equal to the emissivity (ε). And,

$$\alpha + \rho + \tau = 1 \tag{2.8}$$

When α is absorptivity, ρ is reflectivity, and τ is transmissivity

The radiation power can be expressed by the Stefan-Boltzmann's law,

$$P_{rad} = \varepsilon_{rad} \delta A T^4 \tag{2.9}$$

When P_{rad} is radiation power (W), ε_{rad} is emissivity (0-1), δ is Stefan-Boltzmann constant (5.67 x 10^8 W/m^2K^4), A is surface material (m^2), and T is temperature (K)

2.3 Electromagnetic interference (EMI)

Electromagnetic interference (EMI), also called radio-frequency interference (RFI) when in the radio frequency spectrum, is a disturbance generated by an external source that affects an electrical circuit by electromagnetic induction, electrostatic coupling, or conduction. EMI is an unwanted signal at the signal receiver, and in general methods are sought to reduce the level of the interference.

Types of EMI - Electromagnetic Interference [21]

EMI categorizes by origins;

- Man-made EMI: This type of EMI generally arises from other electronic circuits, although some EMI can arise from switching of large currents, and etc.
- Naturally occurring EMI: This type of EMI can arise from many sources cosmic noise as well as lightning and other atmospheric types of noise.

EMI categorized by its duration:

- Continuous interference: This type of EMI generally arises from a source such as a circuit that is emitting a continuous signal. However background noise,

which is continuous, may be created in a number of ways, either manmade or naturally occurring.

- Impulse noise: Again, this type of EMI may be man-made or naturally occurring. Lightning, ESD, and switching systems all contribute to impulse noise which is a form of EMI.

EMI categorized by their bandwidth:

- Narrowband: Typically this form of EMI is likely to be a single carrier source - possibly generated by an oscillator of some forms. Another form of narrowband EMI is the spurious signals caused by intermodulation and other forms of distortion in a transmitter such as a mobile phone of Wi-Fi router. These spurious signals will appear at different points in the spectrum and may cause interference to another user of the radio spectrum. As such these spurious signals must be kept within tight limits.
- Broadband: There are many forms of broadband noise which can be experienced. It can arise from a great variety of sources. Man-made broadband interference can arise from sources such as arc welders where a spark is continuously generated. Naturally occurring broadband noise can be experienced from the sun - it can cause sun-outs for satellite television systems when the sun appears behind the satellite and noise can mask the wanted satellite signal. Fortunately these episodes only last for a few minutes.

EMI coupling mechanisms [21] [38]

There are many ways in which the electromagnetic interference can be coupled from the source to the receiver. Understanding which coupling method brings the interference to the receiver is the key to be able to address the problem.

- Radiated: So called radiative coupling or electromagnetic coupling. This type of EMI coupling is probably the most obvious. It is the type of EMI coupling

that is normally experienced when the source and victim are separated by a large distance - typically more than a wavelength. Source and victim act as radio antennas. The source emits or radiates an electromagnetic wave when propagates across the open space in between and is picked up or received by the victim. The source radiates a signal which may be wanted or unwanted, and the victim receives it in a way that disrupts its performance.

- Conducted: Conducted emissions occur as the name implies when there is a conduction route along which the signals can travel. This may be along power cables or other interconnection cabling. The conduction may be in one of two modes:
    - Common mode: This type of EMI coupling occurs when the noise appears in the same phase on the two conductors, e.g. out and return for signals, or +ve and -ve for power cables.
    - Differential mode: This occurs when the noise is out of phase on the two conductors.
- Capacitive coupling: Occurs when a varying electrical field exists between two adjacent conductors typically less than a wavelength apart, inducing a change in voltage across gap.
- Inductive coupling: Occurs where the source and receiver are separated by a short distance (typically less than a wavelength). Strictly, "inductive coupling" can be of two kinds , electrical induction and magnetic induction. It is common to refer to electrical induction as capacitive coupling and magnetic induction as inductive coupling
- Magnetic coupling: Occurs when a varying magnetic field exists between two parallel conductors typically less than a wavelength apart, inducing a change in voltage along the receiving conductor.

By determining the form of coupling that exists and the way in which it is reaching the victim, it may prove to be that the most effective method of reducing

the EMI is by putting measurement in place to reduce the coupling and reduce the level of interference to an acceptable level.

Electromagnetic interference (EMI) is present in all areas of electronic and electrical applications. By understanding the source, the coupling methods and the susceptibility of the victim, the level of interference can be reduced to a level where the EMI causes no undue degradation in performance.

2.4 Basic hard disk drive assembly parts and processes

Hard disk drive is a data storage device used for storing and retrieving digital information using one or more rigid ("hard") rapidly rotating disks (platters) coated with magnetic material. The platters are paired with magnetic heads arranged on a moving actuator arm, which read and write data to the platter surfaces [22]. Data is accessed in a random-access manner, meaning that individual blocks of data can be stored or retrieved in any order and not only sequentially. HDDs are a type of non-volatile memory, retaining stored data even when powered off [23]. Basic components of hard disk drive are shown in Figure 2.2.

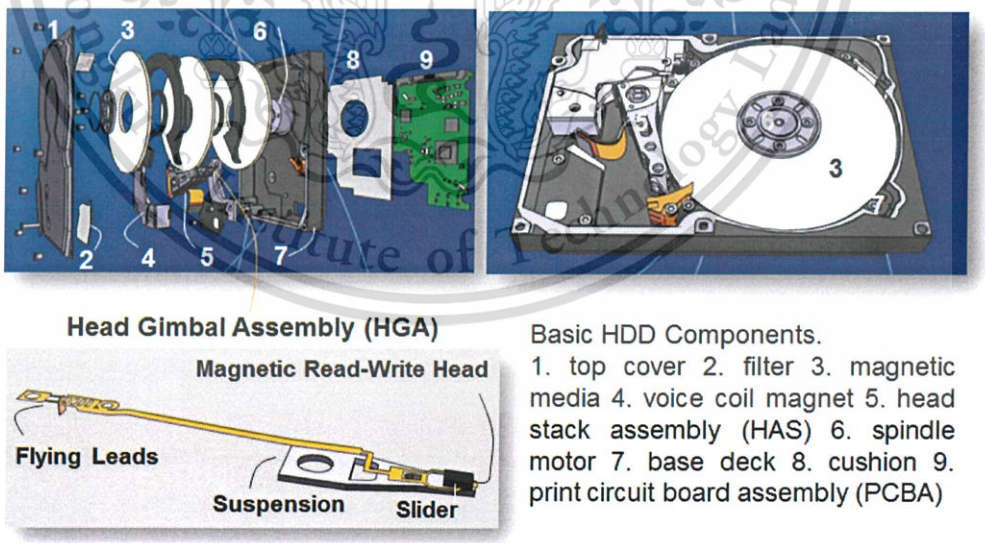

Figure 2.2 Basic hard disk drive components [24]

Modern hard disk drive assembly process is automation base. Basis of the process steps is pick-and-place, mechanical connection, electrical connection and performance testing, as shown in figure 2.3.

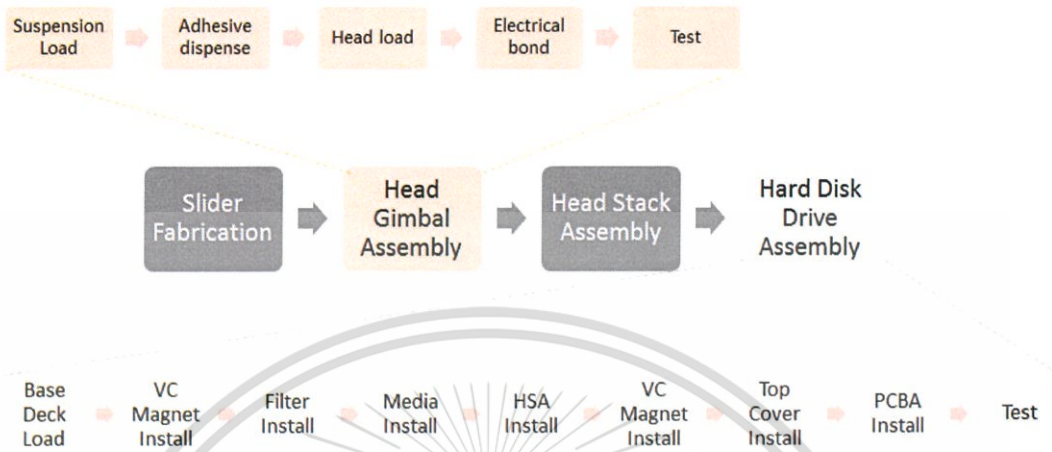

Figure 2.3 Basic hard disk drive assembly processes

Head-Gimbal Assembly (HGA) is an important piece part of Hard Disk Drive in which slider body, which containing read-write head, located and flies above magnetic recording media. The manufacturing process of Head-Gimbal Assembly is basically in full automation.

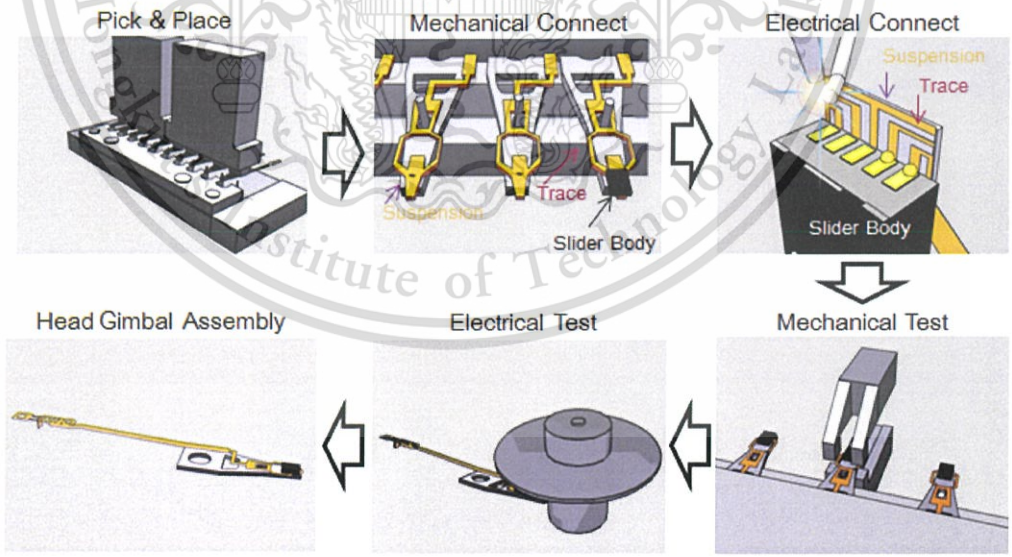

Figure 2.4 Head Gimbal Assembly processes [24]

As shown in Figure 2.4, robot end-effector pick-and-place each piece part, make mechanical connection and electrical connection between Trace-Gimbal Assembly (TGA) and Slider body. Then check performance via mechanical test and electrical test processes. Piece parts of HGA are contacted and in-contacted with grounded metal or static dissipative material many times along the automated process.

2.5 Magnetic read head technologies

The hard disk drive (HDD) industry has been facing strong competition from other data storage devices such as solid state drive. In order to keep HDD's advantages in cost and capacity, the areal density (AD) should maintain an annual growth rate of 30% to 40% [25]. For data storage industry, the innovation drives areal density growth. One of the challenges to increase drive capacity is to increase areal density [26].

Most dramatic change in disk drive technology has happened in magnetic head development and manufacturing. The ranking of head performance is basically base on favorable properties such as linear density, track density, data rate, and cost per complexity [27].

Read head technology started from thin-film effect sensor. Nowadays, read head technology applies magneto-resistance phenomenal effect to extract the information back from the magnetic recording medium. The technology develops from thin film, AMR (Anisotropic Magnetoresistance), GMR (Giant Magnetoresistance) and TGMR (Tunneling Giant Magnetoreistance) read sensor.

GMR Current-in-Plane (CIP) architecture used in longitudinal recording technology has been replaced by TGMR Current-Perpendicular (CPP) architecture

with perpendicular recording technology to allow higher data recording density (Figure 2.5.1).

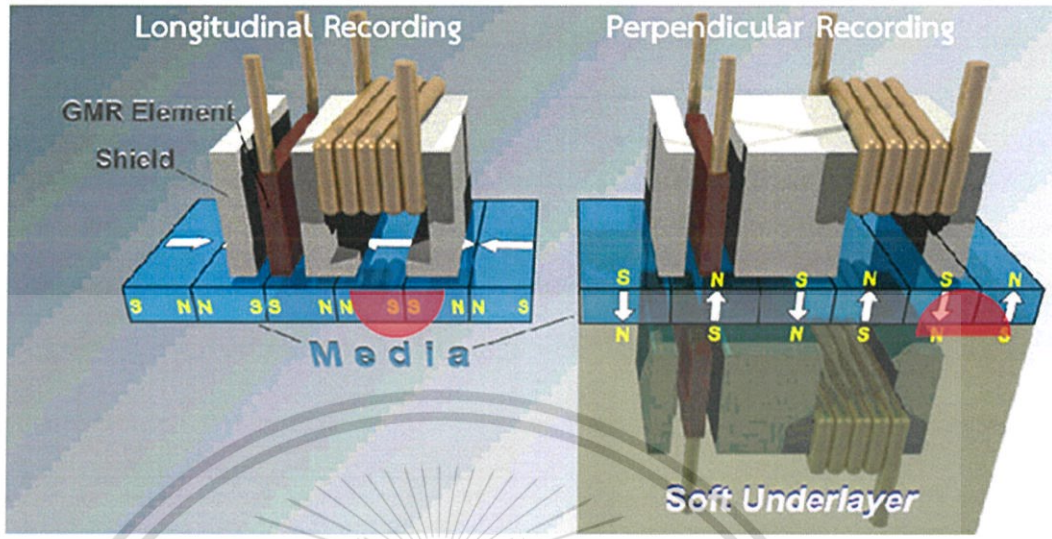

Figure 2.5.1. Current-in-plane and current perpendicular magnetic recording. [28]

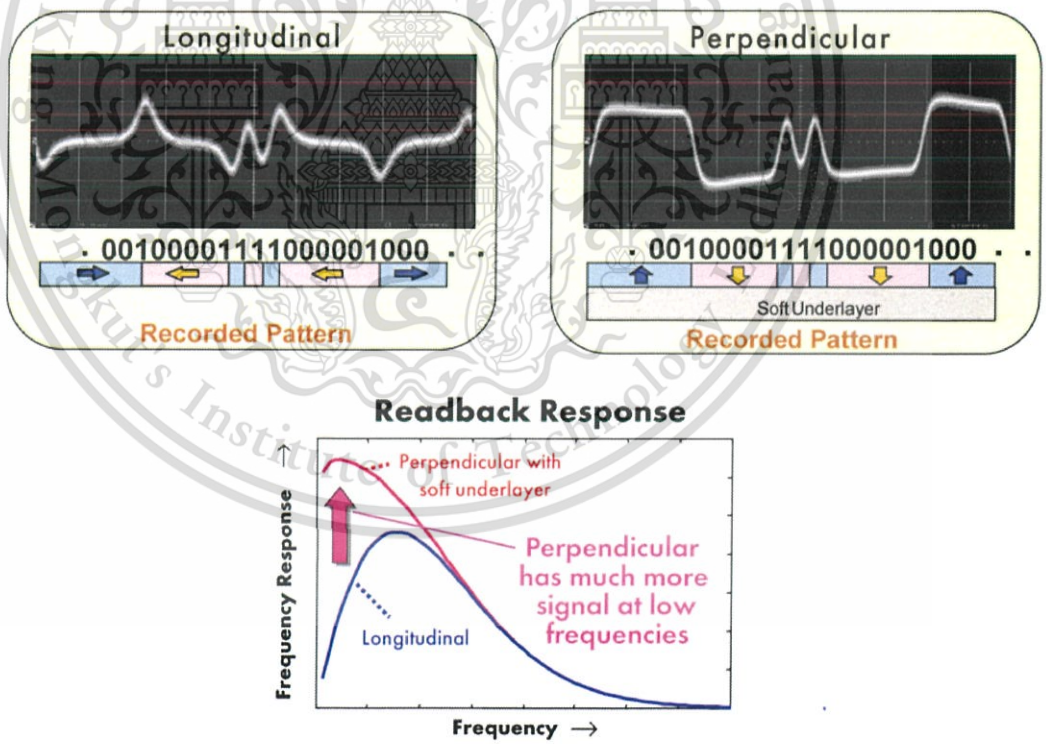

Figure 2.5.2. Readback signal of longitudinal and perpendicular reader sensor [39]

Key distinguishing element of TGMR is Magnetic Tunnel Junction (MTJ), which consists of two ferromagnets separated by an angstrom-thin insulator. Electrons can tunnel from one ferromagnet to the other if the barrier is thin enough (Figure 2.6). With this quantum mechanical phenomenon, the MTJ can be switched between two states of electrical resistance, high resistance and low resistance, then provides higher MR Ratio (ΔR/R0: change of TGMR resistance/minimum resistance of TGMR), higher readout amplitude (Figure 2.5.2) and speed as well as lower areal resistance (RA: Resistance x Area) and head noise [8].

TGMR resistance is ten times higher than GMR resistance. This makes TGMR undergoing ten times higher joule heat than GMR. The angstrom-thin metal oxide barrier makes TGMR more susceptive to external energy. Fortunately, not like GMR, the TGMR head do not have insulator between buffer and shield, so TGMR can dissipate thermal directly through top and bottom metal shield. Example of simplified structure of GMR and TGMR recording reader head are explained in Figure 2.7.1 and Figure 2.7.2. Actual structure and material may be difference base on design and fabrication.

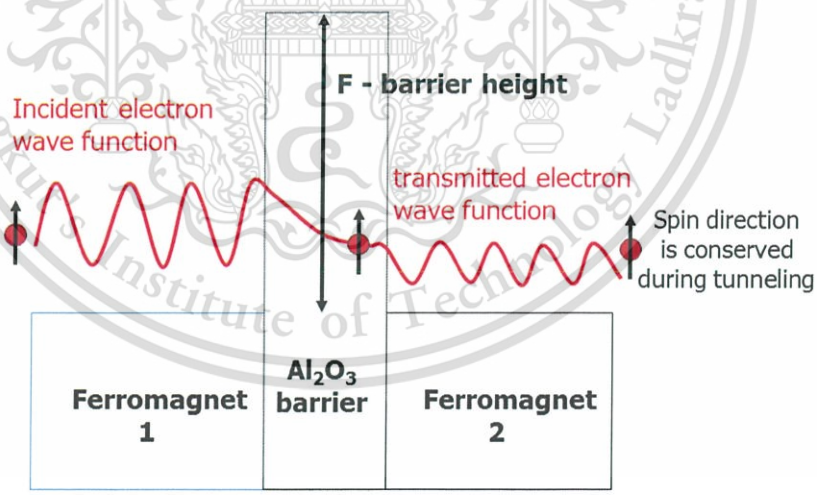

Figure 2.6 Basic of Magnetic Tunnel Junction (MTJ) Resistance of device depending on electrons undergoing spin-dependent tunneling through the barrier layer. Band structure effects in Co(Fe)-MgO-Co(Fe) can lead to very large magneto-resistance [29]

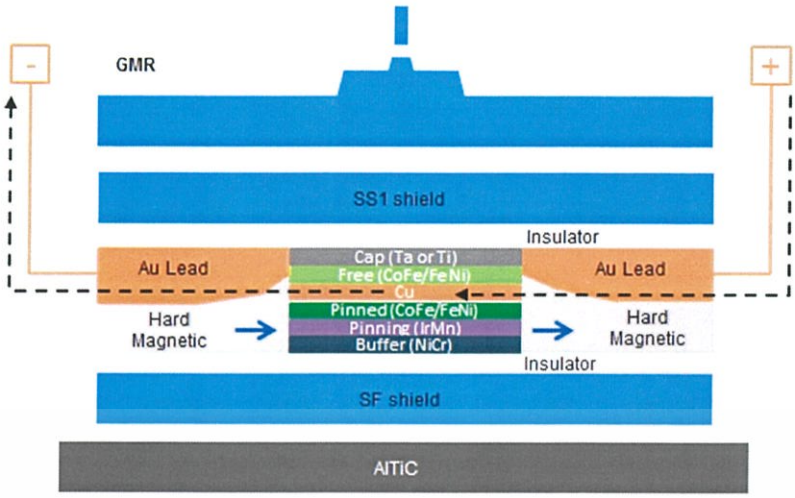

Figure 2.7.1. GMR Structure, Current-In-Plane, Conductive Spacer (Cu) [30]

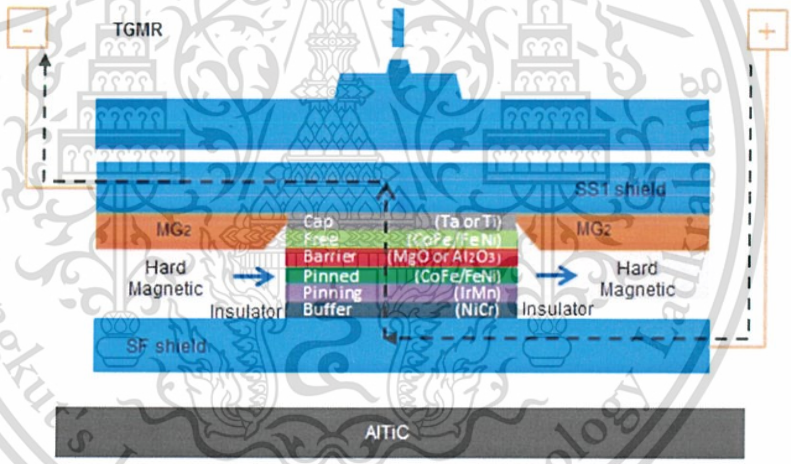

Figure 2.7.2 TGMR Structure, Current-Perpendicular, Insulative Spacer (MgO or Al_2O_3) [30]

2.6 Difference-end temperature coefficient resistor in magnetic head

Differential-Ended Temperature Coefficient of Resistivity (DETCR) is a build-in sensor supported by a head transducer has a temperature coefficient of resistance (TCR) and a sensor resistance. The sensor operates at a temperature above ambient and is responsive to changes in sensor-medium spacing. Conductive contacts connected to the sensor have a contact resistance and across-sectional area adjacent to the sensor larger than that of the sensor, such that the contact resistance is small relative to the sensor resistance and negligibly contributes to a signal generated by the sensor. A multiplicity of head transducers each support a TCR sensor and a power source can supply bias power to each sensor of each head to maintain each sensor at a fixed temperature above an ambient temperature in the presence of heat transfer changes impacting the sensors. A TCR sensor of a head transducer can include a track-oriented TCR sensor wire for sensing one or both of asperities of the medium. [9][10][28]

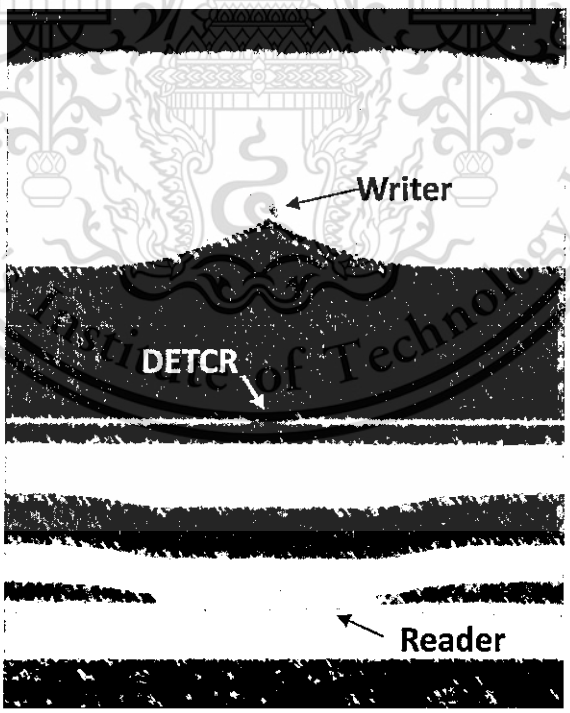

Figure 2.8 Build-in DETCR proximity to TGMR in the magnetic read-write head [9][10] [28]

The response to local changes in temperature at the DETCR sensor is based on equation (2.10) and (2.11). The change of DETCR resistance ($\Delta R_{DETCR} = R_{DETCR} - R_{0\_DETCR}$) is proportional to the change of DETCR temperature ($\Delta T_{DETCR} = T_{DETCR} - T_{0\_DETCR}$) while R_{0_DETCR} is original resistance of the DETCR, R_{DETCR} is resistance of the DETCR at the point of time to compare, T_{0_DETCR} is original temperature of the DETCR, T_{DETCR} is temperature of the DETCR at the point of time to compare, and α is specific to DETCR material.

$$\Delta R_{DETCR} = \alpha \quad \Delta T_{DETCR} \tag{2.10}$$

$$R_{DETCR} - R_{0\_DETCR} = \alpha * (T_{DETCR} - T_{0\_DETCR}) \tag{2.11}$$

2.7 Failure mode of TGMR read head and Quasi-static test

2.7.1 Failure mode of TGMR read head

TGMR read head failure can be classified into three modes, Hard failure, Soft failure and Latent failure. [33]

Hard failure mode is defined as magnetoresistive elements, which are physically damaged [34]. TGMR head with the ultra-thin oxide layer as an insulator acts as capacitor which can induce voltage across and prone for dielectric breakdown and pinhole. Example of oxide layer made of MgO, susceptible to the electric field of 0.5 GV/m, allow voltage across is approximately 2 volts [35]. The dielectric breakdown or pin hole result sudden TGMR resistance drops to low value, so the read out amplitude will drop as well.

In soft failure mode, magnetoresistive elements have no physical damag or resistance changed, but magnetic properties changed. This level of failure sometimes leads to long term reliability issues. Examples of this failure mode are defect in

reference layer, Pinned layer or Antiferromagnet such as temporary magnetization reversal.

Latent failure mode is most likely hard to detect, since it sometimes comes and goes. There may be no abnormal sign of TGMR resistance or amplitude. Small defect of magnetic layers leads to instability of the read sensor. It requires special technique to test and analysis to discover the instability.

2.7.2 Quasi Static Test

Quasi Static Tester (QST) is used to evaluate GMR/TGMR head performance without performing flying head over the recording media. The measurement is independent from external influence such as disk flying height, variation of the magnetic properties and surface properties of the disk. Magnetoresistive effect read head element is tested by applying a varying magnetic field and measuring the resulting output signals from the read head element. The output signals are digitized and a processor calculates [11].

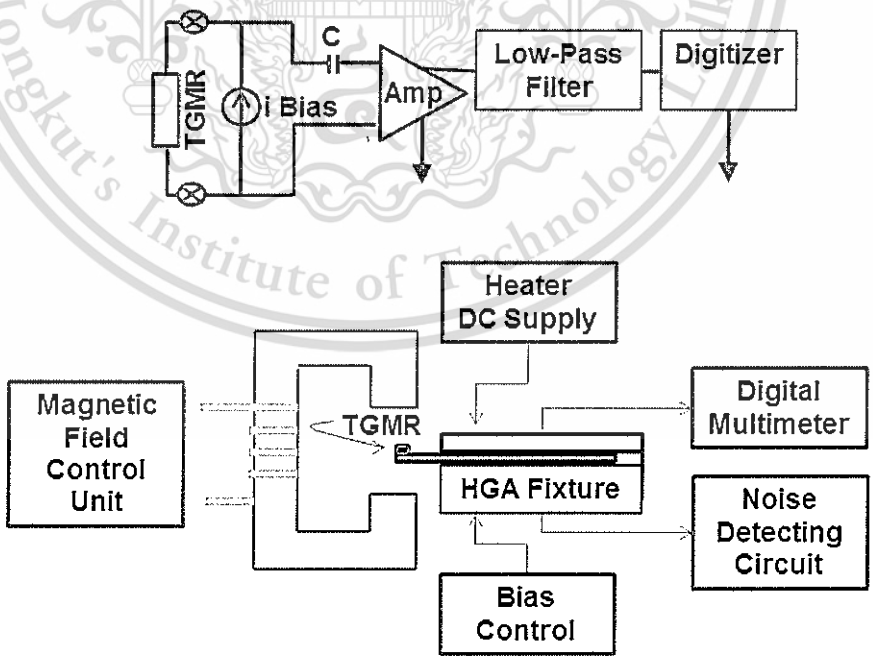

Figure 2.9 Basic diagram of Quasi-Static Test

2.7.2.1 TGMR RESISTANCE

QST TGMR resistance measurement is static test and frequency response test. Actually, the resistance of the GMR is dependent on the magnetic field applied. In ideal case, the relationship of GMR resistance to applied field is linear. But, in reality, each magnetoresistive effect read heads response to the magnetic field differently.

2.7.2.2 QUASI TRANSVERSE TESTING

Quasi transverse testing is fixed bias current (mA) and measure voltage (V) during sweep or varying magnetic field. This method is to characterize the head performance using the magnetic properties such as magnetic domain and also magnetization change causing magnetoreisistive resistance change proportional to the applied field and affect to voltage amplitude over magnetoresistive element changed. All measurement has been controlled and measured through pre-amplifier circuit.

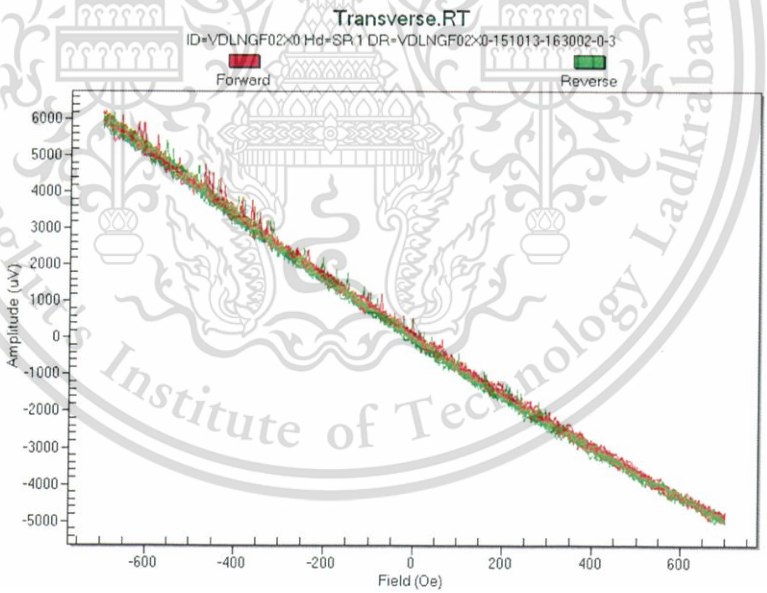

Figures 2.9.1 Example of good TGMR transverse tested by QST

2.7.2.2 (a) TGMR AMPLITUDE

Amplitude is the key performance of reader sensor. There are 2 types of QST amplitude test. One is Amplitude test, the test measures peak amplitude in micro-volt (μV) at defined point of magnetic field. Amplitude is directly related to the change of TGMR resistance as shown in (12). While *I* is the bias current, *V* is the voltage dropped on the sensor, $\Delta R/R_0$ is the intrinsic TGMR ratio, ε is the efficiency or amount of free layer rotation.

$$\text{Amplitude} = I \times \Delta R \times \varepsilon = I \times R_0 \times \frac{\Delta R}{R_0} \times \varepsilon = V \times \frac{\Delta R}{R_0} \times \varepsilon \tag{2.12}$$

Another is peak to peak amplitude which has been calculated by the difference of maximum and minimum amplitude in the transverse transfer curve.

$$Pk - PkAmp(uV) = MaxMmp(uV) - MinAmp(uV) \tag{2.13}$$

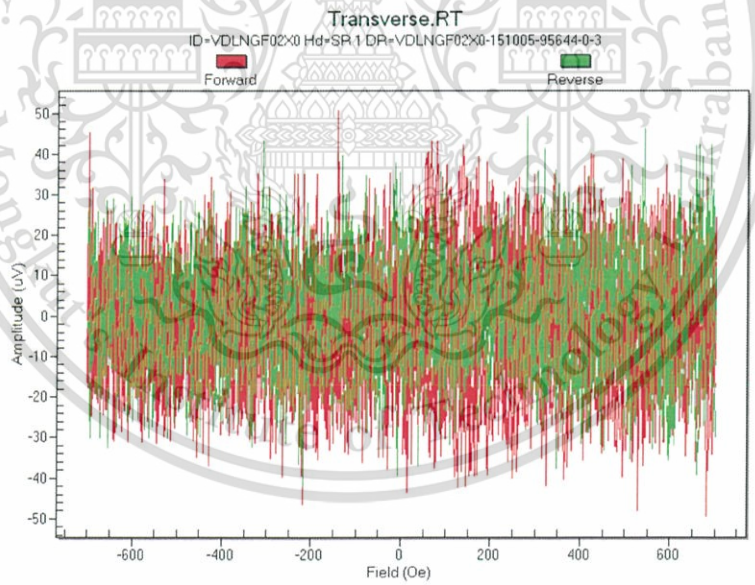

Figure 2.9.2 Example of Amplitude failure (no amplitude) on QST transverse test

The other following parameters are measured and calculated from the transverse transfer curve as shown in Fig.2.9.1

7.7.2.2 (b) SLOPE / MAGNETIC POLARITY

External energy such as Thermal, EOS/ESD can cause Pinned Layer magnetic polarity reversal in TGMR. Weak Pinned Layer, AFM or Reference Layer coupling also cause polarity issue in some points of field. Slope test checks transfer curve slope opposite to the readers with the correctly oriented reference layer. It can reveal the magnitude and location of reversal over the sweep test range. Parameter of slope testing includes,

'Maximum slope (μV/Oe)' which is absolute value of maximum slope detected on either forward or reverse curves, in order to detect slope variations such as direction of the transfer curve that is calculated by fitting a best-fit line cross the data taken from both curves.

'Maximum slope signed (μV/Oe)' which is similar to maximum slope but the window size is defined by the user as 'maximum slope field range' (not absolute value).

'Maximum slope (%)' is percentage change of maximum slope in the field range.

'Maximum slope at (Oe)' is the field location, where maximum slope (μV/Oe) occurred.

'Maximum slope amp (μV)' is the peak-to-peak amplitude within window where maximum slope (μV/Oe) occurred.

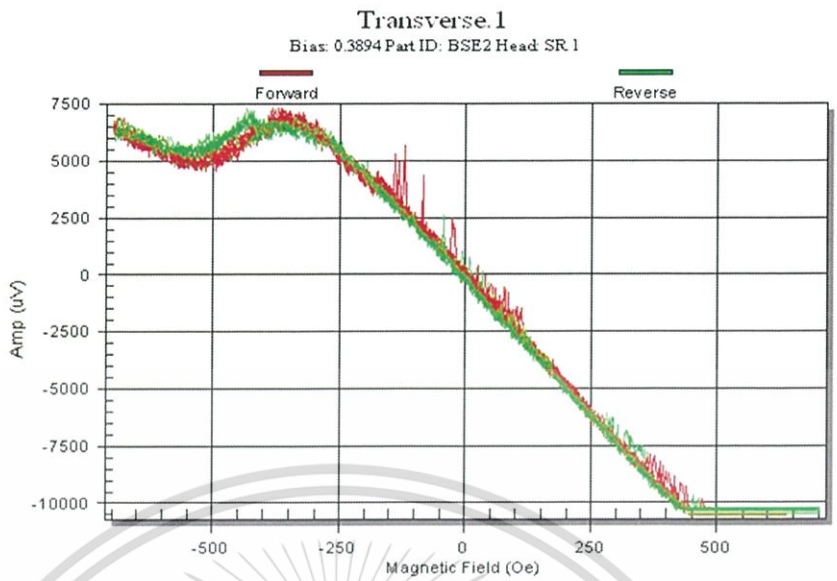

Figure 2.9.3 Example of partially reverse slope failure on QST transverse test

2.7.2.2 (c) AMPLITUDE ASYMMETRY

While magnetic recording head is driven into the magnetic saturation (Ms), there is no longer linear response of the transfer curve, which causes positive and negative peaks amplitudes. Asymmetry test basically shows the symmetry of the transfer curve which can indicate performance of magnetic layers in TGMR. Equation (2.14) shows calculation of asymmetry from absolute value of the maximum and minimum amplitude.

$$\text{Asymmetry}(\%) = \frac{|MAX.amp| - |MIN.amp|}{|MAX.amp| + |MIN.amp|} \times 100 \qquad (2.14)$$

2.7.2.2 (d) HYSTERESIS

Hysteresis test is measurement area between forward amplitude (*Fi*) and reverse amplitude (*Ri*) of the amplitude. Equation (2.15) shows calculation of hysteresis, in the unit of μV/Oe, from amplitude and magnetic field increment (*Inc*). And percentage of Hysteresis (2.16) is calculated from ratio of A to B, where A is Hysteresis in μV/Oe and B is referring to (2.17). Likely cause of large Hysteresis is AFM/SAF failure or shield or Magnetic seed issue.

$$Hysteresis(\mu V / Oe) = Inc \times \sum |Fi - Ri| \tag{2.15}$$

$$Hysteresis\,(\%) = (A / B) \times 100\% \tag{2.16}$$

$$B = Inc \times \sum \frac{(Max_i + Min_i)}{2} - AmpMin \tag{2.17}$$

2.7.2.2 (e) BARKHAUSEN-JUMP

Barkhausen-jump (μV) is maximum amplitude jumping between two adjacent measurement points. Percentage of Barkhausen jump (*%BJ*) can be calculated with peak-to-peak amplitude ($Amp._{pk\text{-}pk}$) as shown in (2.18). Barkhausen field (Oe) is the field location where Barkhausen-jump occurred.

$$\%BJ = [BJ(\mu V) / Amp._{Pk-Pk}] \times 100 \tag{2.18}$$

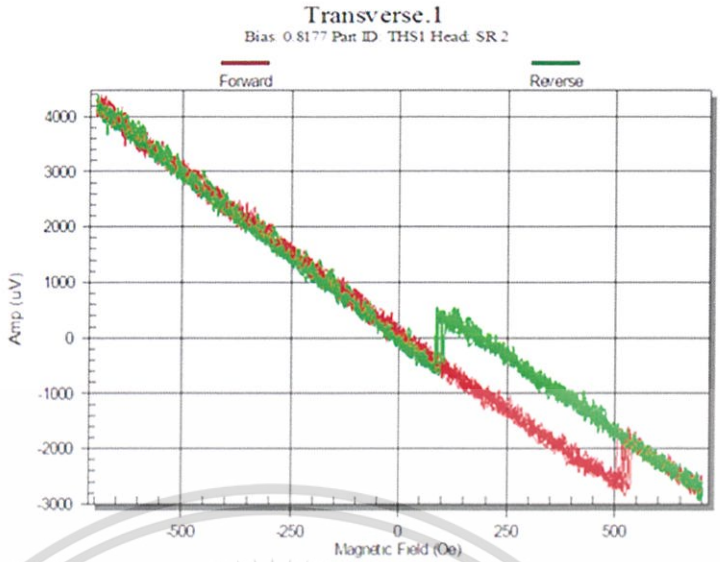

Figure 2.9.4 Example of large Hysteresis from QST transverse test

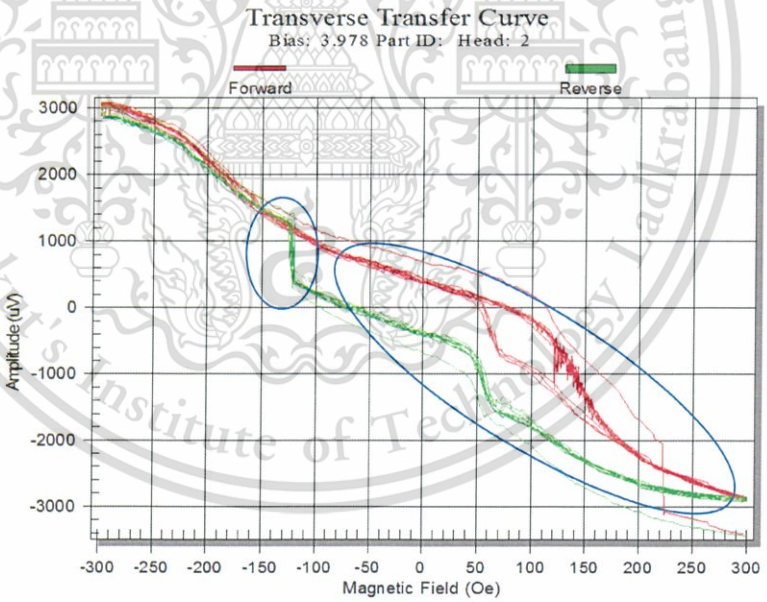

Figure 2.9.5 Example of Barkhausen-jump and large hysteresis on QST transverse test

2.7.2.2 (f) SPECTRAL MAXIMUM AMPLITUDE NOISE (S.M.A.N.)

Spectral Maximum Amplitude Noise (S.M.A.N.) test is designed to quickly measure the spectral noise density as a function of magnetic field utilizing AC channel. It measures noise density by sweeping through a range of DC magnetic fields. This parameter is invented to provide capability of high frequency instability identification [11-12]. Optionally, user can enable write stress to catch both writer induced and field induced noise. Example of S.M.A.N. test is shown in **Figure 2.9.6**.

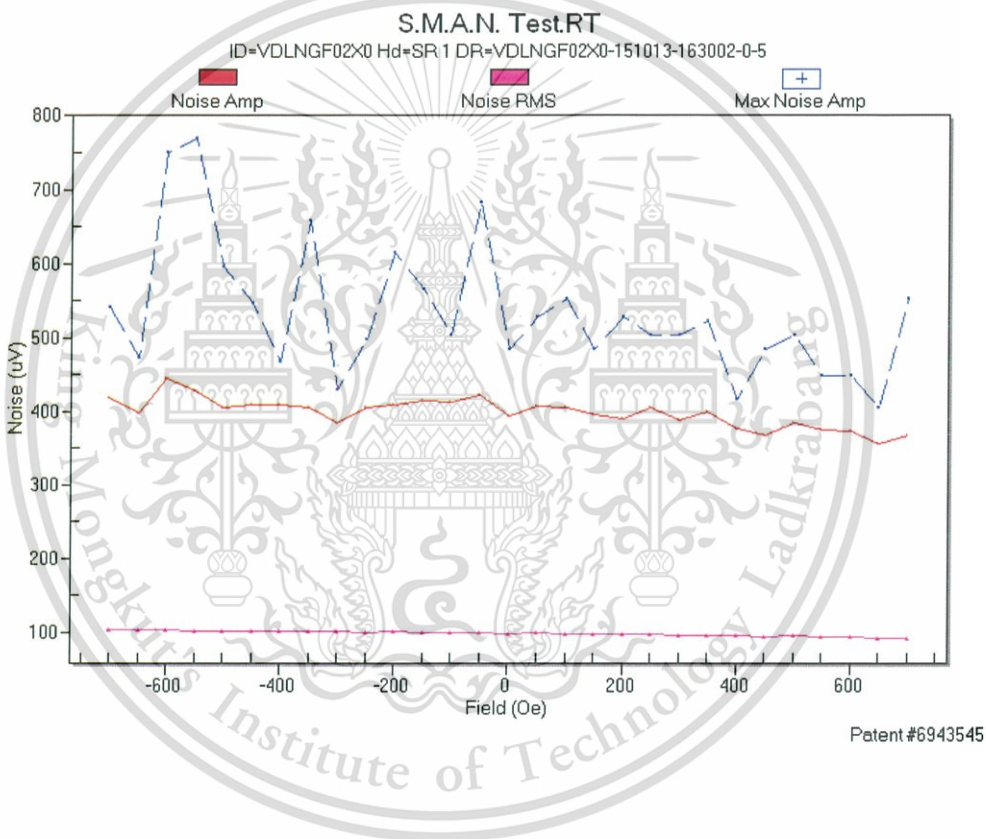

Figure.2.9.6 Example of good TGMR SMAN tested by QST

In summary, TGMR, as the most sensitive part of HGA in assembly process, has specific properties which different from other devices. Wireless communication works in electromagnetic spectrum, which can generate electromagnetic field and interference with power or Joule heat. Knowledge of wireless communication, electromagnetic, thermal theory, hard disk drive assembly, reader technology, and TGMR measurement are all considerable to the study of wireless communication and its effect to TGMR Reader in Head Gimbal Assembly Process.

CHAPTER 3

RESEARCH METHODOLOGY

There are three main experiments in this study.

The first experiment is *A. Wireless communication devices – Electric Field Survey,* to survey overall wireless communication devices potentially be used in manufacturing environment. The experiment will observe direction and distance of placing wireless communication device impact to its electric field strength. Significant field sources, direction and distance from this experiment will be used in the rest of experiments.

The second experiment is *B. Thermal change and DC voltage of TGMR head while placing in the field of wireless communication device,* to know actual thermal change and DC voltage of TGMR head while placing in the field of wireless communication device to compare with TGMR failure threshold. Prediction model from regression analysis could tell the critical distance of specific wireless communication device to be installed in the controlled environment such as in Head Gimbal Assembly process.

And the third experiment is *C. Electrical Performance of TGMR pre and post actions simulating HGA assembly process,* to see accordance from previous experiment to the actual result of electrical performance of TGMR. If thermal change or DC voltage, of TGMR head during assembly and exposing in the field of wireless communication device, is higher than with TGMR failure threshold, the electrical performance of TGMR on HGA process would have same negative change of trend and vice versa.

A. Wireless communication devices – Electric Field Survey

Purpose of this experiment is to see how direction placing wireless communication device and distance impact to electric field strength.

Measuring equipment:

- CTM048 EM Field Meter with CTS001 directional antenna and electromagnetic field module.

Other Tools/Equipment:

- Acrylic insulative test bed
- Ruler for distance measuring and marking
- Design Of Experiment (DOE) table of Multi Level Factorial Design

Field sources:

- Walkie-talkie
- WiFi router
- WiFi phone
- Cellular phone
- Laptop computer
- Tablet computer
- Wireless mouse & keyboard

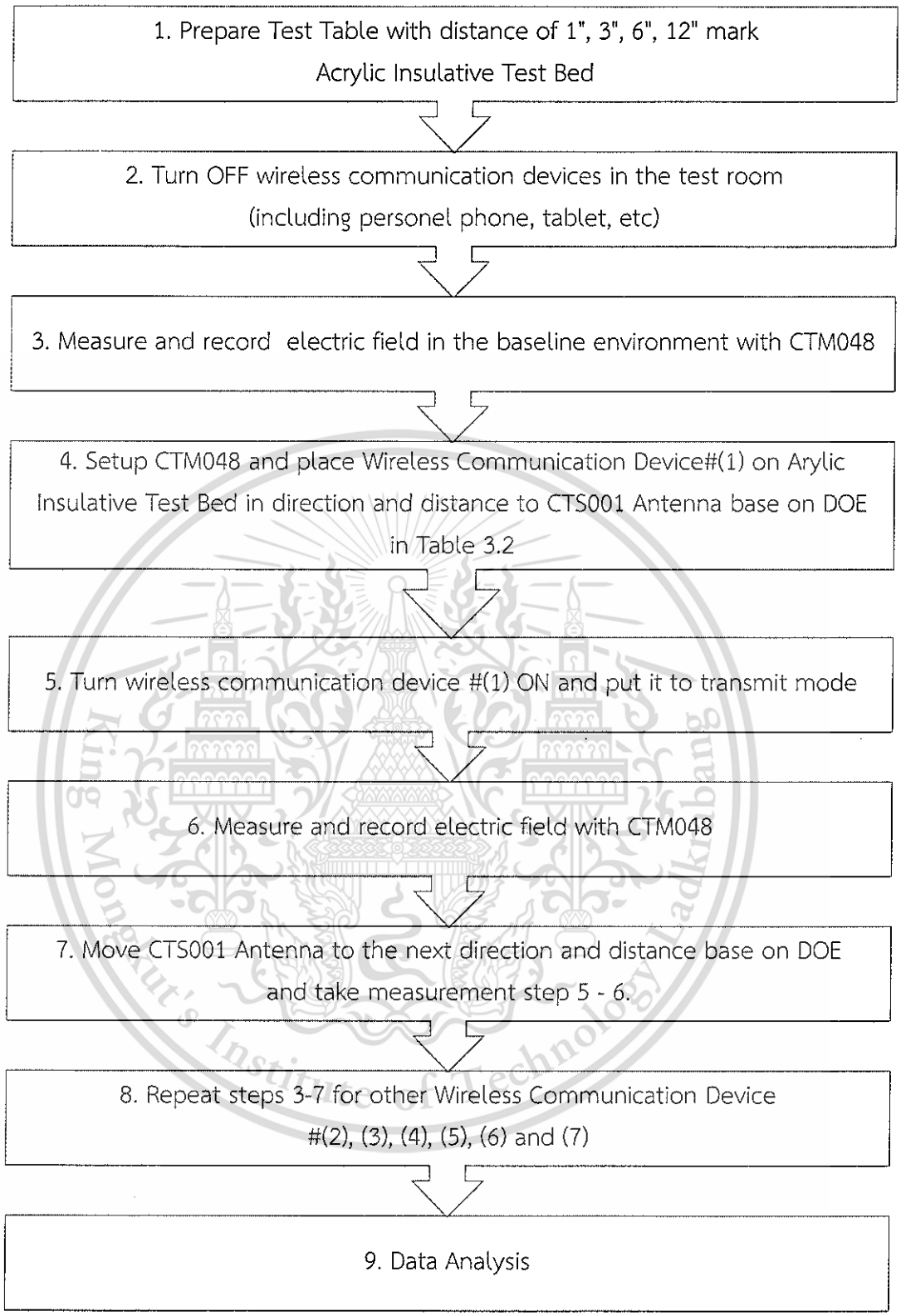

Figure 3.1 Experiment A steps diagram

Detail of Experiment

Electric field from wireless communication devices is measured using CTM048, EM Field Meter with CTS001 directional antenna and electromagnetic field module. This measuring instrument has Peak and Average Measurement Range of 0.001 V/m - 20.00 V/m, Frequency Bandwidth of 1 MHz to 2.5 GHz, Antenna Factor Range of -40.0 to 40.0 dBm-1, Antenna Frequency Response of 10 MHz – 2.5 GHz.

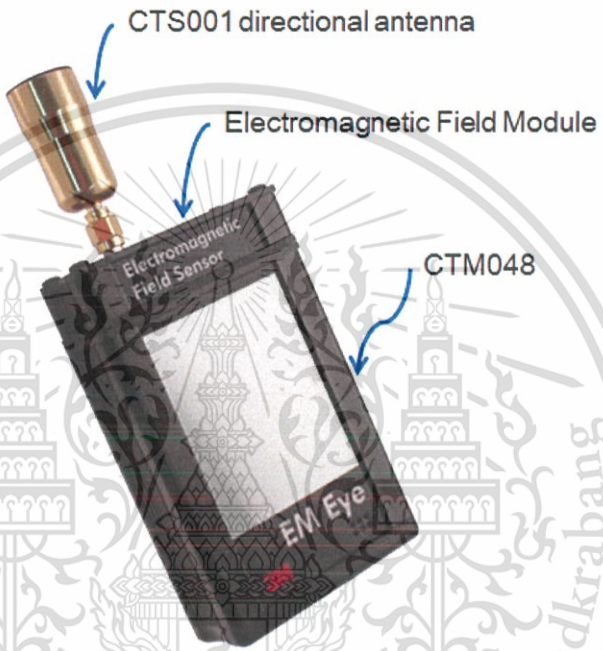

Figure 3.2. CTM048, EM field meter with CTS001 directional antenna and electromagnetic field module [40]

Electromagnetic Field Sensor			
Function Modes	**Electromagnetic Field**	**Power Density Meter**	**EIRP Meter**
Peak Range	Min: 0.001 V/m Max: 20.00 V/m	Min: 0.027 nW/cm² Max: 106.1 uW/cm²	Min: 0.001W Max: 5333 W @ 20 m.
Average Range	Min: 0.001 V/m Max: 20.00 V/m	Min: 2.65 nW/m² Max: 1.06 Watts/m²	
Memory Reference Range	Min: 0.01 V/m Max: 20.00 V/m	Min: 0.027 nW/cm² Max: 106.1 uW/cm²	
Current Reference Range	Min: 0.01 V/m Max: 20.00 V/m	Min: 0.027 nW/cm² Max: 106.1 uW/cm²	
Units	V/m, dBuV/m	W/cm²	Watts
EIRP Distance	Na	Na	0.25 – 20.0 m 0.82 – 65.60 ft
Frequency Bandwidth	1 MHz to 2.5 GHz		
Antenna Factor Range	-40.0 to 40.0 dBm⁻¹		
Hardware Setup	Brightness, Off-time, Antenna factor (AF)		
Frequency Response	10 MHz – 2.5 GHz		
Antenna Options	Local, or remote (CTC113 for regular use, or CTC115 for high temp use)		
Record Interval Range	1 – 360 seconds		
Record Average Range	0.1 – 360 seconds		

Figure 3.3 CTS001 directional antenna and electromagnetic field module specification [40]

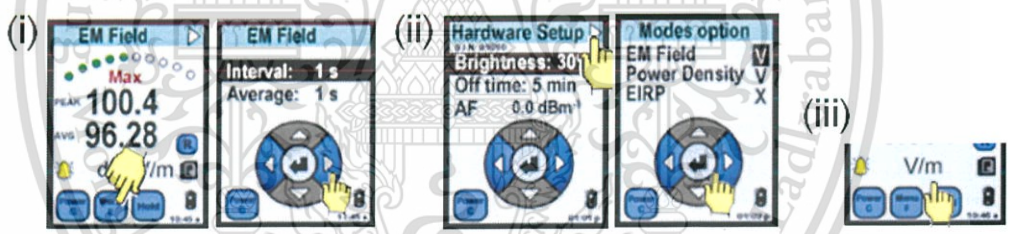

Figure 3.4. CTM048 setting up [40]

(i) Press 'Menu F button' and select 'INTERVAL' of '10' seconds. It is the sampling time for PEAK data to be recorded. Then set 'AVERAGE' at 10 seconds as well.

(ii) At the 'HARDWARE SETUP' menu, press the triangle 'MODE OPTION' button located at the upper right side of the display. Then 'enable' 'EM field' mode. "V" – enabled; "X" – disabled.

(iii) Press the 'UNITS' button toggles to 'V/m' unit.

Observe electric field from the sources which are wireless communication devices, typically used in business and factory environment, (1) Portable Two-way Radio Transceiver (walkie-talkie), (2) Wireless LAN Access Point (WiFi router), (3) GSM Cellular phone, (4) Cordless WiFi phone, (5) Laptop computer, (6) Tablet Computer and (7) Wireless mouse & Keyboard set.

Table 3.1. Sample of wireless communication devices to be studied

Wireless Devices	Working Frequency	Power at Transmit Mode	Brand / Model
(1) Portable Two-way Radio Transceiver (walkie-talkie)	245 MHz	1-5 W	icom / IC-3FGX
(2) Wireless LAN Access Point (WiFi router)	2400 MHz	0.78-200 mW	Cisco / Aironet 3500
(3) Cordless WiFi phone	2400 MHz	1-50 mW	Cisco / 7926G
(4) GSM Cellular phone	900, 1800, 2100 MHz	50-500 mW	Samsung / Galaxy Note2
			Apple / iPhone 5
(5) Laptop computer	2400 MHz	1-40 mW	Dell / Latitude 6430s
(6) Tablet Computer	2400 MHz	1-500 mW	Samsung / Galaxy Tab S
(7) Wireless mouse & Keyboard	2400 MHz	0.1-20 mW	Logitech / M185

Performed electric field measurement in empty large room, at distance of 1 inch (25.4 mm), 3 inches (76.2 mm), 6 inches (152.4 mm) and 12 inches (304.8 mm) between CTS001 antenna and transmitting wireless communication devices in X, Y, and Z direction and record 5 repeats measurement.

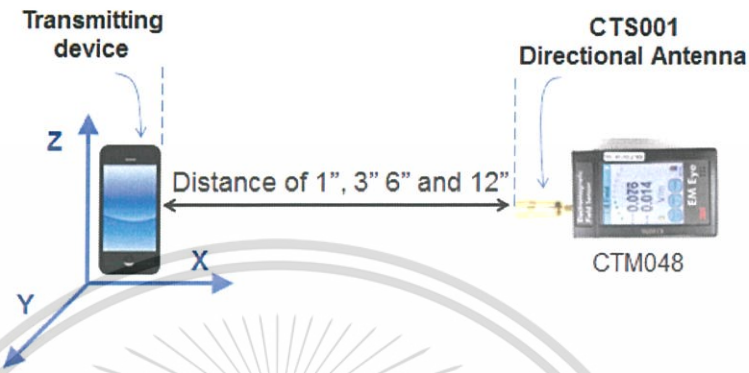

Figure 3.5. Observation of electric field from wireless communication device at different distance.

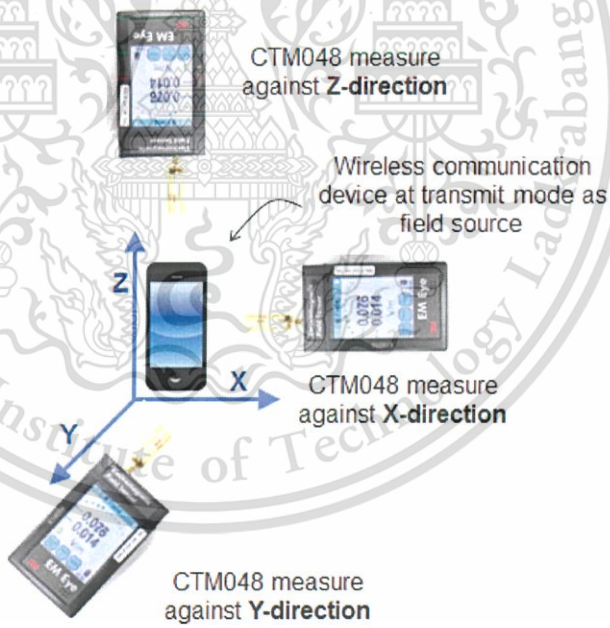

Figure 3.6. Observation of electric field from wireless communication device at different directions.

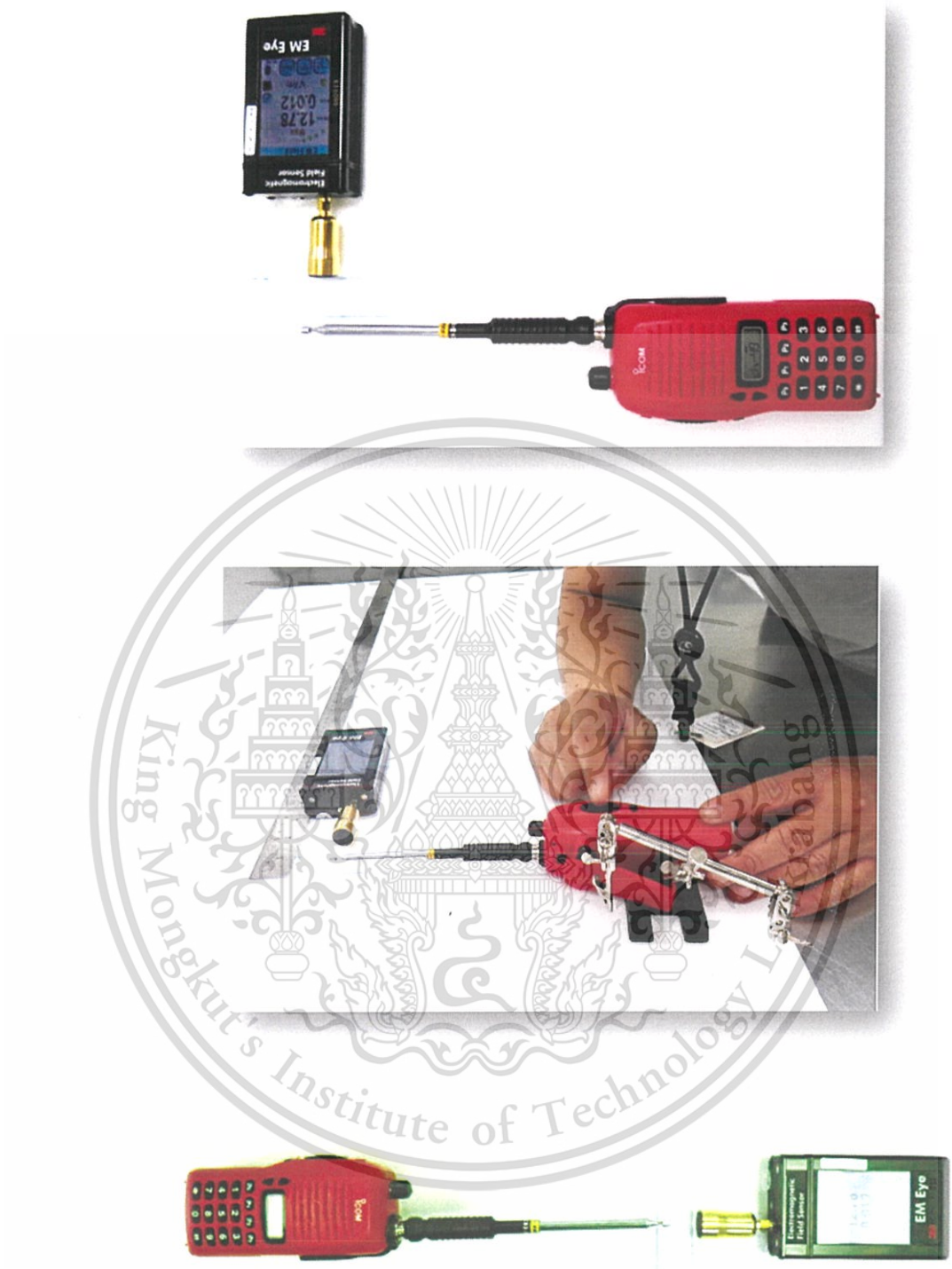

Figure 3.7. Example of experiment A setup. Walkie-talkie in X-Y-Z direction at distance of one inch.

Table 3.2 Example of 'wireless communication devices – electric field survey' record table based on DOE Multi-Level Factorial Design

DOE Multi-Level Factorial Design				Electric field (V/m)		
StdOrder	RunOrder	Direction	Distance (mm)	Source(1)	Source(X)	Source(N)
47	1	Z	152.4			
56	2	Y	304.8			
28	3	X	304.8			
30	4	Y	76.2			
45	5	Z	25.4			
39	6	X	152.4			
23	7	Z	152.4			
27	8	X	152.4			
9	9	Z	25.4			
12	10	Z	304.8			
20	11	Y	304.8			
18	12	Y	76.2			
59	13	Z	152.4			
42	14	Y	76.2			
36	15	Z	304.8			
53	16	Y	25.4			
52	17	X	304.8			
54	18	Y	76.2			
31	19	Y	152.4			
29	20	Y	25.4			
40	21	X	304.8			
49	22	X	25.4			
21	23	Z	25.4			
8	24	Y	304.8			
1	25	X	25.4			
34	26	Z	76.2			
41	27	Y	25.4			
3	28	X	152.4			
25	29	X	25.4			
43	30	Y	152.4			

Table 3.2 (Continued) Example of 'wireless communication devices – electric field survey' record table based on DOE Multi-Level Factorial Design

DOE Multi-Level Factorial Design				Electric field (V/m)		
StdOrder	RunOrder	Direction	Distance (mm)	Source(1)	Source(X)	Source(N)
19	31	Y	152.4			
7	32	Y	152.4			
26	33	X	76.2			
60	34	Z	304.8			
50	35	X	76.2			
37	36	X	25.4			
35	37	Z	152.4			
11	38	Z	152.4			
24	39	Z	304.8			
32	40	Y	304.8			
16	41	X	304.8			
51	42	X	25.4			
48	43	Z	304.8			
10	44	Z	76.2			
6	45	Y	76.2			
2	46	X	76.2			
13	47	X	152.4			
17	48	Y	25.4			
15	49	X	152.4			
5	50	Y	25.4			
57	51	Z	25.4			
22	52	Z	76.2			
44	53	Y	304.8			
14	54	X	76.2			
38	55	X	76.2			
46	56	Z	76.2			
58	57	Z	76.2			
55	58	Y	152.4			
33	59	Z	25.4			
4	60	X	304.8			

B. Thermal change and DC voltage of TGMR head while placing in the field of wireless communication device

The purpose of this experiment is to know actual thermal change and DC voltage of TGMR head while placing in the field of wireless communication device to compare with TGMR failure threshold. Prediction model from regression analysis could tell the controlled distance of specific wireless communication device to be installed in the controlled environment such as in Head Gimbal Assembly process.

Measuring equipment:

- Agilent 34410A 6 ½ Digit Multimeter with shielded-cables
- Modified Gryphic probe to match with HGA leads to be probed

Other tools/equipment:

- Fixture to hold HGA
- Current divider TGMR Protection Circuit Box
- Dissipative Tweezes to pick up HGA
- Wrist straps and ground cords for persons who handle HGA
- Design Of Experiment (DOE) table of Multi Level Factorial Design

Field sources:

- Walkie-talkie
- WiFi router
- Cellular phone
- Tablet computer
- WiFi phone

Sample:

HGAs with build-in DETCR. Good HGAs, passed electrical test, random from normal HGA processes total 150 HGAs. Measure 25 repeats per sources per distance.

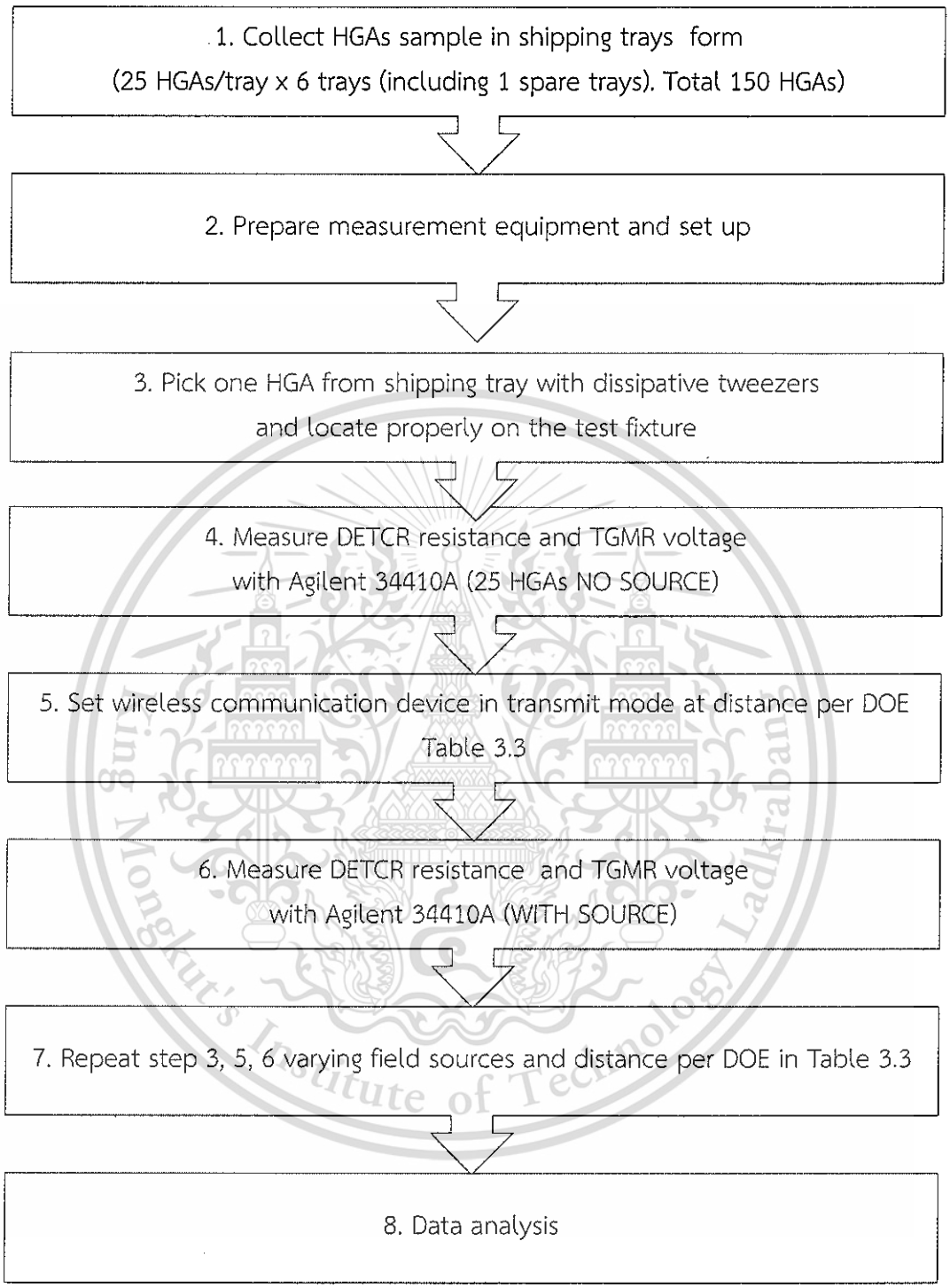

Figure 3.8 Experiment B steps diagram

Detail of Experiment:

From the results of experiment A, significant electric field sources, distance and directions had been selected to be electric field source of this experiment. HGA is placed at distance of 1 inch, 6 inches and 12 inches from the electric field source.

Build-in Differential-Ended Temperature Coefficient of Resistivity (DETCR) sensor [9] [10] has been used to observe actual thermal change at TGMR head. In this experiment, the build-in DETCR sensor was located inside the slider body, approximately 1 micron ($1x10^{-6}$ m) from TGMR reader.

Agilent 34410A 6 ½ Digit Multimeter with shielded-cables and Gryphic probe was modified to measure DETCR resistance and DC voltage of TGMR while placing TGMR head in the field of wireless communication devices.

The response to local changes in temperature at the DETCR sensor is based on equations (3.1) and (3.2). The change of DETCR resistance ($\Delta R_{DETCR} = R_{DETCR} - R_{0\_DETCR}$) is proportional to the change of DETCR temperature ($\Delta T_{DETCR} = T_{DETCR} - T_{0\_DETCR}$) while R_{0_DETCR} is original resistance of the DETCR, R_{DETCR} is resistance of the DETCR at the point of time to compare, T_{0_DETCR} is original temperature of the DETCR, T_{DETCR} is temperature of the DETCR at the point of time to compare, and α is specific to DETCR material.

$$\Delta R_{DETCR} = \alpha \ \Delta T_{DETCR} \tag{3.1}$$

$$R_{DETCR} - R_{0\_DETCR} = \alpha * (T_{DETCR} - T_{0\_DETCR}) \tag{3.2}$$

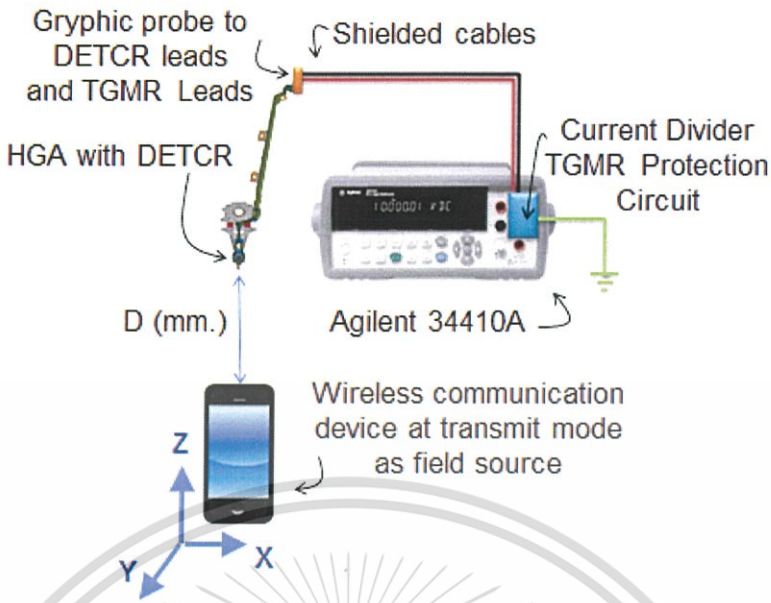

Figure 3.9 Measurement setup on thermal change and DC voltage of TGMR head while placing in the field issued from wireless communication device

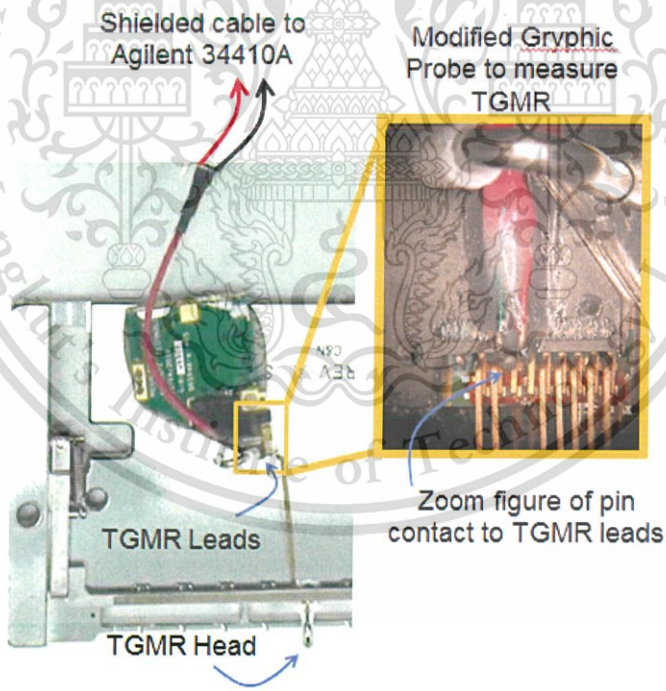

Figure 3.10 Example of modified Gryphic probe from electrical tester to measure TGMR

Measurement precaution

1. Only open one HGA tray under simulation or testing. Always keeps other waiting HGAs in closed trays. Follow ESD handling protocol and packaging plan while handling and transfer HGAs in this experiment.

2. Measurement loading errors occur when the resistance of the device–under–test (DUT) is an appreciable percentage of the meter's own input resistance. The diagram below shows this error source. Set the meter's input resistance to >10 GΩ (the HI–Z setting) for the 100 mVdc, 1 Vdc, and 10 Vdc ranges reduce the effects of loading errors, and to minimize noise pickup.

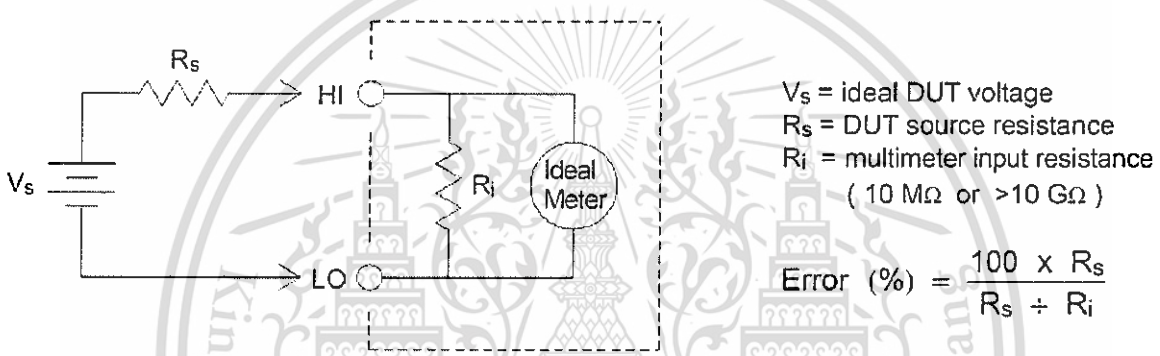

Figure 3.11 Diagram of measurement loading error source [41]

3. To prevent DETCR and TGMR from electrical over stress during the measurement, custom made current divider TGMR protection circuit been connected to Agilent 34410A meter to reduce electrical overstress on DETCR and TGMR.

DC Characteristics

Accuracy Specifications ±(% of reading + % of range) [1]

Function	Range [3]	Test Current or Burden Voltage	24 Hour [2] T_{CAL} ± 1 °C	90 Day T_{CAL} ± 5 °C	1 Year T_{CAL} ± 5 °C	Temperature Coefficient/°C 0 °C to (T_{CAL} – 5 °C) (T_{CAL} + 5 °C) to 55 °C
DC	100.0000 mV		0.0030+0.0030	0.0040+0.0035	0.0050+0.0035	0.0005+0.0005
	1.000000 V		0.0020+0.0006	0.0030+0.0007	0.0035+0.0007	0.0005+0.0001
	10.00000 V		0.0015+0.0004	0.0020+0.0005	0.0030+0.0005	0.0005+0.0001
	100.0000 V		0.0020+0.0006	0.0035+0.0006	0.0040+0.0006	0.0005+0.0001
	1000.000 V [5]		0.0020+0.0006	0.0035+0.0006	0.0040+0.0006	0.0005+0.0001
Resistance [4]	100.0000 Ω	1 mA Current Source	0.0030+0.0030	0.008+0.004	0.010+0.004	0.0006+0.0005
	1.000000 KΩ	1 mA	0.0020+0.0005	0.007+0.001	0.010+0.001	0.0006+0.0001
	10.00000 KΩ	100 µA	0.0020+0.0005	0.007+0.001	0.010+0.001	0.0006+0.0001
	100.0000 KΩ	10 µA	0.0020+0.0005	0.007+0.001	0.010+0.001	0.0006+0.0001
	1.000000 MΩ	5.0 µA	0.0020+0.0010	0.010+0.001	0.012+0.001	0.0010+0.0002
	10.00000 MΩ	500 nA	0.0100+0.0010	0.030+0.001	0.040+0.001	0.0030+0.0004
	100.0000 MΩ	500 nA || 10 MΩ	0.200+0.001	0.600+0.001	0.800+0.001	0.1000+0.0001
	1.000000 GΩ	500 nA || 10 MΩ	2.000+0.001	6.000+0.001	8.000+0.001	1.0000+0.0001

[1] Specifications are for 90 minute warm–up and integration setting of 100 NPLC.
For <100 NPLC, add the appropriate "RMS Noise Adder" from the table on the following page.
[2] Relative to calibration standards.
[3] 20% overrange on all ranges, except 1000 VDC, 3 A range.
[4] Specifications are for 4–wire ohms function, or 2–wire ohms using Math Null. Without Math Null, add 0.2 Ω additional error in 2–wire ohms function.

Figure 3.12 Agilent 34410A Specification: DC Characteristics [41]

Figure 3.13 Connecting of Agilent 34410A with current divider TGMR protection circuit to prevent TGMR damage during measurement

Table 3.3 Example of DOE record sheet of 'DETCR resistance (°C) and TGMR DC Volts (μV)

StdOrder	RunOrder	Source	Distance (mm)	DETCR Temp (C)	TGMR DC (μV)
30	1	WiFiPhone	304.8		
364	2	WiFiRouter	25.4		
371	3	Tablet	152.4		
76	4	WalkieTalkie	25.4		
283	5	WiFiPhone	25.4		
323	6	CellPhone	152.4		
292	7	CellPhone	25.4		
230	8	WiFiRouter	152.4		
146	9	Tablet	152.4		
10	10	Tablet	25.4		
252	11	Tablet	304.8		
19	12	WiFiRouter	25.4		
199	13	WiFiRouter	25.4		
148	14	WiFiPhone	25.4		
316	15	WalkieTalkie	25.4		
46	16	WalkieTalkie	25.4		
98	17	CellPhone	152.4		
337	18	CellPhone	25.4		
189	19	CellPhone	304.8		
299	20	WiFiPhone	152.4		
324	21	CellPhone	304.8		
214	22	WiFiRouter	25.4		
365	23	WiFiRouter	152.4		
370	24	Tablet	25.4		
343	25	WiFiPhone	25.4		
207	26	Tablet	304.8		
226	27	WalkieTalkie	25.4		
243	28	WalkieTalkie	304.8		
366	29	WiFiRouter	304.8		
284	30	WiFiPhone	152.4		
...	...	....	...		
113	375	CellPhone	152.4		

C. Electrical Performance of TGMR pre and post actions simulating HGA assembly process

Purpose of this experiment is to see agreement from previous experiment to the actual result of electrical performance of TGMR. If thermal change or DC voltage of TGMR head while placing in the field of wireless communication device is lower than with TGMR failure threshold, the electrical performance of TGMR on HGA process should not have negative change and vice versa.

Measuring equipment:

- CTM048 EM Field Meter with CTS001 directional antenna and electromagnetic field module.
- QST2002 Quasi-Static Tester with HGA probing fixture

Other tools/equipment:

- HGA automation trays (22 sets)
- Grounded metal, Grounded non-metal, Pick & Place module
- Wrist straps and ground cords for persons who handle HGA

Field sources:

- Walkie-talkie
- WiFi router
- Cellular phone
- Tabliet computer
- WiFi phone

Sample:

Good HGAs, passed electrical test, random from normal HGA processes total 220 HGAs. Prepare sample in automation trays, 10 HGAs per tray on the mark position 1-10.

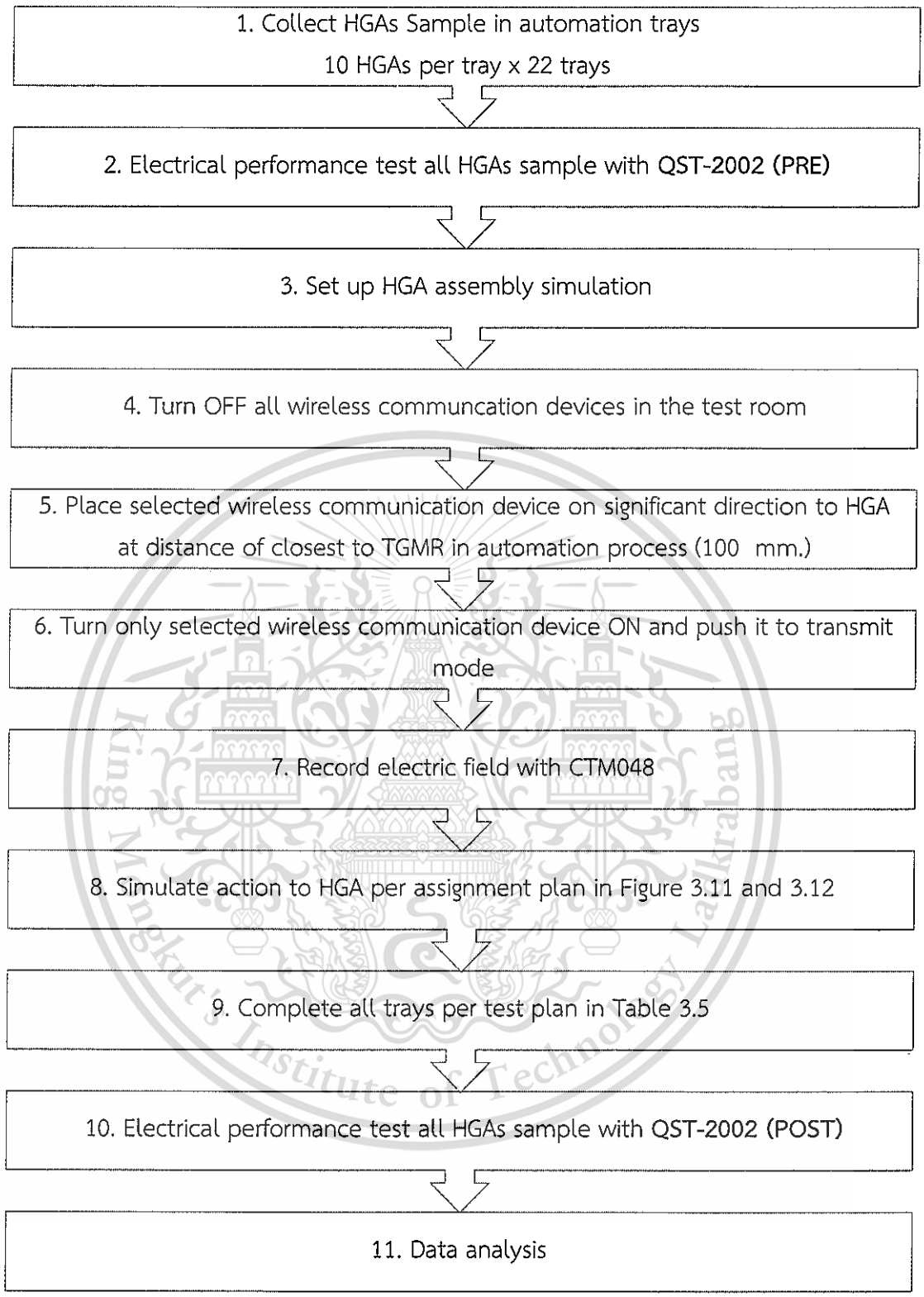

Figure 3.14 Experiment C steps diagram

Detail of experiment:

Wireless communication devices, which are in top five of electric field from experiment A, have been chosen to be field sources in this experiment. HGAs are placed in the field generated from each wireless communication device at significant direction from previous experiment. From experiment B, calculated distance to the TGMR failure threshold is too short to be set up in HGA automation process. So the closest distance set in this experiment is 100 mm far between HGA and field source. And the other distance is at 600 mm, which is typical rule limit that wireless communication devices are allowed to come close to TGMR in the HGA automation process. Set up and assignment of actions are illustrated in **Figure 3.15 and 3.16**.

Measurement precaution:

Only open one HGA tray under simulation or testing. Always keeps other waiting HGAs in closed trays. Follow ESD handling protocol and packaging plan while handling and transfer HGAs in this experiment.

Four actions of HGA process have been simulated during the HGAs are in electric field of wireless communication device as shown in **Figure 3.15**. There are,

(I) No contact to HGA at all

(II) Grounded-Metal: 10 times contact to open traces of TGMR

(III) Grounded-Non-Metal: 10 times contact to open traces of TGMR

(IV) 10 times pick-and-place on base plate with Non-Metal End-Effector

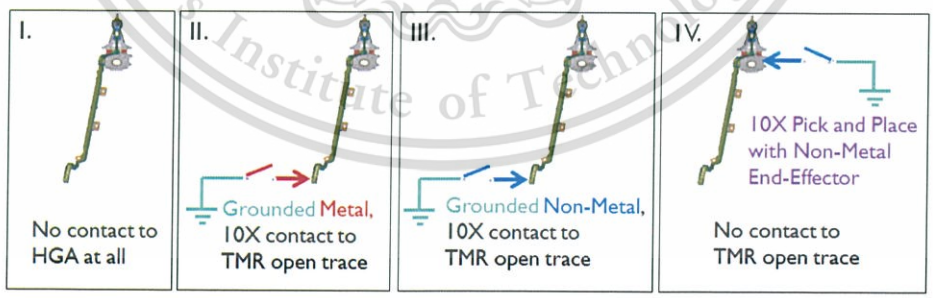

Figure 3.15 Four simulation actions representing HGA process

Table 3.4 Test plan for 'Simulating HGA assembly processes during the HGAs are in electric-field of wireless communication device'

Tray	Field Source	Direction	Experiment C. Distance	Sample quantity of HGA for each action				Total HGA sample
				Action (I)	Action (II)	Action (III)	Action (IV)	
2	No source	none	none	1+1	3+3	3+3	3+3	20
2	Walkie-Talkie	[X]	100 mm	1+1	3+3	3+3	3+3	20
2			600 mm	1+1	3+3	3+3	3+3	20
2	WiFi router	[Y]	100 mm	1+1	3+3	3+3	3+3	20
2			600 mm	1+1	3+3	3+3	3+3	20
2	Cellular phone	[X]	100 mm	1+1	3+3	3+3	3+3	20
2			600 mm	1+1	3+3	3+3	3+3	20
2	Tablet Computer	[Z]	100 mm	1+1	3+3	3+3	3+3	20
2			600 mm	1+1	3+3	3+3	3+3	20
2	WiFi phone	[Z]	100 mm	1+1	3+3	3+3	3+3	20
2			600 mm	1+1	3+3	3+3	3+3	20

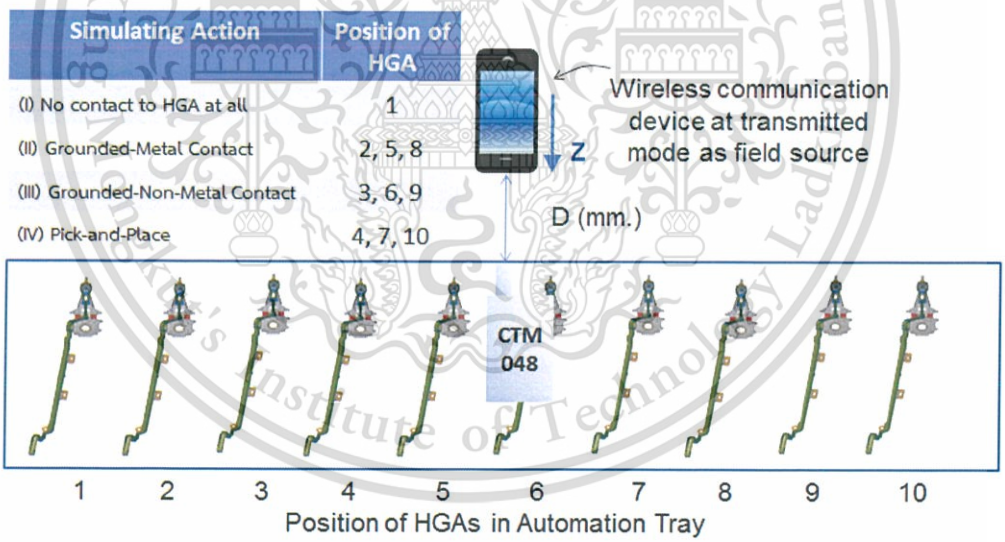

Figure 3.16 Setup and assignment of simulating actions for HGAs in automation tray.

Electrical performance of HGAs has been tested before and after the actions simulating HGA process, with Quasi-Static Tester QST-2002, to see how the

experiment impacts to electrical performance of HGAs. Both catastrophic failure parameters (TGMR resistance, amplitude, slope) and instability parameters (asymmetry, Barkhausen jump, hysteresis loop, and Spectral Maximum Amplitude Noise/ S.M.A.N.) were observed and compared with total sample size of 220 HGAs.

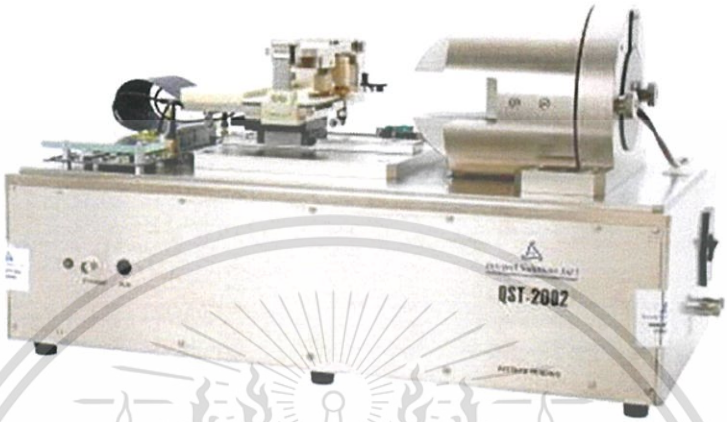

Figure 3.17 QST-2002 Quasi-Static Tester

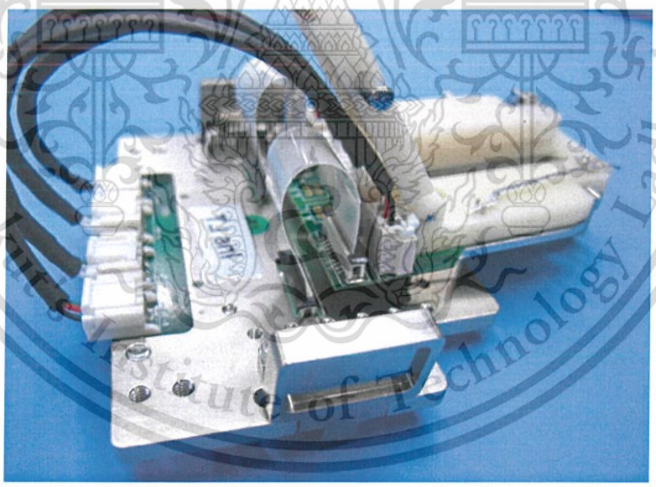

Figure 3.18 QST-2002 fixture and probing for HGA

Quasi-Static test parameters in this experiment

- TGMR resistance (ohms)
- TGMR amplitude (μV)
- Slope (μV/Oe)
- Asymmetry (%)
- Barkhausen jump (%)
- Hysteresis loop (%)
- Spectral Maximum Amplitude Noise/ S.M.A.N.) (μV)

V-bias mode: Read Bias 140 mV , starts current at 0.1 mA, Maximum 3 mA.

Transverse: field sweep +/- 700 Oe in 2 Oe increments [Oe pk-pk]

SMAN Test: +/- 700 Oe field sweep, 50 Oe increments. 10 μs read window, 25 cycles, frequency 235 MHz, 80 MHz filter.

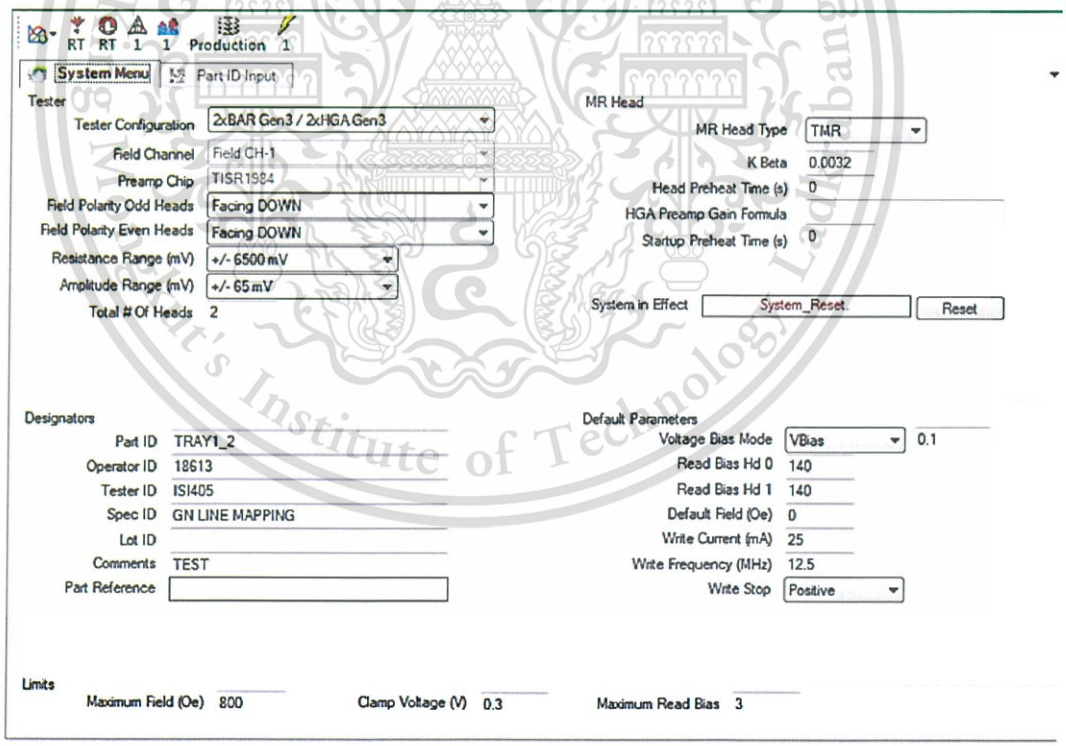

Figure 3.19 QST V-bias setting

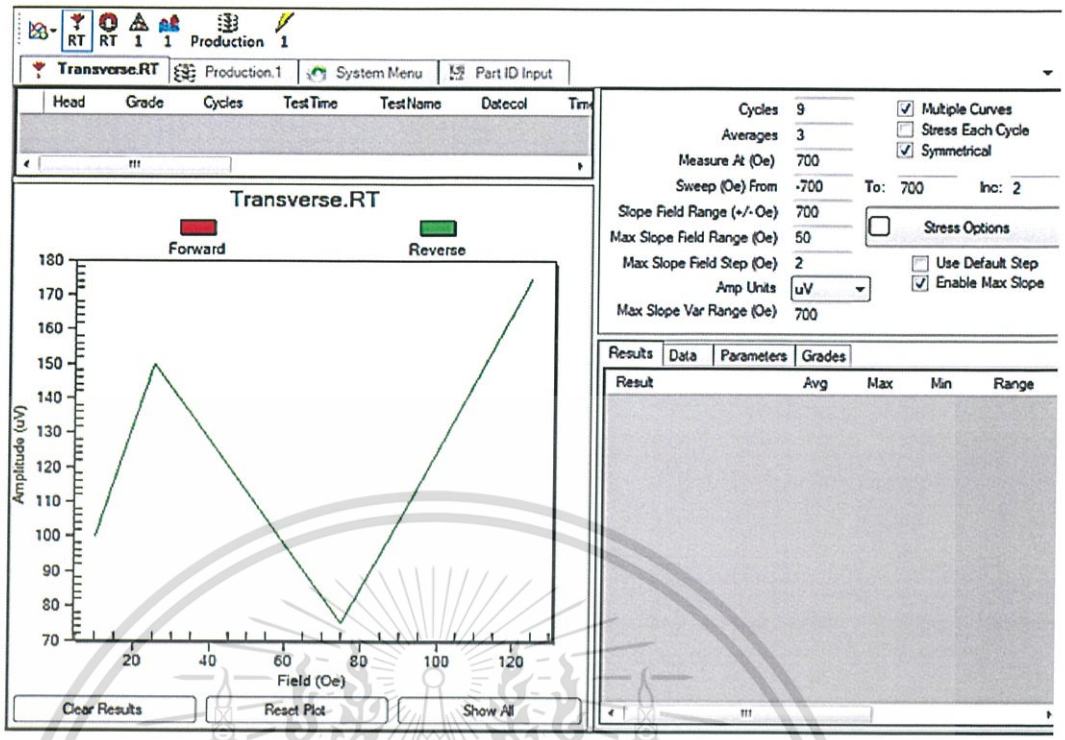

Figure 3.20 QST transverse test setting

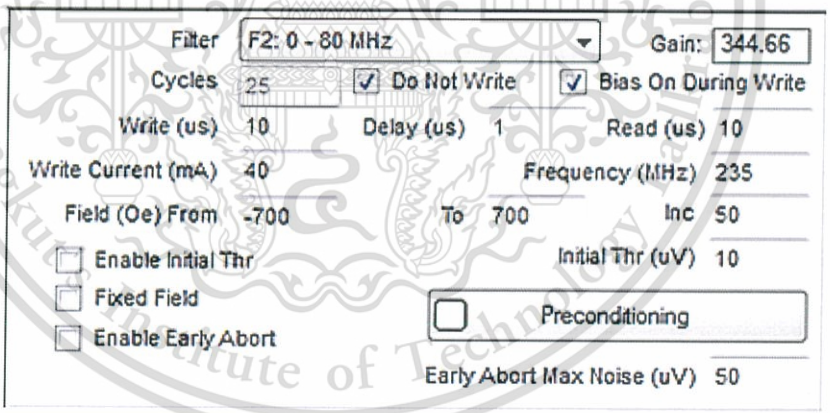

Figure 3.21 QST S.M.A.N. test setting

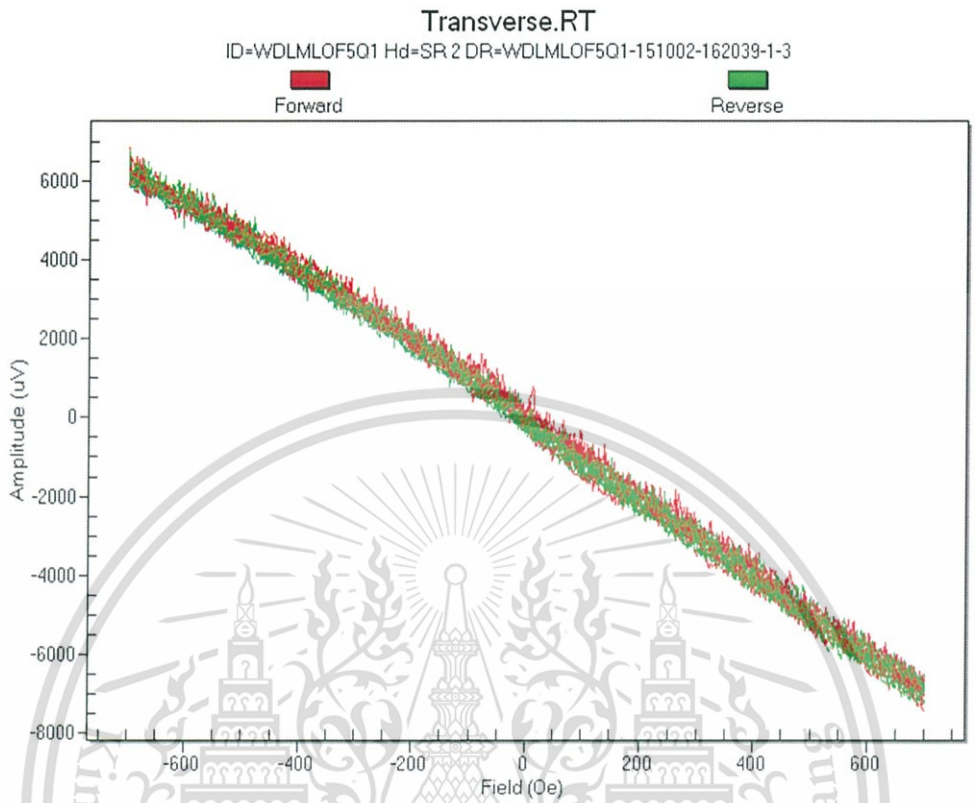

Figure 3.22 Example of QST-2002 Transfer Curve to be recorded PRE & POST simulating HGA process action

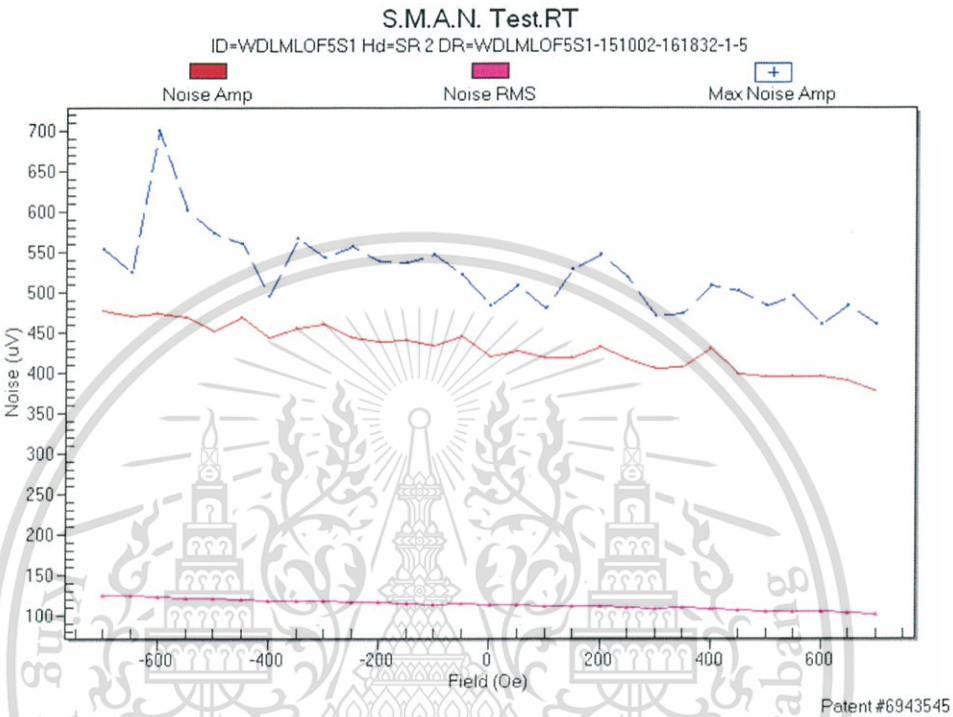

Figure 3.23 Example of QST-2002 S.M.A.N graph to be recorded PRE & POST simulating HGA process action

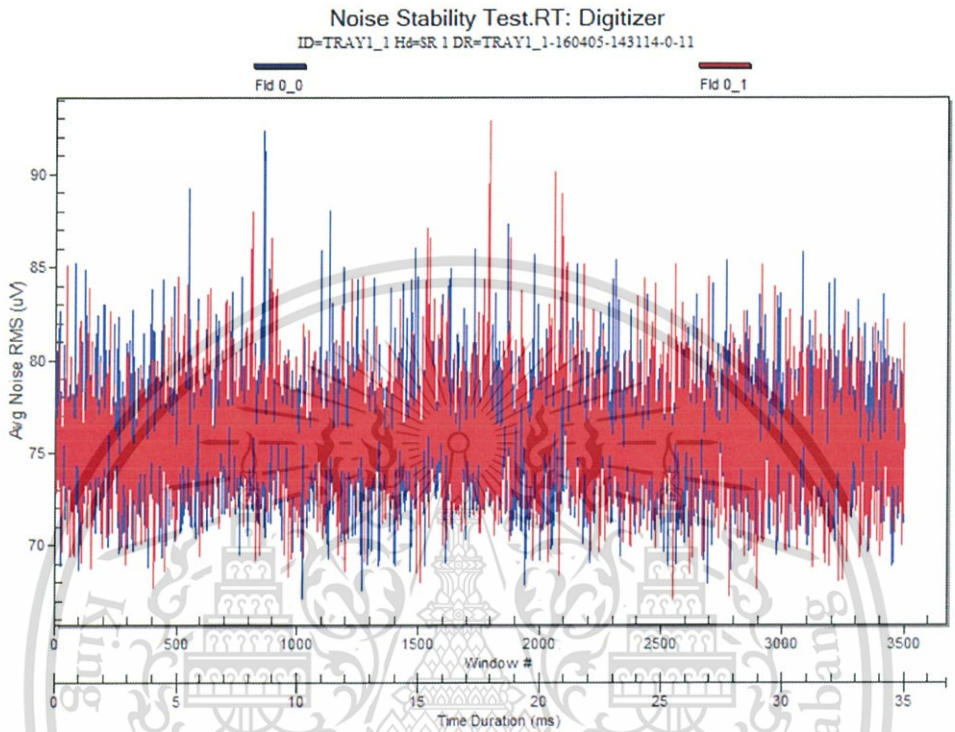

Figure 3.24. Example of QST-2002 Noise Instability graph to be recorded PRE & POST simulating HGA process action

CHAPTER 4

EXPERIMENTAL RESULT AND DISCUSSION

In this chapter, detailed result and discussion from methodology in chapter 3, is elaborated. There are three main experiments,

A. *Wireless communication devices – electric field survey*, how direction placing wireless communication device and distance impact to electric field magnitude had been observed. Result of significant type of electric field sources, direction and distance from this experiment were used for the setup in the rest of experiments.

B. *Thermal change and DC voltage of TGMR head while placing in the field of wireless communication device*, actual thermal change and DC voltage of TGMR head while placing in the field of wireless communication device had been observed and compared with TGMR failure threshold. From this experiment, we can get prediction model and preliminary result of possibility of wireless communication device to damage or not damage TGMR head in HGA process.

C. *Electrical performance of TGMR pre and post actions simulating HGA assembly process.* Result of thermal change and DC voltage of TGMR head while placing in the field of wireless communication devices against TGMR failure threshold from previous experiment, had been confirmed by the actual electrical performance of TGMR whether they are in the same way.

A. Result of wireless communication devices – electric field survey

Figure 4.1 illustrates overall result of electric field survey from experiment A. Distance and direction between field sources and target play important role. Obviously, the shorter distance reflects higher electric field from the strong field sources such as walkie-talkie, WiFi router, cell phone, tablet, WiFi phone.

The Bubble plot in Figure 4.1 also compares different types of wireless communication as electric field sources, power range of the devices can inform tendency of the electric field they generate while transmitting. Ranking of the electric field strength is from walkie-talkie, WiFi router, cell phone 1, tablet, WiFi phone, cell phone 2, laptop, wireless mouse and wireless keyboard, used in the experiment, respectively. We do not have sample of electric field sources which have different frequencies but same transmitting power in this experiment. So the conclusion about relationship between frequency of the wireless communication device and electric field could not be drawn.

Electric field interval plot, main effect plot, interaction plot and analysis of variance from individual sources inform that distance is more significant to the electric field strength than direction. Anyway, it can tell the most influence direction of some wireless communication devices and the directional antenna as shown in Figure 4.2.1-4.2.7.2. Here is the legend of the graphs, Distance 1 = 25.4 mm, Distance 2 = 76.2 mm, Distance 3 = 152.4 mm, Distance 4 = 304.8 mm, Direction 1 = X, Direction 2 = Y, Direction 3 = Z. Direction X is the most influence direction of walkie-talkie and cell phone 1. Direction Y is the most influence direction of WiFi router. Direction Z is the most influence direction of the tablet and WiFi phone. There is no sign of influence direction of electric field from laptop computer, wireless mouse and wireless keyboard since the magnitude of their electric filed strength is about the same as background baseline.

In Figure 4.2.1-4.2.7.2, the analysis of variance is based on null hypothesis for direction H_0: $\mu_x = \mu_y = \mu_z$, distance H_0: $\mu_1 = \mu_2 = \mu_3 = \mu_4$, and interaction H_0: *No interaction*. The risks involved in these hypothesis tests are type I Error, rejecting the null hypothesis when it is true. Probability of this error equals α (by convention).

The critical value, α, is the level of significant in hypothesis testing. It is the threshold tolerable error probability. In this experiment, H_0 is rejected at P-Value less than α, which is 0.05.

Analysis of variance in Figure 4.2.1 for walkie-talkie results the P-Value of 0.487 for direction, 0.000 for distance and 0.428 for direction interact to distance. It means, only distance is significant to the electric field strength from walkie-talkie. Direction and interaction are not significant. Analysis of variance from Figure 4.2.6 and 4.2.7.2 for tablet and wireless keyboard can be interpreted in the same way.

Analysis of variance in Figure 4.2.2, 4.2.3 and 4.2.4.1 for WiFi router, WiFi phone, and cell phone 1 result the P-Value of 0.000 for direction, 0.000 for distance and 0.000 for direction interact to distance. It means, distance, direction and their interaction are significant to the electric field strength from WiFi router, WiFi phone, and cell phone 1. Analysis of variance in Figure 4.2.7.1 can be interpreted in the same way.

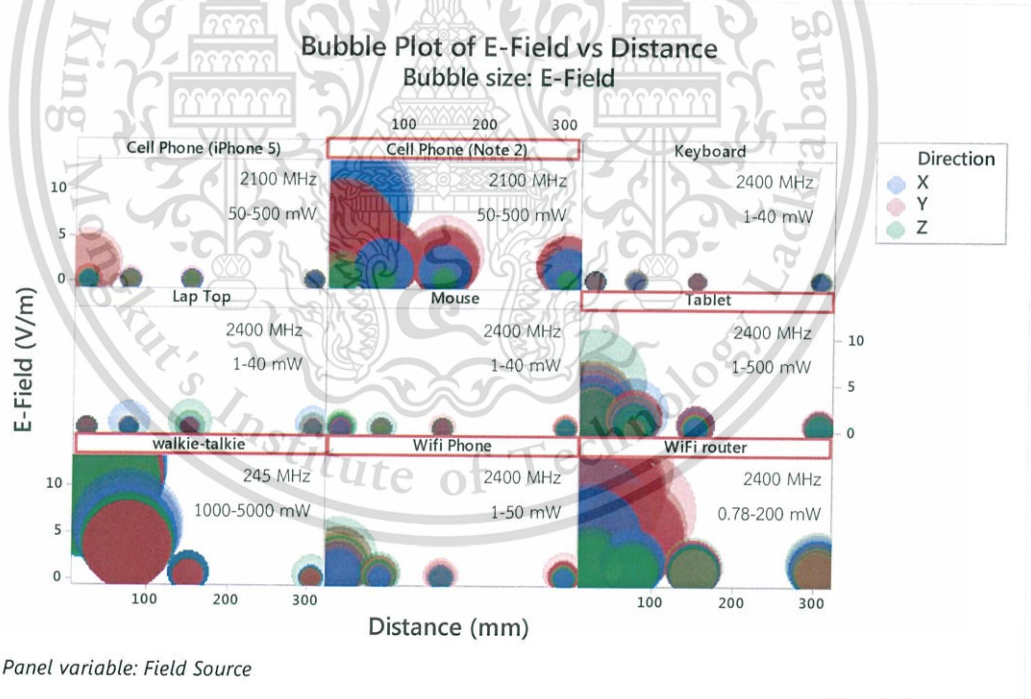

Figure 4.1 Overall result of electric field survey from experiment A: distance and direction between field sources and target playing important role.

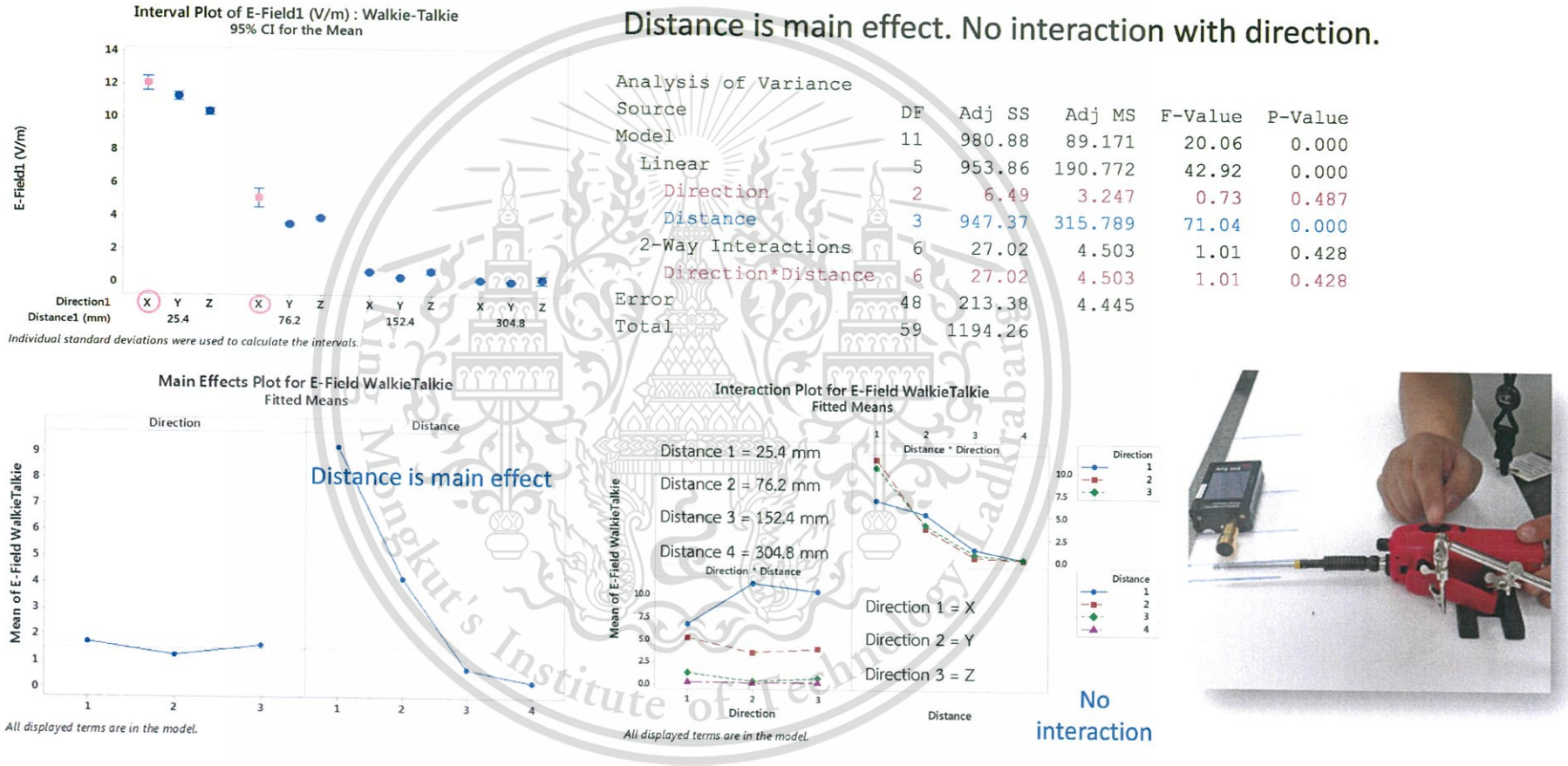

Figure 4.2.1 Electric field interval plot, main effect plot and interaction plot from experiment A - Walkie-talkie

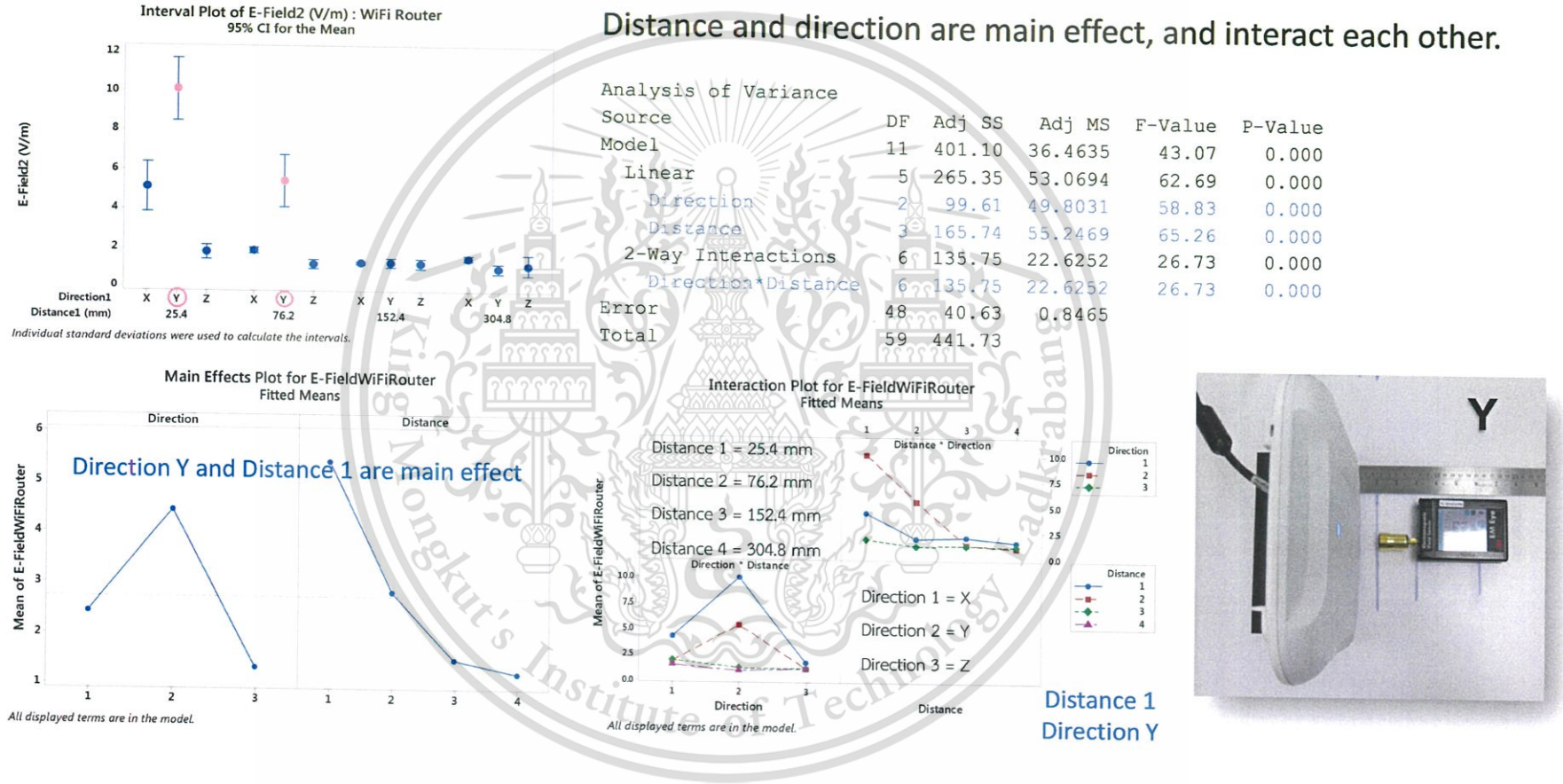

Figure 4.2.2 Electric field interval plot, main effect plot and interaction plot from experiment A – WiFi router

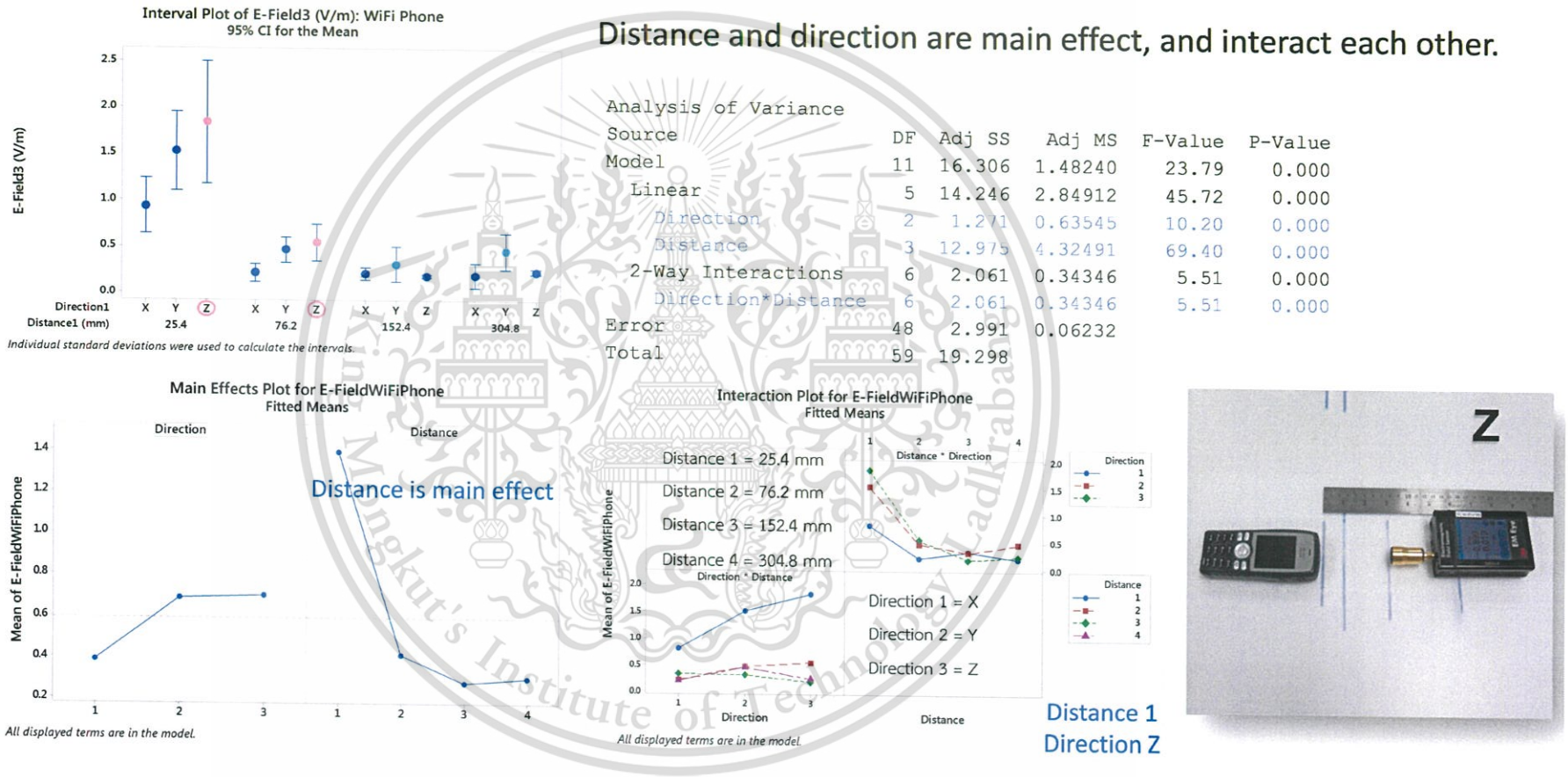

Figure 4.2.3 Electric field interval plot, main effect plot and interaction plot from experiment A – WiFi phone

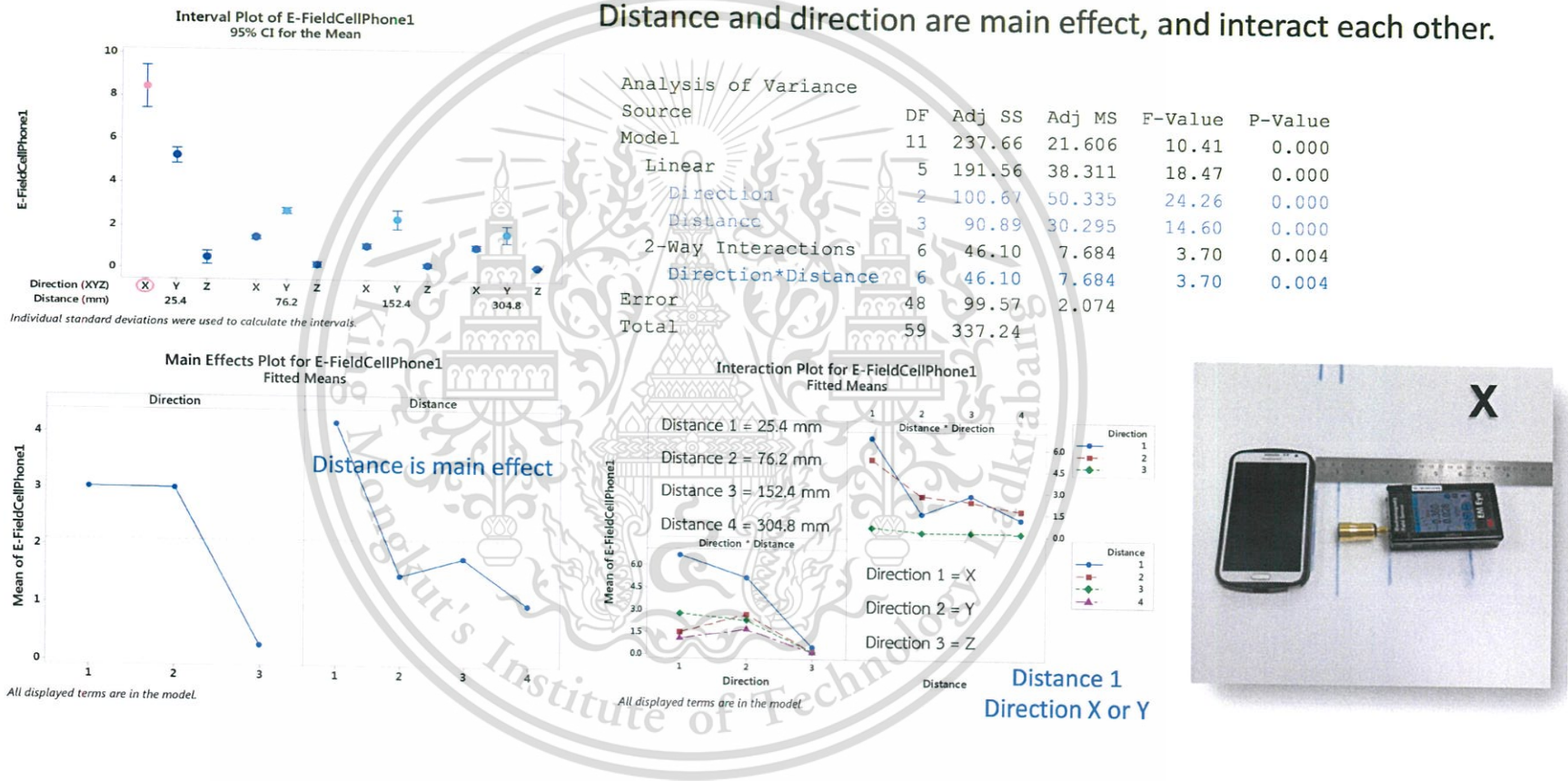

Figure 4.2.4.1 Electric field interval plot, main effect plot and interaction plot from experiment A – Cell phone1

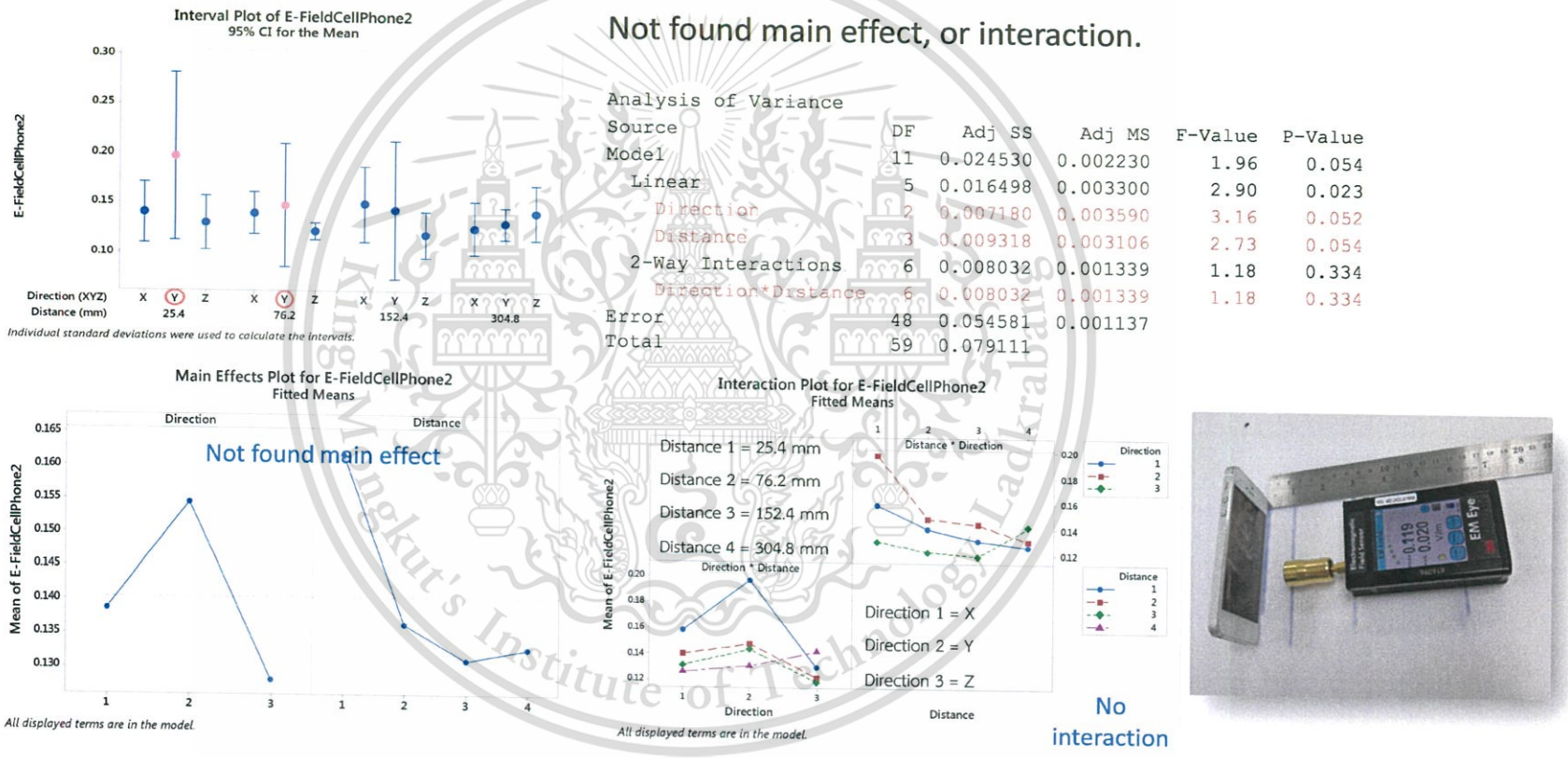

Figure 4.2.4.2 Electric field interval plot, main effect plot and interaction plot from experiment A – Cell phone2

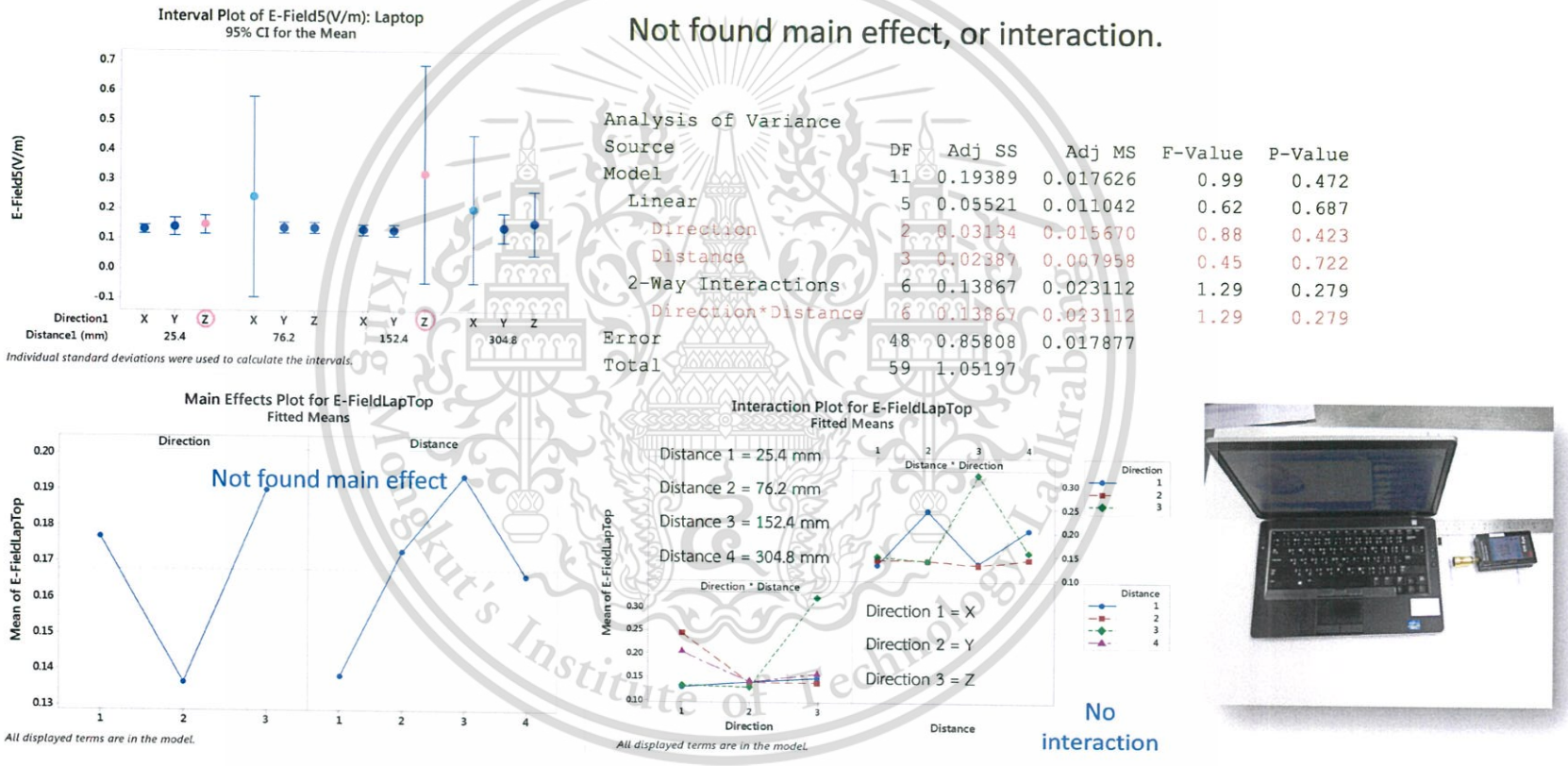

Figure 4.2.5 Electric field interval plot, main effect plot and interaction plot from experiment A - Laptop

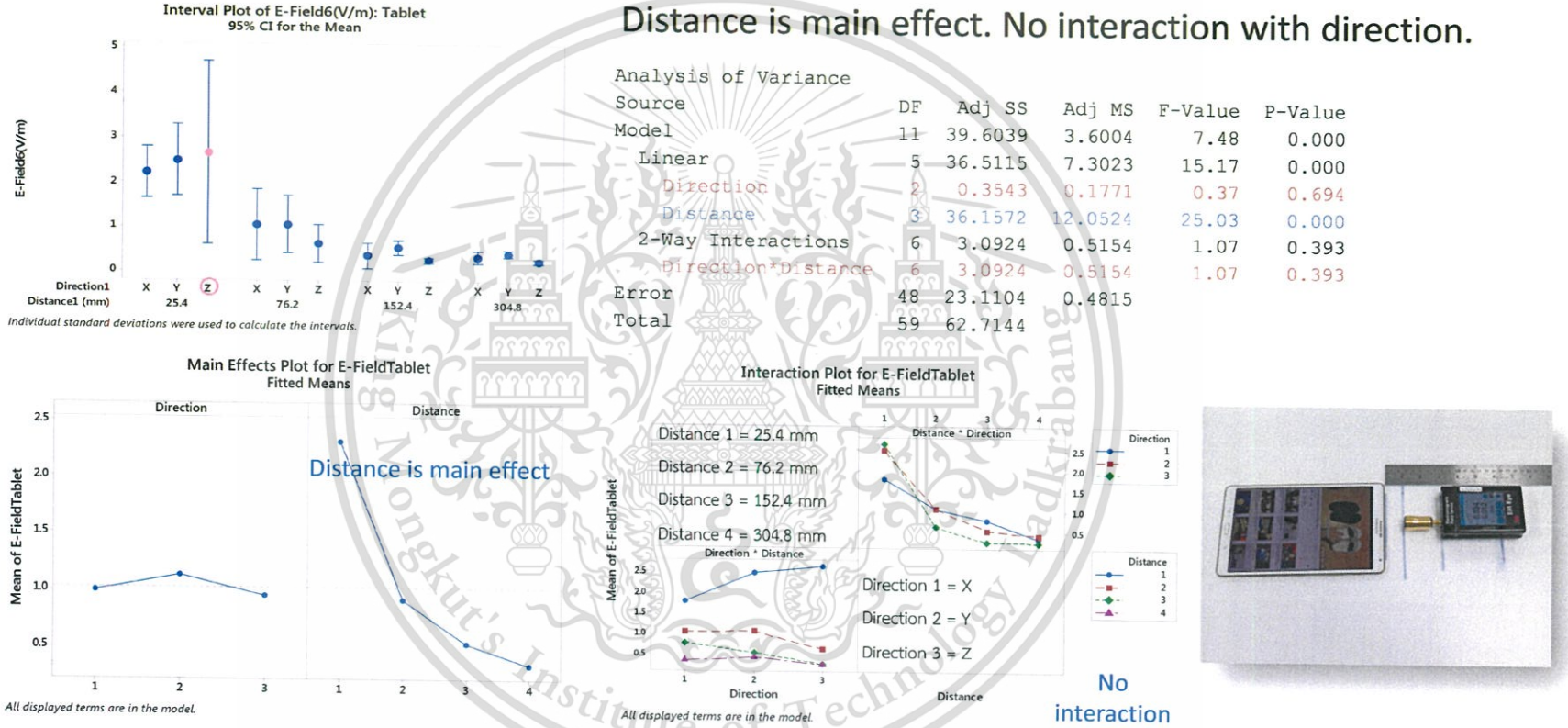

Figure 4.2.6 Electric field interval plot, main effect plot and interaction plot from experiment A – Tablet

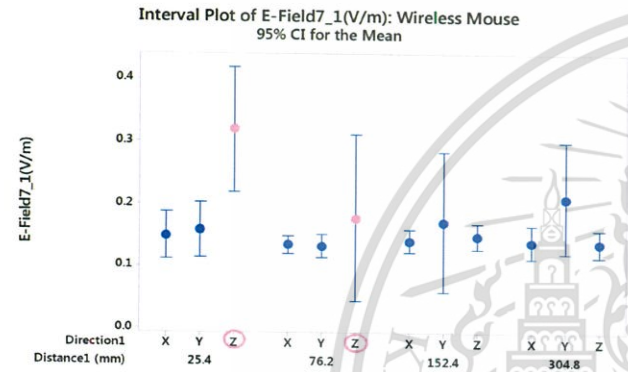

Distance and direction are main effect, and interact each other.

Analysis of Variance

Source	DF	Adj SS	Adj MS	F-Value	P-Value
Model	11	0.15200	0.013818	4.74	0.000
Linear	5	0.05715	0.011429	3.92	0.005
Direction	2	0.02949	0.014743	5.06	0.010
Distance	3	0.02766	0.009220	3.17	0.033
2-Way Interactions	6	0.09485	0.015809	5.43	0.000
Direction*Distance	6	0.09485	0.015809	5.43	0.000
Error	48	0.13981	0.002913		
Total	59	0.29181			

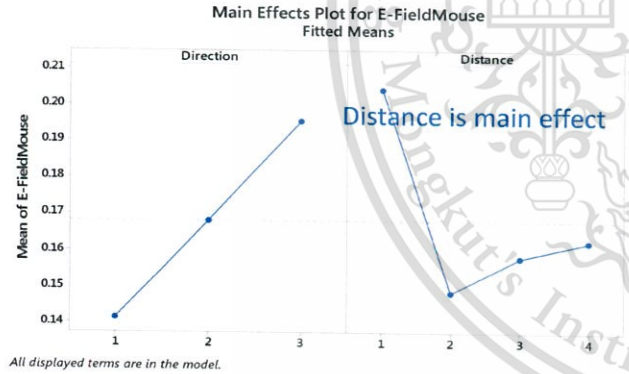

Distance is main effect

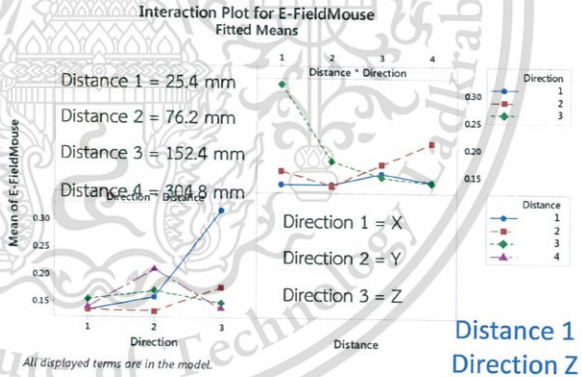

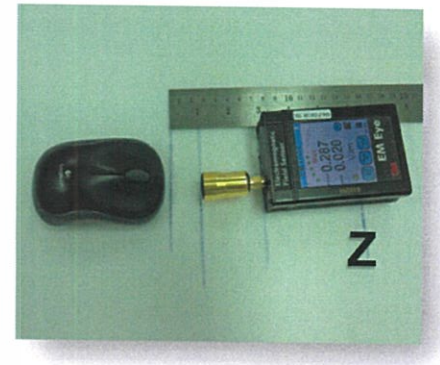

Distance 1
Direction Z

Figure 4.2.7.1 Electric field interval plot, main effect plot and interaction plot from experiment A – Wireless mouse

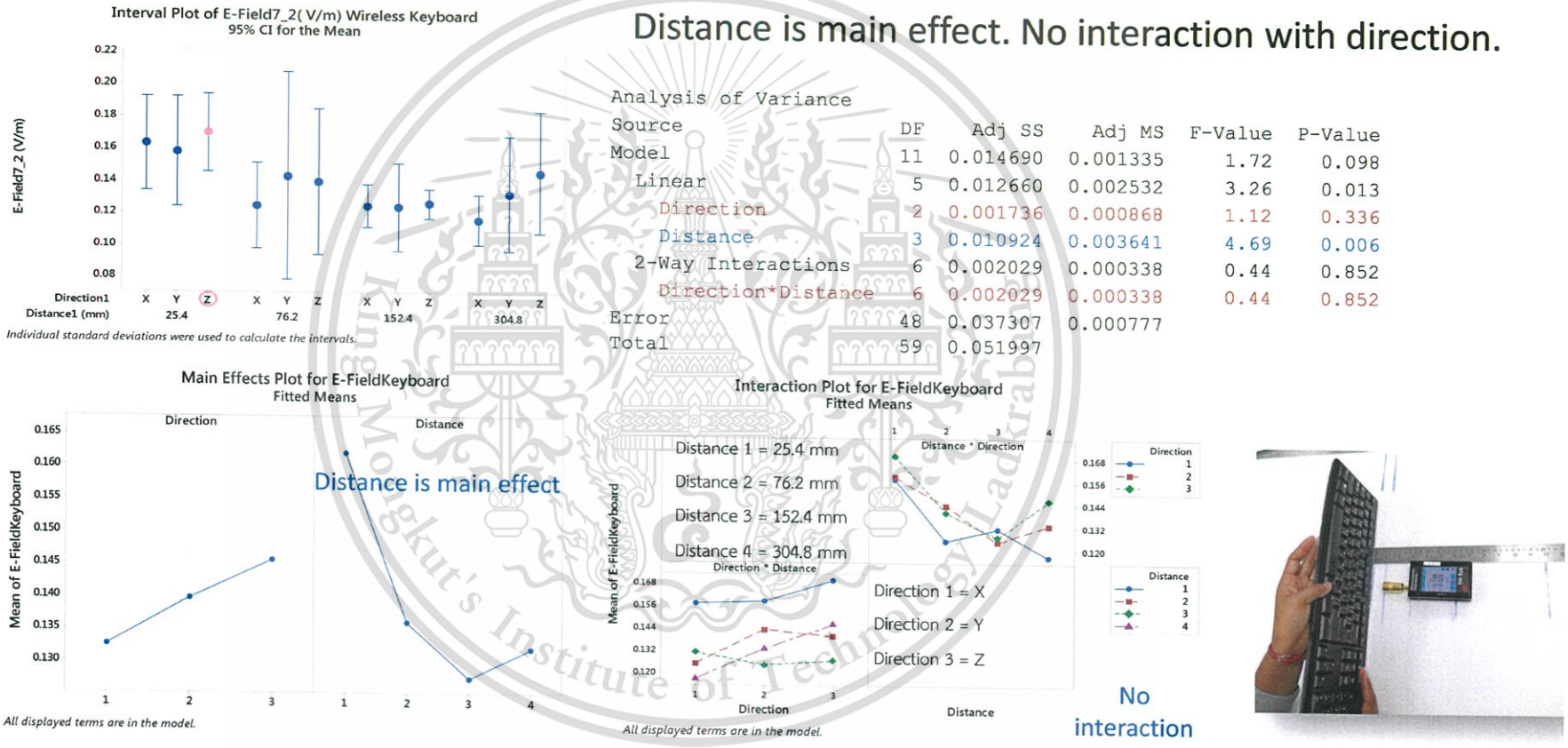

Figure 4.2.7.2 Electric field interval plot, main effect plot and interaction plot from experiment A – Wireless keyboard

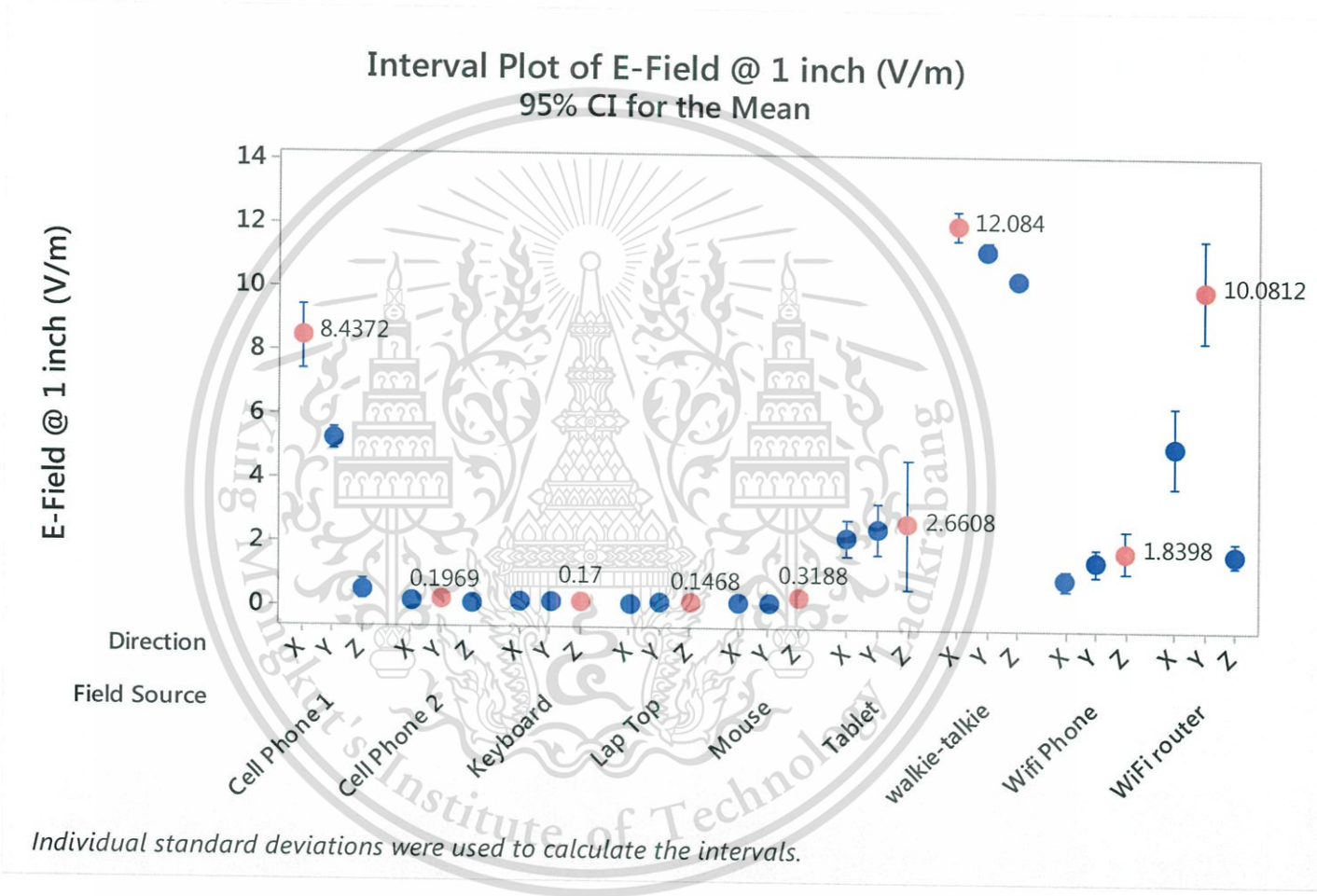

Figure 4.3 Electric field of wireless communication devices at 1 inch distance

Table 4.1 Regression analysis: Electric field (V/m) VS distance (mm), direction (X, Y, Z). Categorical predictor coding (1, 0), Box-Cox transformation $\lambda = 0$. Blue fonts indicate prediction with $R^2 > 50\%$

Source	Direction	Regression Equation
1: Walkie-Talkie:	X	R^2 = 92.61% : ln(E-Field1 (V/m)_X) = 2.591 - 0.014606 Distance(mm)
	Y	R^2 = 88.46% : ln(E-Field1 (V/m)_Y) = 2.358 - 0.01539 Distance(mm)
	Z	R^2 = 90.87% : ln(E-Field1 (V/m)_Z) = 2.390 - 0.01381 Distance(mm)
2: WiFi Router	X	R^2 = 44.98% : ln(E-Field2 (V/m)_X) = 1.205 - 0.003487 Distance(mm)
	Y	R^2 = 79.94% : ln(E-Field2 (V/m)_Y) = 2.216 - 0.008395 Distance(mm)
	Z	R^2 = 24.76% : ln(E-Field2 (V/m)_Z) = 0.4217 - 0.001249 Distance(mm)
3: WiFi Phone	X	R^2 = 38.96% : ln(E-Field3 (V/m)_X) = -0.646 - 0.00441 Distance(mm)
	Y	R^2 = 25.82% : ln(E-Field3 (V/m)_Y) = -0.155 - 0.00333 Distance(mm)
	Z	R^2 = 56.04% : ln(E-Field3 (V/m)_Z) = 0.097 - 0.00646 Distance(mm)
4_1: Cell Phone 1	X	R^2 = 50.26% : ln(E-Field4_1 (V/m)_X) = 1.474 - 0.00573 Distance(mm)
	Y	R^2 = 74.78% : ln(E-Field4_1 (V/m)_Y) = 1.4998 - 0.003556 Distance(mm)
	Z	R^2 = 34.59% : ln(E-Field4_1 (V/m)_Z) = -1.068 - 0.00324 Distance(mm)
4_2: Cell Phone2	X	R^2 = 6.17% : ln(E-Field4_2 (V/m)_X) = -1.9351 - 0.000385 Distance(mm)
	Y	R^2 = 15.10% : ln(E-Field4_2 (V/m)_Y) = -1.764 - 0.001065 Distance(mm)
	Z	R^2 = 7.54% : ln(E-Field4_2 (V/m)_Z) = -2.1183 + 0.000374 Distance(mm)
5: Laptop computer	X	R^2 = 0.28% : ln(E-Field5(V/m)_X) = -1.958 + 0.00025 Distance(mm)
	Y	R^2 = 0.10% : ln(E-Field5(V/m)_Y) = -1.9989 - 0.000048 Distance(mm)
	Z	R^2 = 0.11% : ln(E-Field5(V/m)_Z) = -1.847 + 0.00015 Distance(mm)
6: Tablet computer	X	R^2 = 54.03% : ln(E-Field6(V/m)_X) = 0.495 - 0.00649 Distance(mm)
	Y	R^2 = 52.03% : ln(E-Field6(V/m)_Y) = 0.573 - 0.00549 Distance(mm)
	Z	R^2 = 55.59% : ln(E-Field6(V/m)_Z) = 0.342 - 0.00694 Distance(mm)
7_1: Wireless mouse	X	R^2 = 0.96% : ln(E-Field7_1(V/m)_X) = -1.9499 - 0.000118 Distance(mm)
	Y	R^2 = 15.87% : ln(E-Field7_1(V/m)_Y) = -2.001 + 0.001172 Distance(mm)
	Z	R^2 = 34.47% : ln(E-Field7_1(V/m)_Z) = -1.406 - 0.002306 Distance(mm)
7_2: Wireless keyboard	X	R^2 = 30.62% : ln(E-Field7_2V/m)_X) = -1.9078 - 0.000926 Distance(mm)
	Y	R^2 = 6.85% : ln(E-Field7_2V/m)_Y) = -1.9164 - 0.000552 Distance(mm)
	Z	R^2 = 4.86% : ln(E-Field7_2V/m)_Z) = -1.8907 - 0.000380 Distance(mm)

Comparison of electric field at one inch (25.4 mm) distance from all wireless communication devices in this experiment are illustrated in Figure 4.3. Again ranking of the electric field is from walkie-talkie, WiFi router, cell phone 1, tablet, WiFi phone, cell phone 2, laptop, wireless mouse and wireless keyboard, used in the experiment, respectively. The red dots illustrate the direction with has maximum electric field at one inch (25.4 mm) distance.

Regression analysis results exponential decay function of distance, as shown in (4.1) as well as in table 4.1.

$$ln\ (Electric\ field(V/m)) = -\ a_1\ Distance\ (mm) - b_1 \quad (4.1)$$

The coefficient a_1 is specific to a wireless communication device while constant b_1 related to the X Y Z directions. Coefficient of determination, R^2, is a number that indicates the proportion of the variance in the dependent variable that is predictable from the independent variable. The R^2 of walkie-talkie and cell phone 1's regression equations are about 90%. While R^2 of WiFi router, WiFi phone and tablet's regression equation are around 50%. The R^2 of laptop computer, wireless mouse and keyboard's regression equations are less than 40%. Thought the regression equation does not fit for the weak-power field sources.

Table 4.2 summarized analysis result of this experiment. Five out of nine wireless communication devices , as shown in blue fonts, been chosen to be field sources in experiments B and C, as they have significant magnitude of the electric field strength. They are walkie-talkie, WiFi router, cell phone 1, tablet, WiFi phone. Summary of the analysis of variance, electric field at 25.4 mm, and the most influencing direction is illustrated

Table 4.2 Selected significant electric field sources, distance and direction to be used in experiments B and C.

Significant Electric field source	Analysis of Variance P-value [<0.05, reject H_0]			At 1" distance	
	Direction $H_0: \mu_x = \mu_y = \mu_z$	Distance $H_0: \mu_1 = \mu_2 = \mu_3 = \mu_4$	Interaction H_0: *No interaction*	Electric field (V/m)	The most influence direction
1 Walkie-Talkie	0.487 [Not significant]	0.000 [Significant]	0.428 [Not significant]	12.084	X
2 WiFi Router	0.000 [Significant]	0.000 [Significant]	0.000 [Significant]	10.081	Y
3 WiFi Phone	0.000 [Significant]	0.000 [Significant]	0.000 [Significant]	1.839	Z
4_1 Cell Phone1	0.000 [Significant]	0.000 [Significant]	0.004 [Significant]	8.437	X
4_2 Cell Phone2	0.052 [Not significant]	0.054 [Not significant]	0.334 [Not significant]	0.197	Y
5 Laptop	0.423 [Not significant]	0.722 [Not significant]	0.279 [Not significant]	0.147	Z
6 Tablet	0.694 [Not significant]	0.000 [Significant]	0.393 [Not significant]	2.661	Z
7.1 Mouse	0.010 [Significant]	0.033 [Significant]	0.000 [Significant]	0.319	Z
7.2 Keyboard	0.336 [Not significant]	0.006 [Not significant]	0.852 [Not significant]	0.170	Z

B. Result of Thermal change and DC voltage of TGMR head while placing in the field of wireless communication device

Actual thermal change to the read head and DC voltage dropped on TGMR been observed while HGAs are in the simulated assembly process, and in the electric field of wireless communication device.

In the same way as result from experiment A, magnitude of DC voltage and DETCR temperature of TGMR in the field of walkie-talkie signal are obviously higher than other wireless communication devices. It is about 400 times of DC voltage and 4 times of DETCR temperature of HGAs in the field from WiFi router, which has second magnitude in the rank. Likewise, the ranking order of magnitude from this experiment is consistence with ranking result from experiment A, which is walkie-talkie, WiFi router, cell phone, tablet and WiFi phone, respectively. Figure 4.4.1 and 4.4.2 show voltage dropped on TGMR in electric field of wireless communication devices in different scale. Figure 4.5.1 and 4.5.2 show temperature of DETCR adjacent to TGMR in electric field of wireless communication devices in different scale as well.

From the result of experiment A, the most influence direction of wireless communication device to the HGA has been fixed in this experiment. Meanwhile, distance between wireless communication devices to HGA still plays important role to the magnitude of the DC voltage dropped to TGMR as well as change of DETCR temperature. Regression equation can be explained in exponential decay function, as expressed in equation (4.2) and (4.3). The coefficients a_2, b_2, a_3, *and* b_3 including R^2 for each wireless communication device are identified in the equation in Table 4.3.1 and Table 4.3.2.

$$ln(DC\ \mu V) = -\ a_2\ (Distance\ mm) + b_2 \qquad (4.2)$$

$$ln(DETCR\ Temp\ C) = -\ a_3\ (Distance\ mm) + b_3 \qquad (4.3)$$

Correlation between DETCR temperature and voltage drop on TGMR is observed in Figure 4.6.1 with P-Value of 0.000. The regression equation of voltage drop on TGMR with the DETCR temperature has coefficient of determination, R^2 of 90.5%. It means DETCR temperature can predict voltage drop on TGMR and vice versa.

Now, we need to compare result from this experiment, to TGMR damage threshold, which will be different based on its design and structure. The comparison with current specification or control limit that organization defined is able to do as well. Supposing the TGMR, had been used in this experiment, withstands to the Joule heating power of less than 20 nJ/s to 25 nJ/s and accumulated temperature of not more than 100 °C to 120 °C.

Calculation of the power is basically done through equation $P = V^2 / R$, while V is measurement result of DC voltage dropped on TGMR and R is typical TGMR resistance which average value is about 300 Ω. The calculation result has been plotted and shown in Figure 4.6.2 Joule heating power of TGMR in electric field of wireless communication devices.

Calculation from regression equation (4.4) as expressed in Table 4.3.3 concluded that the electric field from walkie-talkie at the distance of less than 61.06 mm. is possible to result DC voltage dropped on TGMR exceeding its withstanding point of 25 nJ/s and the electric field from walkie-talkie at the distance of less than 70.34 mm. is possible to result DC voltage dropped on TGMR exceed its withstand of 20 nJ/s.

$$ln(Power\ (J/s)) = -16.036 - 0.024048\ Distance\ (mm) \quad (4.4)$$

Temperature is quite direct. Calculation from regression equation (4.5) for walkie-talkie (4.5) concluded that, the calculated distance from walkie-talkie to TGMR is 79.85 mm or closer is possible to make DETCR temperature exceed its withstanding of TGMR damage at 120 °C and at the distance of 110.80 mm or closer is possible to make DETCR temperature exceed its withstanding of TGMR damage at 100 °C.

$$ln(DETCR\ Temperature\ (^{o}C)) = 5.2577 - 0.005889\ Distance\ (mm) \quad (4.5)$$

As walkie-talkie is the worse-case example, it should not come closer to HGA than 61.06, 70.43, 79.85 or 110.80 mm, depend on which threshold number are comparing. Other wireless communication device got negative distance from calculation, as shown in Table 4.4, which means there is not enough power or temperature to harm TGMR even those wireless communication devices come as close as almost contact to TGMR head.

Graph of the prediction models of joule heating power on TGMR (nJ/s) and DETCR temperature (^{o}C), versus distance (mm) from walkie-talkie based on regression analysis are illustrated in Figure 4.7.1 and Figure 4.7.2.

Figure 4.7.1, power in TGMR (nJ/s) is in Y-axial. Figure 4.7.2, DECTR temperature (^{o}C) is on Y-axial. In both figures distance from wireless communication device to the TGMR in millimeters is in X-axial. From the exponential decay function plotting, the critical distance could be found by varying TGMR failure base on design and technology.

With the same calculation and modelling concept from this experiment, we can make decision for setting up proper distance of using wireless communication devices in HGA assembly areas.

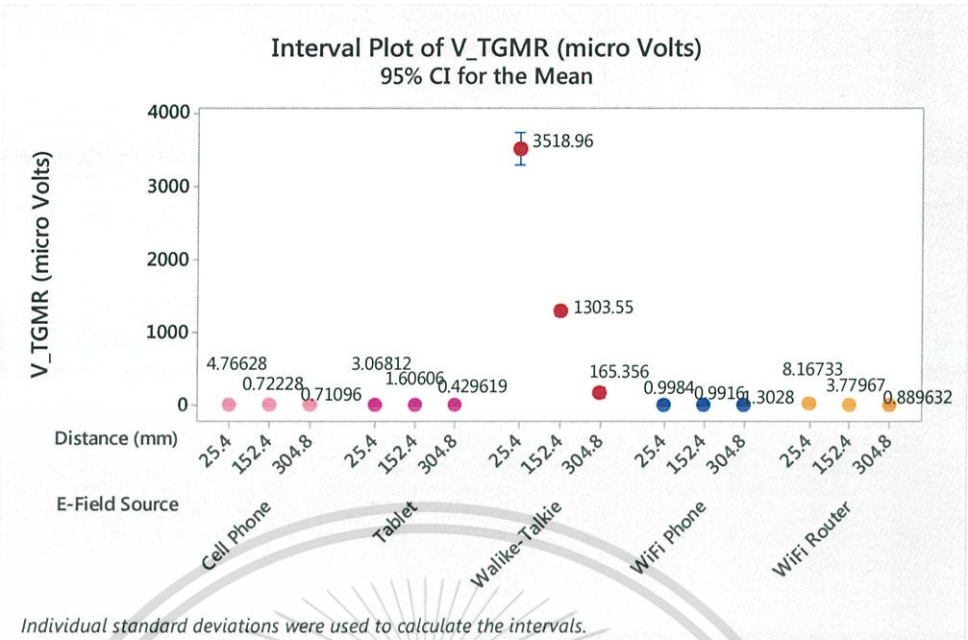

Figure 4.4.1 Voltage dropped on TGMR in electric field of wireless communication devices.

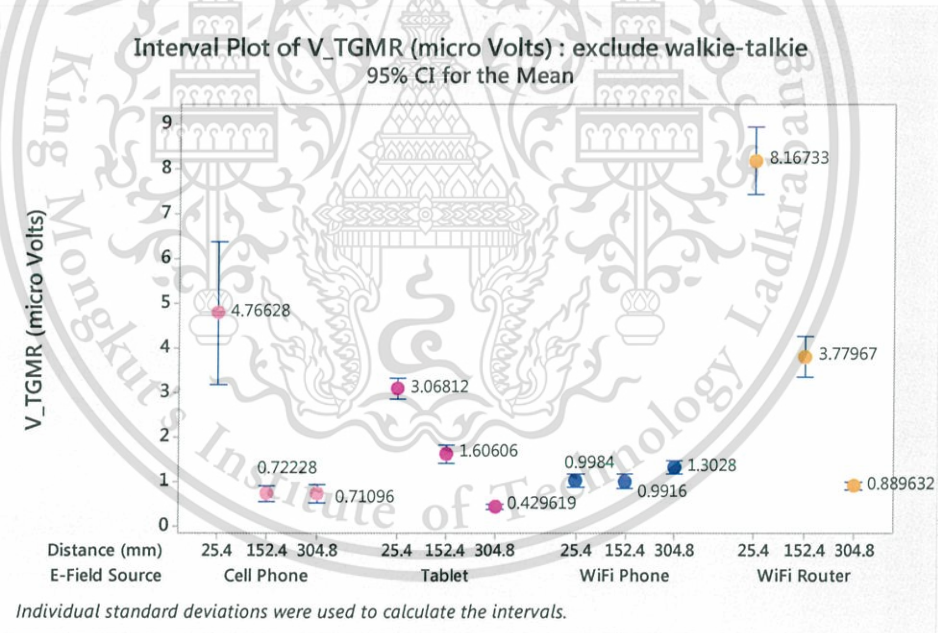

Figure 4.4.2 Interval plot of voltage dropped on TGMR in electric field of wireless communication devices, exclude walkie-talkie.

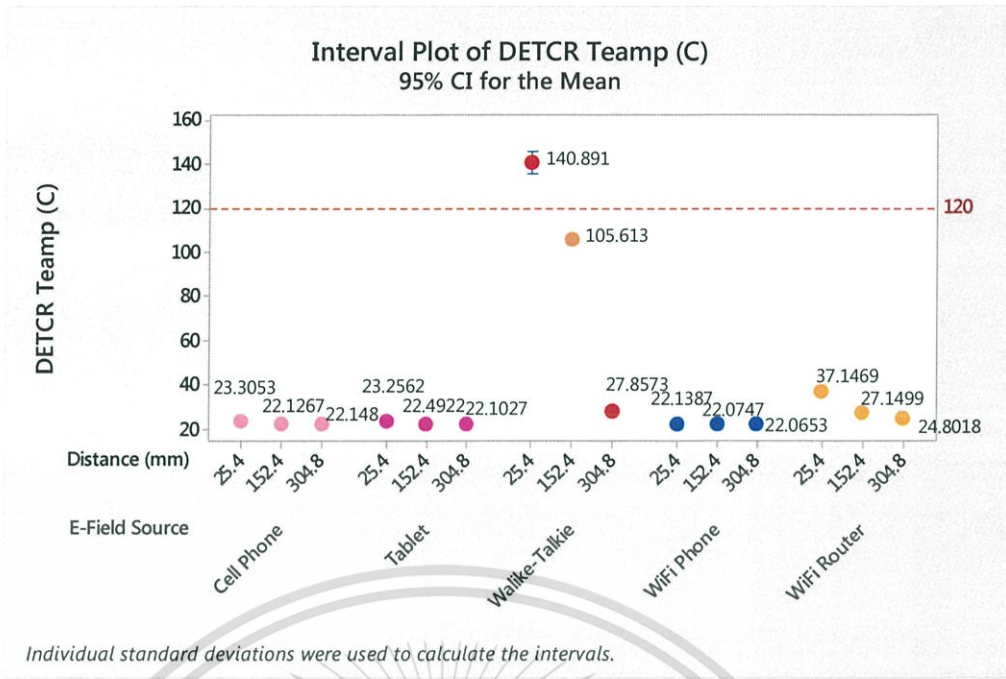

Figure 4.5.1 Temperature of DETCR adjacent to TGMR in electric field of wireless communication devices.

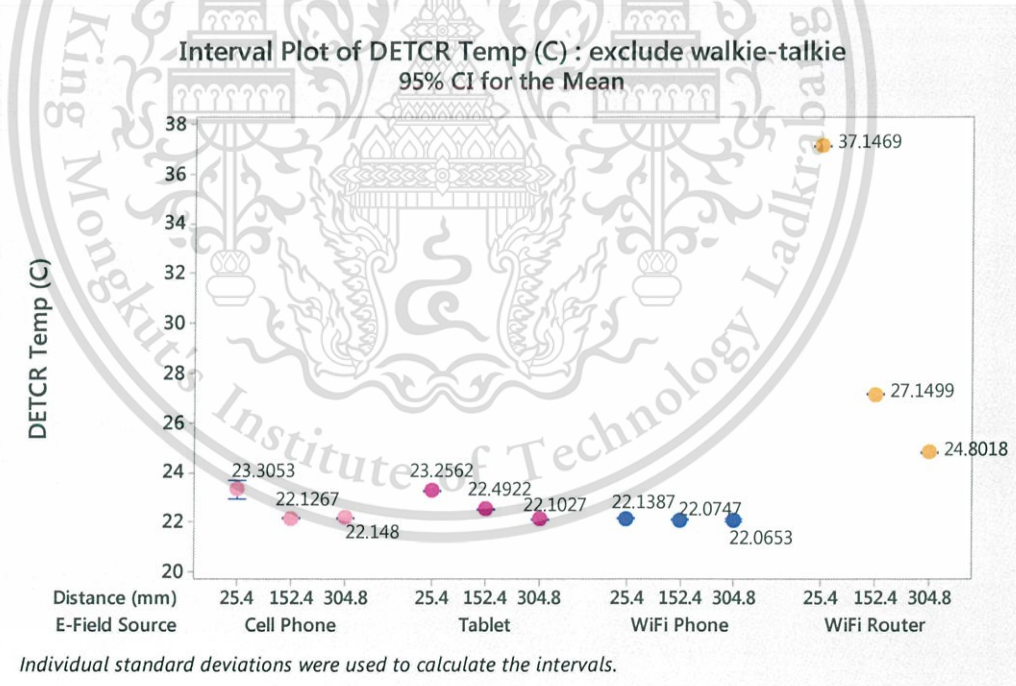

Figure 4.5.2 Temperature of DETCR adjacent to TGMR in electric field of wireless communication devices, excluding walkie-talkie.

Table 4.3.1 Regression Equation; y = TGMR Voltage (μV), x = distance (mm)

	Regression Equation y = TGMR Voltage (μV), x = distance (mm)	
Electric field Source	Linear Regression Equation	Exponential Decay
Walkie-Talkie	R^2 = 94.53% y = -118.5 x + 3569.2	R^2 = 90.04% ln(y) = 8.6493 - 0.012024 x
WiFi Router	R^2 = 97.62% y = -0.253 x + 8.3565	R^2 = 91.46% ln(y) = 2.3581 - 0.007996 x
Cell Phone	R^2 = 71.76% y = -0.1288 x + 4.0068	R^2 = 36.69% ln(y) = 0.988 - 0.006032 x
Tablet	R^2 = 99.37% y = -0.0929 x + 3.1989	R^2 = 87.40% ln(y) = 1.3681 - 0.007205 x
WiFi Phone	R^2 = 77.83% y = 0.0112 x + 0.9173	R^2 = 8.75% ln(y) = -0.1611 + 0.001104 x

Table 4.3.2 Regression Equation; y = DETCR Temperature (°C), x = distance (mm)

	Regression Equation y = DETCR Temperature (°C), x = distance (mm)	
Electric field Source	Linear Regression Equation	Exponential Decay
Walkie-Talkie	R^2 = 97.42% y = -4.0804 x + 157.09	R^2 = 90.51% ln(y) = 5.2577 - 0.005889 x
WiFi Router	R^2 = 85.13% y = -0.4325 x + 36.672	R^2 = 87.51% ln(y) = 3.6038 - 0.001418 x
Cell Phone	R^2 = 67.74% y = -0.0397 x + 23.173	R^2 = 37.89% ln(y) = 3.14212 - 0.000174 x
Tablet	R^2 = 94.72% y = -0.041 x + 23.278	R^2 = 92.01% ln(y) = 3.14740 - 0.000180 x
WiFi Phone	R^2 = 59.38% y = 0.0022 x + 21.872	R^2 = 12.46% ln(y) = 3.09711 - 0.000012 x

Table 4.3.3 Regression Equation; y = Power on TGMR (J/s), x = distance (mm).

	Regression Equation y = Power on TGMR (nJ/s), x = distance (mm)
Electric field Source	Exponential Decay
Walkie-Talkie	R^2 = 90.04% ln(y) = -16.036 - 0.024048 x ln(y(nJ/s)) = 4.687 - 0.024048 x
WiFi Router	R^2 = 91.46 ln(y) = -28.619 - 0.015993 x ln(y(nJ/s)) = -7.895 - 0.015993 x
Cell Phone	R^2 = 36.69% ln(y) = -31.360 - 0.01206 x ln(y(nJ/s)) = -10.636 - 0.01206 x
Tablet	R^2 = 87.40% ln(y) = -30.599 - 0.014410 x ln(y(nJ/s)) = -9.875 - 0.014410 x
WiFi Phone	R^2 = 8.75% ln(y) = -33.657 + 0.002208 x ln(y(nJ/s)) = -12.934 + 0.002208 x

Table 4.4 Distance limit between wireless communication devices to TGMR head

	Distance from Wireless communication devices to TGMR head (mm)			
	Power threshold of		Temperature threshold of	
Electric field Source	25 nJ/s	20 nJ/s	120 °C	100 °C
Walkie-Talkie	61.06	70.33	79.85	110.80
WiFi Router	-694.97	-681.01	-834.76	-834.76
Cell Phone	-1148.89	-1130.39	-9456.16	-9456.16
Tablet	-908.72	-893.23	-9111.62	-9111.62
WiFi Phone	Skip calculation, R^2 is too low due to reading is close to background			

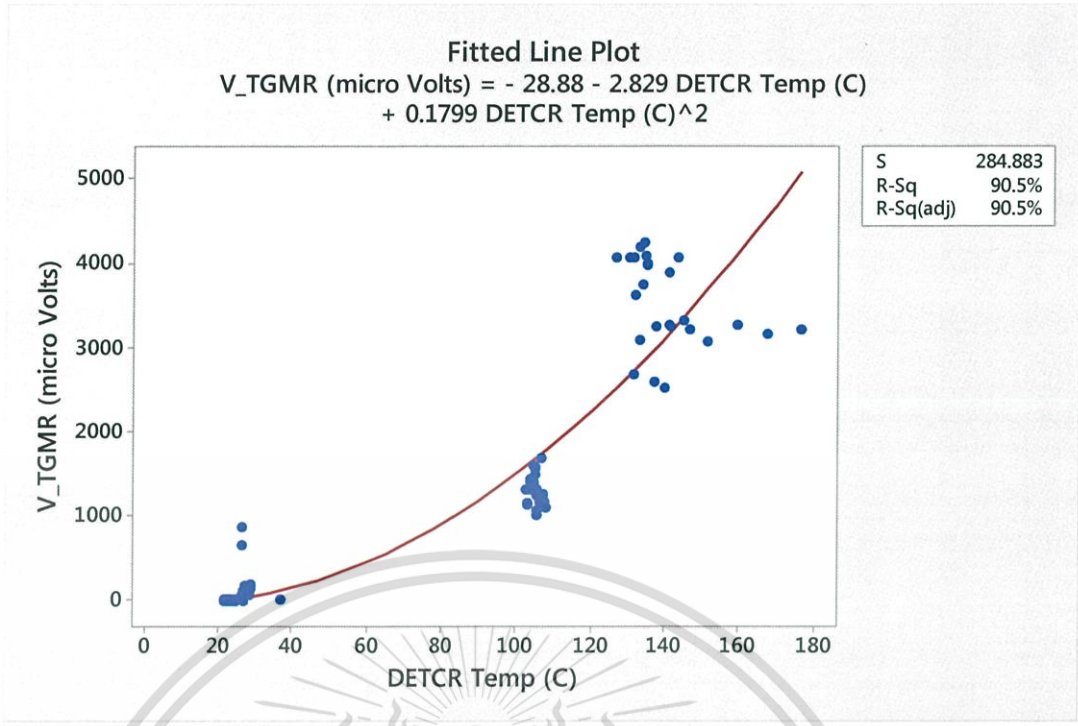

Correlation: DETCR Temp (C), V_TGMR (micro Volts)

```
Pearson correlation of DETCR Temp (C) and V_TGMR (micro Volts) = 0.937
P-Value = 0.000
```

Polynomial Regression Analysis: V_TGMR (micro Volts) versus DETCR Temp (C)

```
The regression equation is
V_TGMR (micro Volts) = - 28.88 - 2.829 DETCR Temp (C) + 0.1799 DETCR Temp (C)^2


S = 284.883   R-Sq = 90.5%   R-Sq(adj) = 90.5%


Analysis of Variance

Source        DF         SS         MS        F      P
Regression     2  288921350  144460675  1779.99  0.000
Error        372   30190825      81158
Total        374  319112175


Sequential Analysis of Variance

Source      DF         SS        F      P
Linear       1  280110178  2678.87  0.000
Quadratic    1    8811172   108.57  0.000
```

Figure 4.6.1 Correlation of DETCR temperature and voltage dropped on TGMR in electric field.

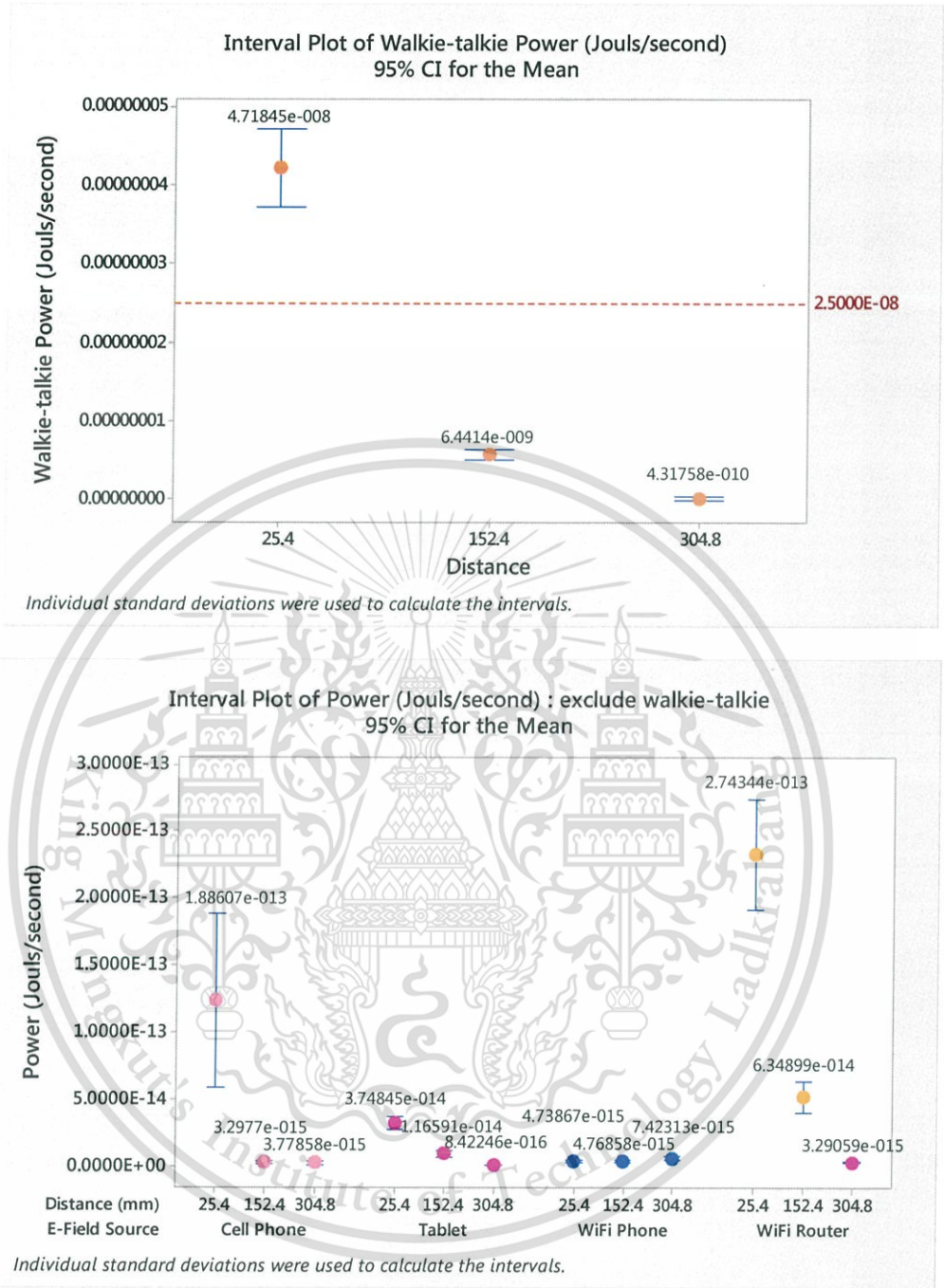

Figure 4.6.2 Joule heating power of TGMR in electric field of wireless communication.

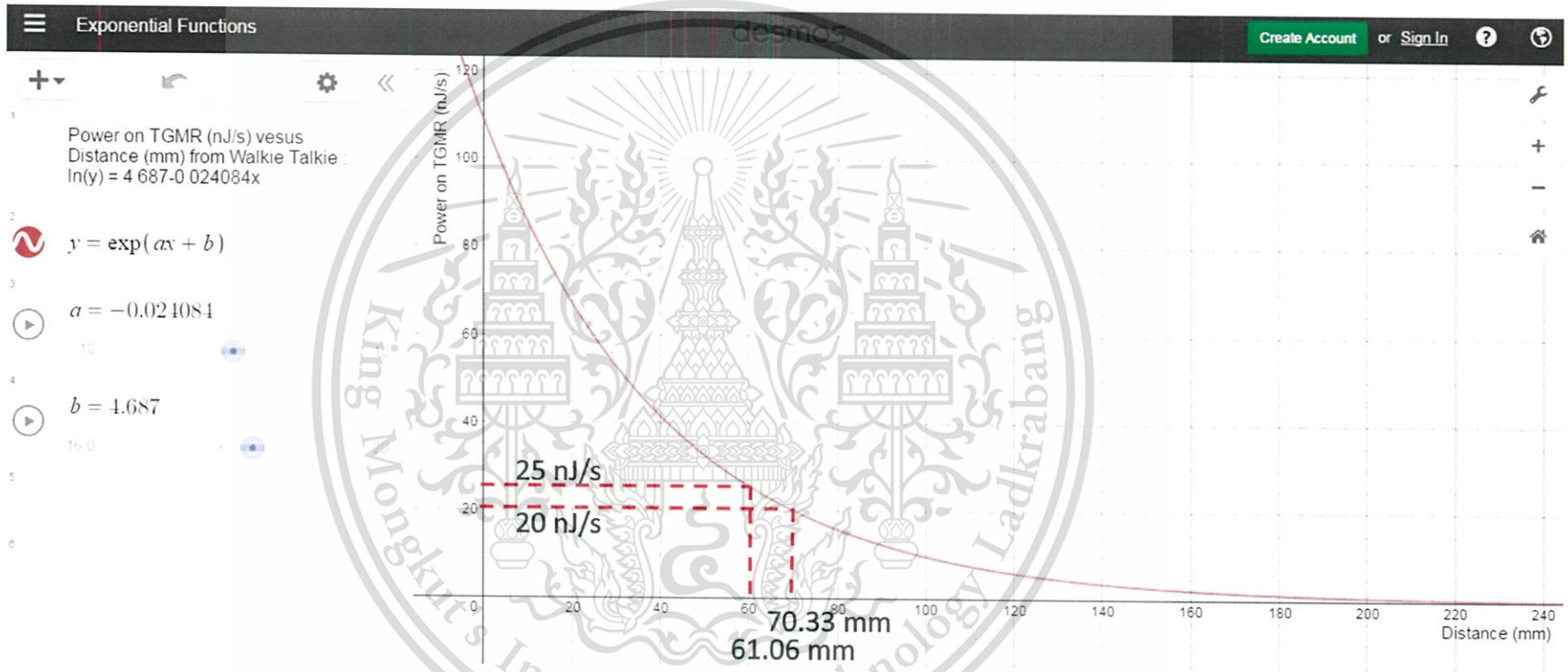

Figure 4.7.1 Graph of prediction model of power on TGMR (nJ/s) versus distance (mm) from walkie-talkie based on regression analysis

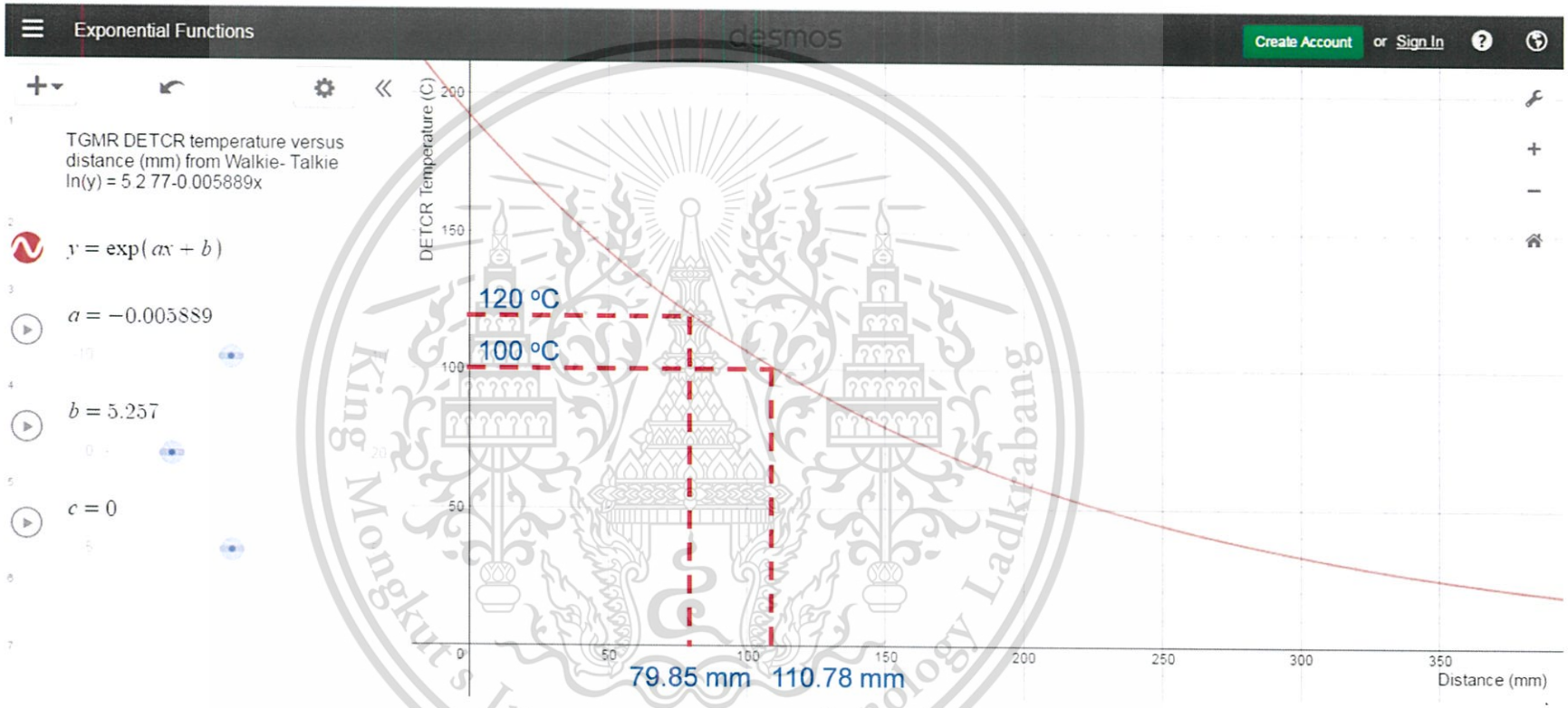

Figure 4.7.2 Graph of prediction model of DETCR temperature (°C) versus distance (mm) from walkie-talkie based on regression analysis

C. Result of Electrical Performance of TGMR pre and post actions simulating HGA assembly process

Wireless communication devices, which are in top five of electric field from experiment A, have been chosen to be field sources in this experiment. HGAs are placed in the field generated from each wireless communication device at the most influence direction as learnt from experiment A. From experiment B, calculated distance to the TGMR failure threshold of 100°C and 120°C are 110.80 mm and 79.85 mm for walkie- talkie, and no close distance limit for other wireless communication devices to harm the TGMR. As limit of the HGA automation tools, the closest distance able to set in this experiment is 100 mm far between HGA and field source. And the distance of 600 mm. had been also studied to confirm whether the typical rule limit of contraband distance, at 600 mm, is able to be applied to control the wireless communication devices. So, the expected result is not to observe obvious electrical or magnetic properties change or damaged on all TGMR at Quasi-Static Tester QST-2002, or in worse case, we might see very little change in stability parameter at studied distance of 100 mm from walkie-talkie or WiFi-router only.

Table 4.5 is summary of QST measurement result from all HGAs samples (220 HGAs), tested pre and post HGA process. It showed that, HGA sample variations are large enough to cover range of all parameters and able to represent normal HGAs in the process. From overall data, there is no significant difference of pre and post test result of all test setup parameters base on Pair-T test, Null Hypothesis is H_0: $\mu_b = \mu_a$, P-Value > 0.05, accept H_0.

Scatter plot of individual measurement data from QST of HGAs in the field of transmitting wireless communication devices, pre-HGA-process versus pose-HGA process in Figure series 4.8 (Figure 4.8.0-4.8.7), confirmed agreement with Experiment B that, there is no change in both catastrophic, or hard failure parameters (TGMR resistance-Figure 4.8.1, Amplitude-Figure 4.8.2, Slope-Figure 4.8.3) and instability parameters (Asymmetry-Figure 4.8.4, Barkhausen Jump-Figure 4.8.5, Hysteresis Loop-Figure 4.8.6, and Spectral Maximum Amplitude Noise-Figure 4.8.7) were observed, with total samples of 220 HGAs in all experiment conditions.

Table 4.5 Summary of QST measurement result from all HGAs samples (220 HGAs), Pair-T test pre and post HGA process with exposure.

QST PARAMETER	TEST SET	MAX	MIN	Mean	STDEV	95% CI for mean difference	P-Value
RESISTANCE (Ohms)	Pre HGA Process	192	447	287.59	37.88	(-0.478, 0.400)	0.860
	Post HGA Process	190	444	287.63	38.20		Not significant difference
AMPLITUDE (mV)	Pre HGA Process	5753	27162	14256	3847	(-64.2, 53.8)	0.826
	Post HGA Process	5871	27300	14261	3869		Not significant difference
SLOPE_AVG (mV/Oe)	Pre HGA Process	-20	-4	-10.006	2.845	(-0.0295, 0.0469)	0.655
	Post HGA Process	-21	-4	-10.075	2.865		Not significant difference
ASYMMETRY (%)	Pre HGA Process	-16	23	4.611	7.138	(-0.251, 0.339)	0.767
	Post HGA Process	-21	22	4.566	7.199		Not significant difference
BARK_JMP (%)	Pre HGA Process	2	23	6.392	3.400	(-0.0802, 0.2452)	0.319
	Post HGA Process	2	22	6.309	3.258		Not significant difference
HYST_PCT (%)	Pre HGA Process	2	15	3.926	2.252	(-0.0364, 0.2158)	0.162
	Post HGA Process	1	13	3.836	2.012		Not significant difference
SMANAMP_MAX (mV)	Pre HGA Process	187	2465	773.0	371.9	(-18.84, 2.98)	0.153
	Post HGA Process	197	2726	781.0	377.6		Not significant difference

Null Hypothesis, H_0: $\mu_b = \mu_a$, P-Value > 0.05, accept H_0

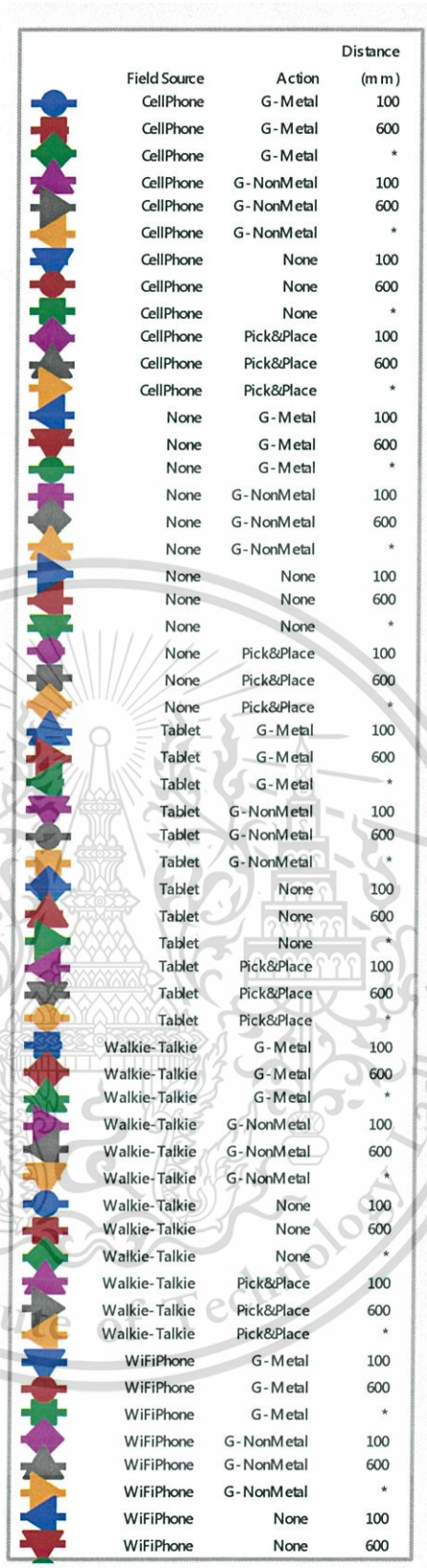

Field Source	Action	Distance (mm)
CellPhone	G-Metal	100
CellPhone	G-Metal	600
CellPhone	G-Metal	*
CellPhone	G-NonMetal	100
CellPhone	G-NonMetal	600
CellPhone	G-NonMetal	*
CellPhone	None	100
CellPhone	None	600
CellPhone	None	*
CellPhone	Pick&Place	100
CellPhone	Pick&Place	600
CellPhone	Pick&Place	*
None	G-Metal	100
None	G-Metal	600
None	G-Metal	*
None	G-NonMetal	100
None	G-NonMetal	600
None	G-NonMetal	*
None	None	100
None	None	600
None	None	*
None	Pick&Place	100
None	Pick&Place	600
None	Pick&Place	*
Tablet	G-Metal	100
Tablet	G-Metal	600
Tablet	G-Metal	*
Tablet	G-NonMetal	100
Tablet	G-NonMetal	600
Tablet	G-NonMetal	*
Tablet	None	100
Tablet	None	600
Tablet	None	*
Tablet	Pick&Place	100
Tablet	Pick&Place	600
Tablet	Pick&Place	*
Walkie-Talkie	G-Metal	100
Walkie-Talkie	G-Metal	600
Walkie-Talkie	G-Metal	*
Walkie-Talkie	G-NonMetal	100
Walkie-Talkie	G-NonMetal	600
Walkie-Talkie	G-NonMetal	*
Walkie-Talkie	None	100
Walkie-Talkie	None	600
Walkie-Talkie	None	*
Walkie-Talkie	Pick&Place	100
Walkie-Talkie	Pick&Place	600
Walkie-Talkie	Pick&Place	*
WiFiPhone	G-Metal	100
WiFiPhone	G-Metal	600
WiFiPhone	G-Metal	*
WiFiPhone	G-NonMetal	100
WiFiPhone	G-NonMetal	600
WiFiPhone	G-NonMetal	*
WiFiPhone	None	100
WiFiPhone	None	600

Figure 4.8.0 Reference legend for Figure 4.8.1-4.8.7

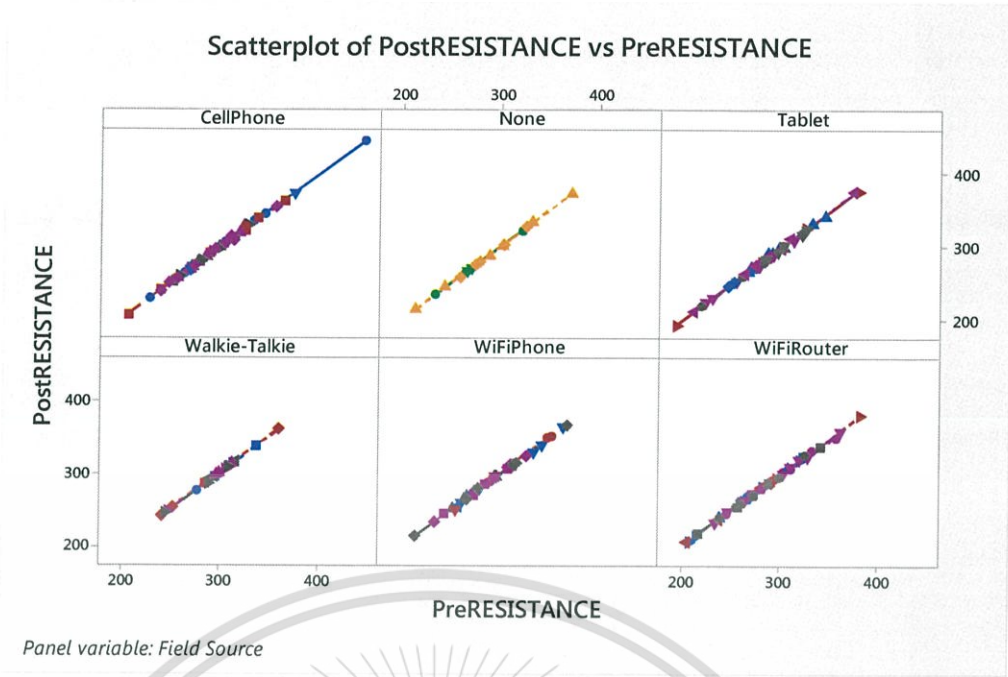

Figure 4.8.1 Scatter plot from QST TGMR resistance (ohms) measurement of HGAs in the field of transmitting wireless communication devices, pre-HGA-process VS post-HGA process.

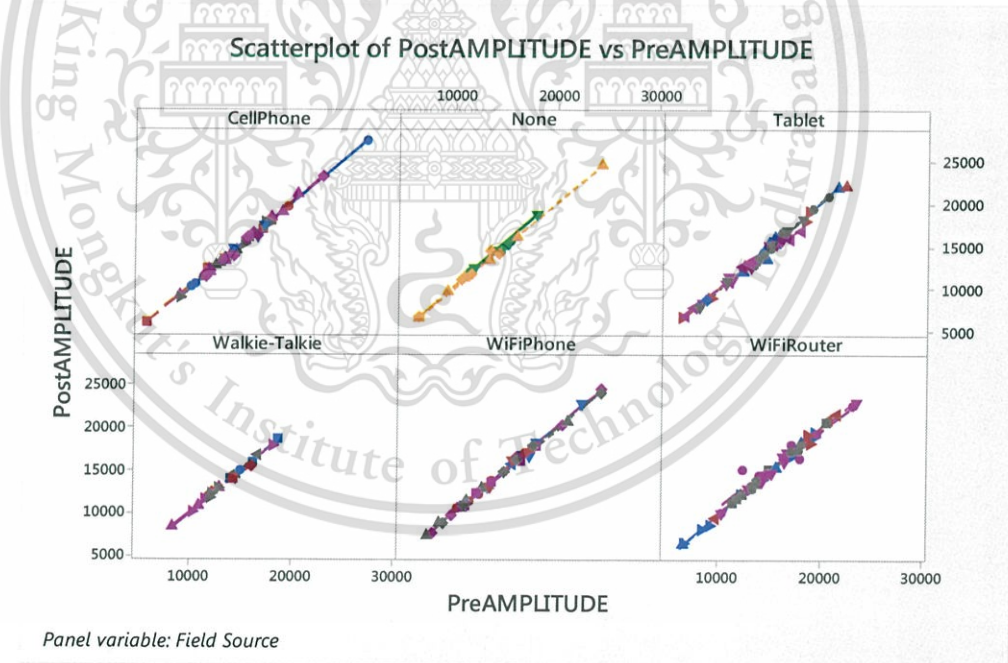

Figure 4.8.2 Scatter plot from QST TGMR amplitude (μV) measurement of HGAs in the field of transmitting wireless communication devices, pre-HGA-process VS Post-HGA process.

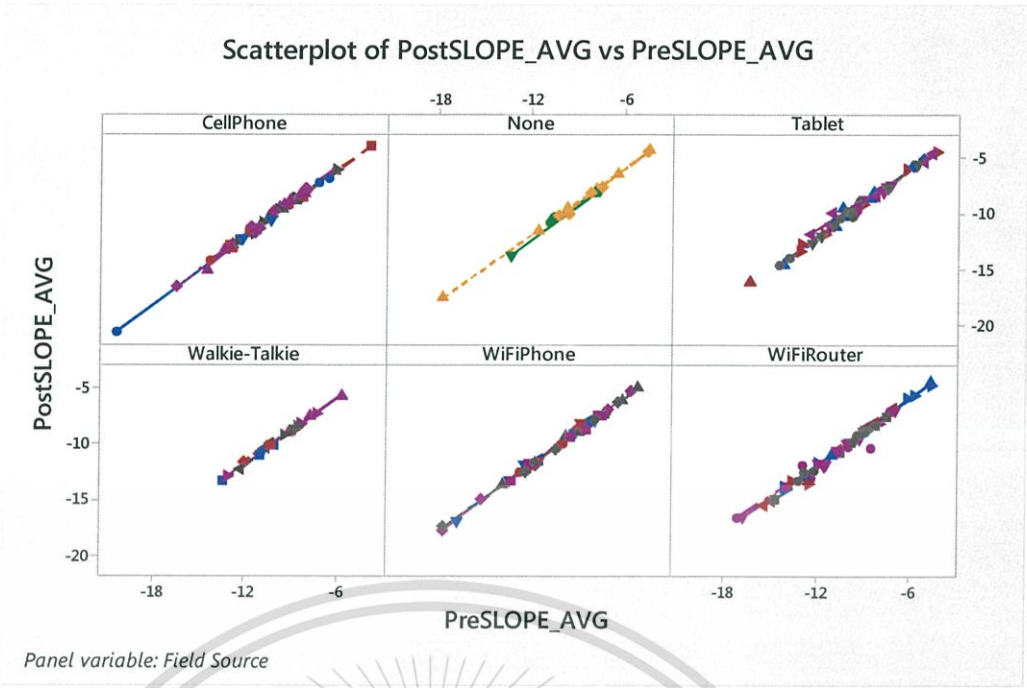

Figure 4.8.3 Scatter plot from QST TGMR slope (μV/Oe) measurement of HGAs in the field of transmitting wireless communication devices, pre-HGA-process VS post-HGA process.

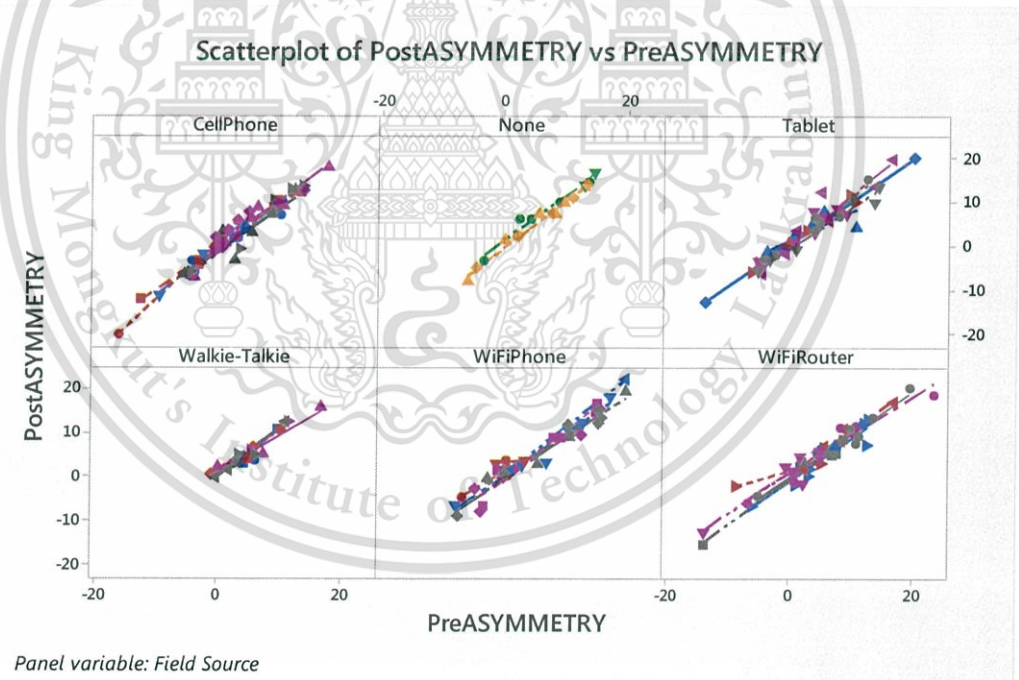

Figure 4.8.4 Scatter plot from QST TGMR asymmetry (%) measurement of HGAs in the field of transmitting wireless communication devices, pre-HGA-process VS post-HGA process.

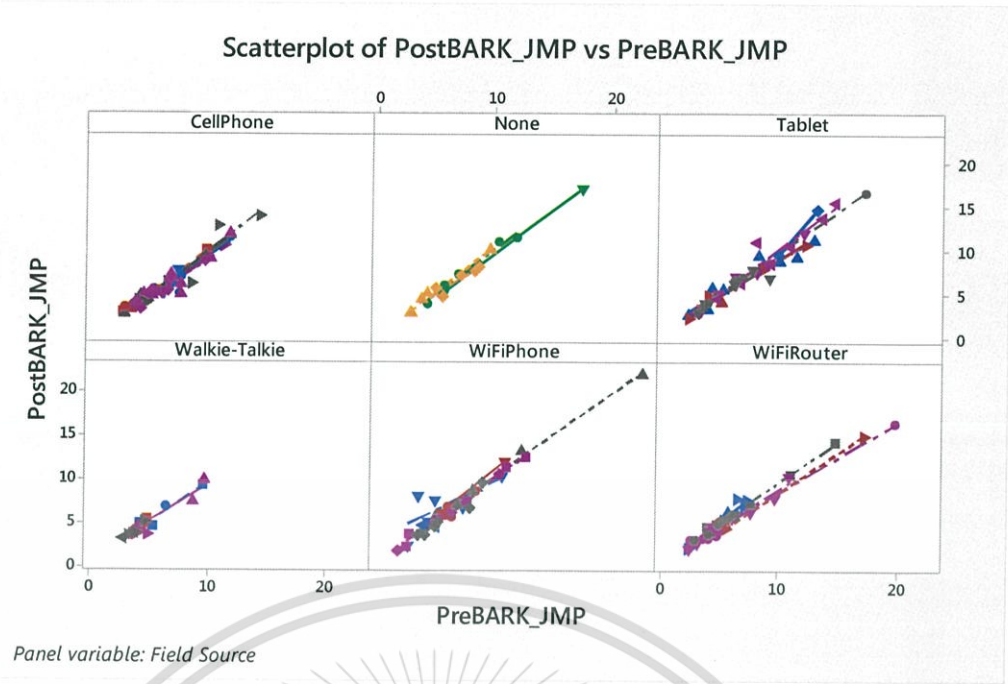

Figure 4.8.5 Scatter plot from TGMR Barkhausen jump (%) measurement of HGAs in the field of transmitting wireless communication devices, pre-HGA-process VS post-HGA process.

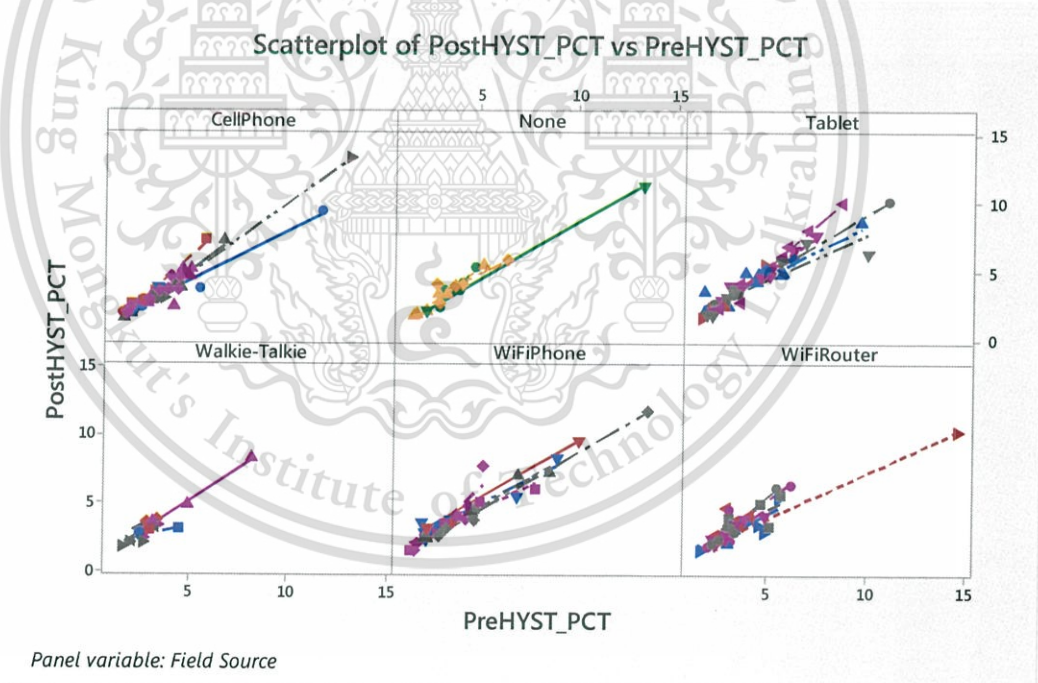

Figure 4.8.6 Scatter plot from QST TGMR hysteresis (%) measurement of HGAs in the field of transmitting wireless communication devices, pre-HGA-process VS post-HGA process.

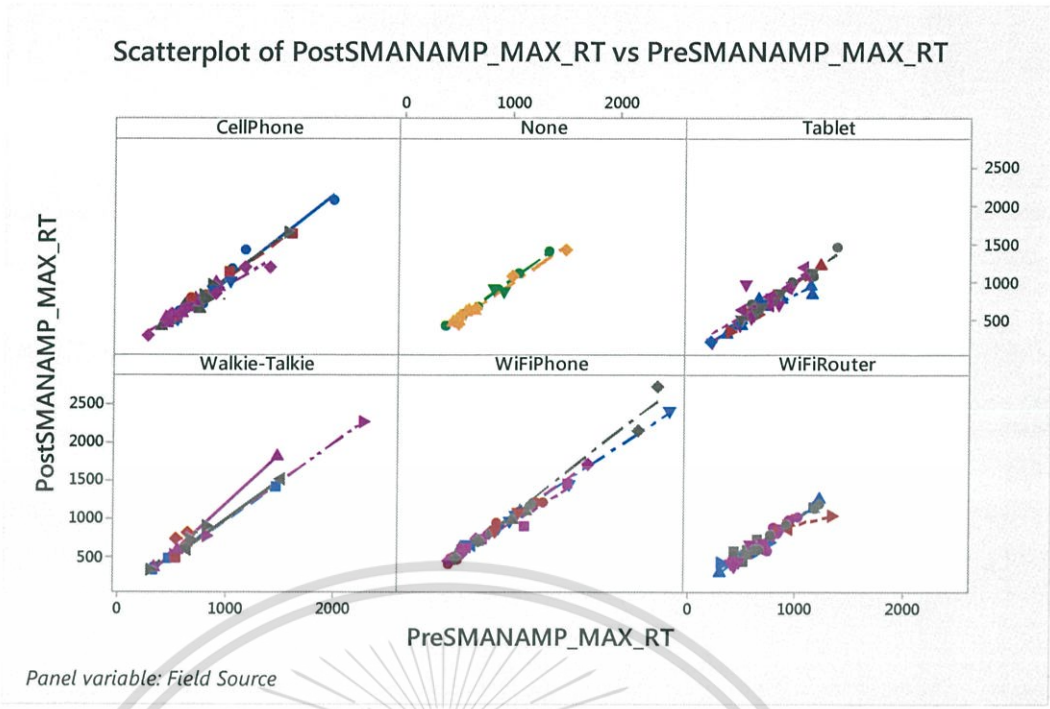

Figure 4.8.7 Scatter plot from QST TGMR Spectral Maximum Amplitude Noise S.M.A.N. (μV) measurement of HGAs in the field of transmitting wireless communication devices, pre-HGA-process VS post-HGA process.

Figure 4.9.1, 4.10.1, 4.11.1, 4.12.1, 4.13.1 show actual example of QST transverse of TGMR Amplitude (μV) sweep range +/-700 Oe, while HGA is on the field of transmitting wireless communication devices at distance of 100 mm far from TGMR while operating Ground-Metal-Contact actions. There is no significant difference between (a) pre-HGA process and (b) post HGA process.

Figure 4.9.2, 4.10.2, 4.11.2, 4.12.2, 4.13.2 show actual example of QST S.M.A.N. (μV) sweep range +/-700 Oe, while HGA is on the field of transmitting wireless communication devices at distance of 100 mm far from TGMR while operating Ground-Metal-Contact actions. There is no significant difference between (a) pre-HGA process and (b) post HGA process.

Figure 4.9.3, 4.10.3, 4.11.3, 4.12.3, 4.13.3 show actual example of QST Noise Stability (μV) sweep range +/-700 Oe, while HGA is on the field of transmitting wireless communication devices, at distance of 100 mm far from TGMR while operating Ground-Metal-Contact actions. There is no significant difference between (a) pre-HGA process and (b) post HGA process.

QST transverse, S,M,A,N, and Noise Stability of all other HGAs for all conditions in this experiment act the same way. There is no significant difference between test result of pre-HGA process and post HGA process in the field of wireless communication devices.

The results are in agree with result and calculation in experiment B that if the wireless communication devices been placed at the distance of larger than significant distance to reach TGMR failure threshold, the thermal stress and Joule heating power will not high enough to make change to electrical and magnetic properties of the TGMR in HGA process.

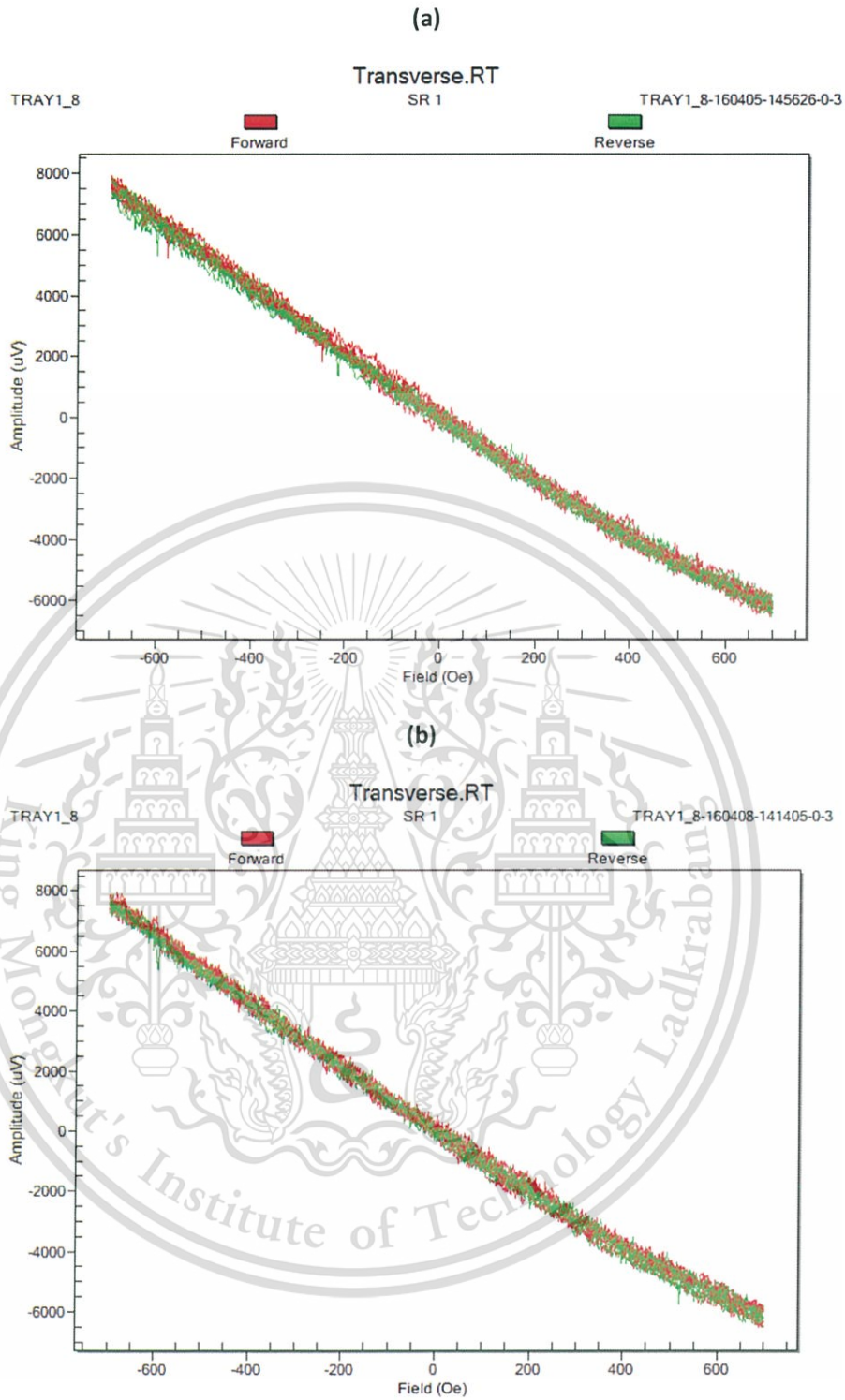

Figure 4.9.1 Example of QST transverse of TGMR amplitude (μV), source = **walkie-talkie,** D = 100 mm, Ground-Metal-Contact, (a) pre-HGA process (b) post HGA process.

(a)

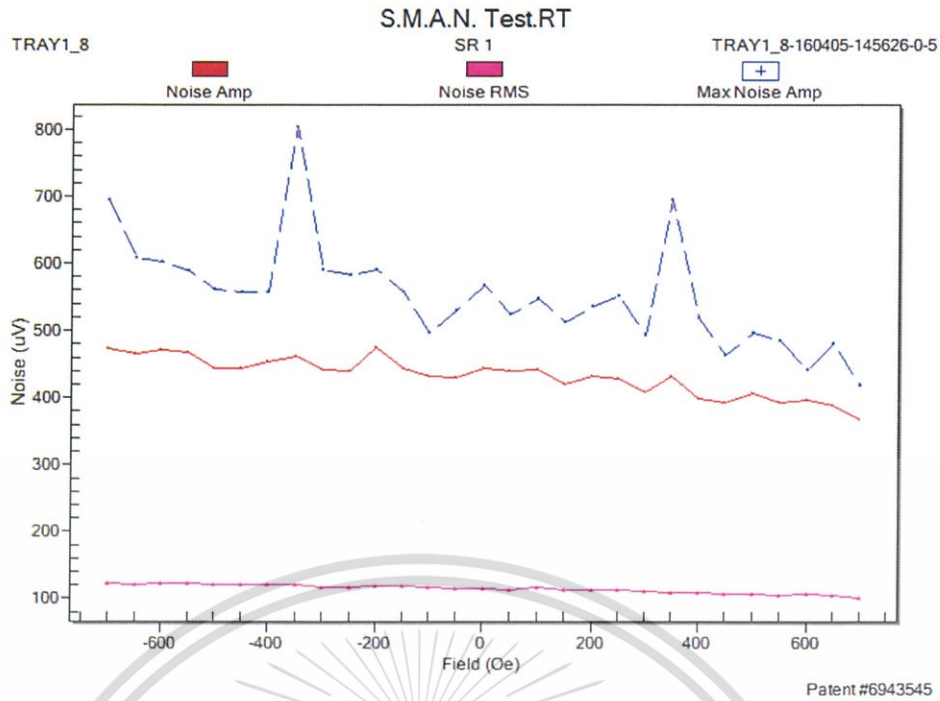

(b)

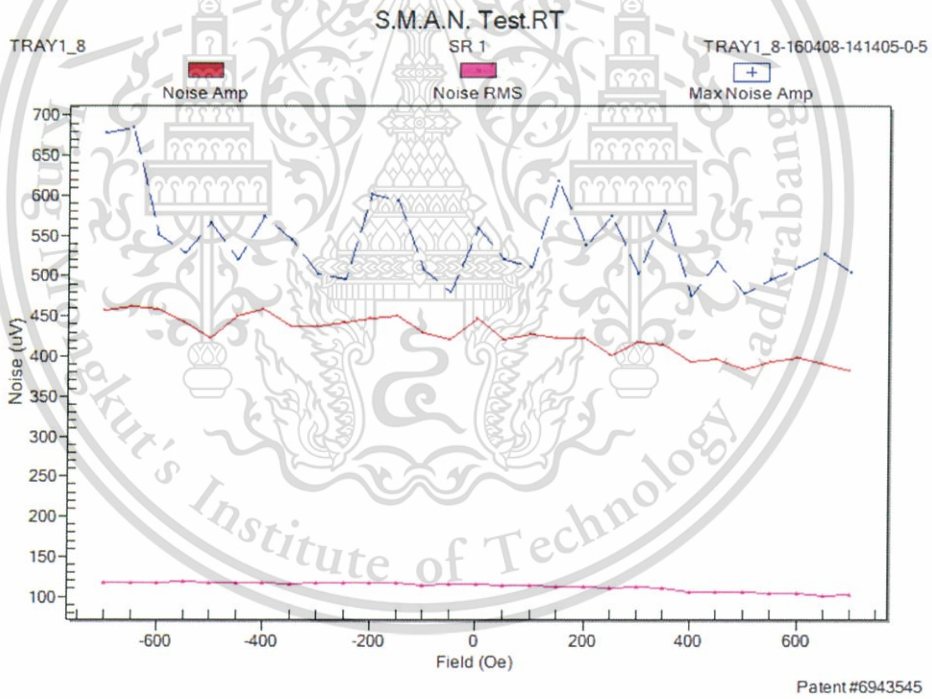

Figure 4.9.2 Example of QST S.M.A.N. (μV), source = **walkie-talkie,** D = 100 mm., Ground-Metal-Contact, (a) pre-HGA process (b) post HGA process

(a)

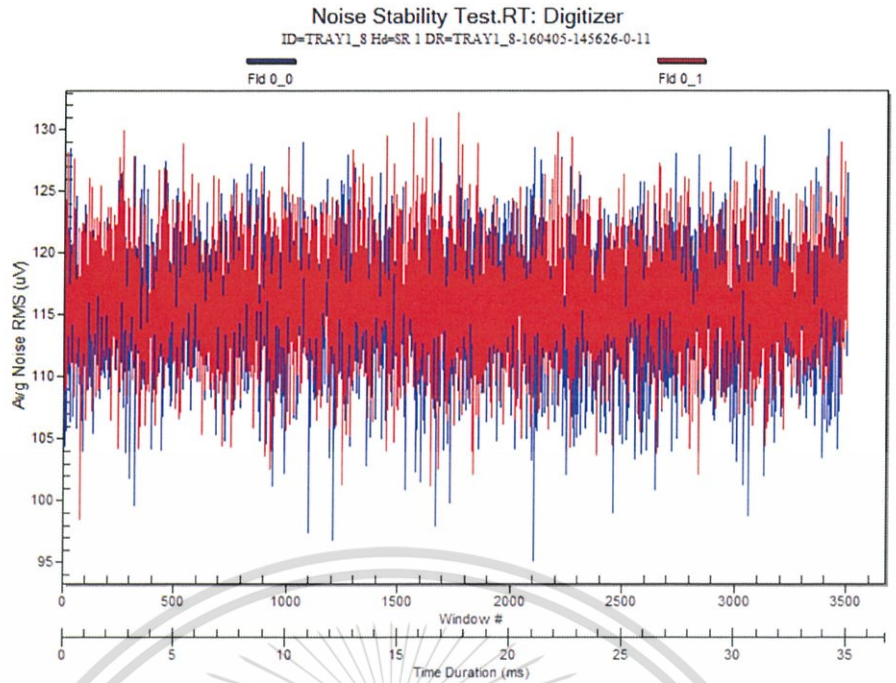

(b)

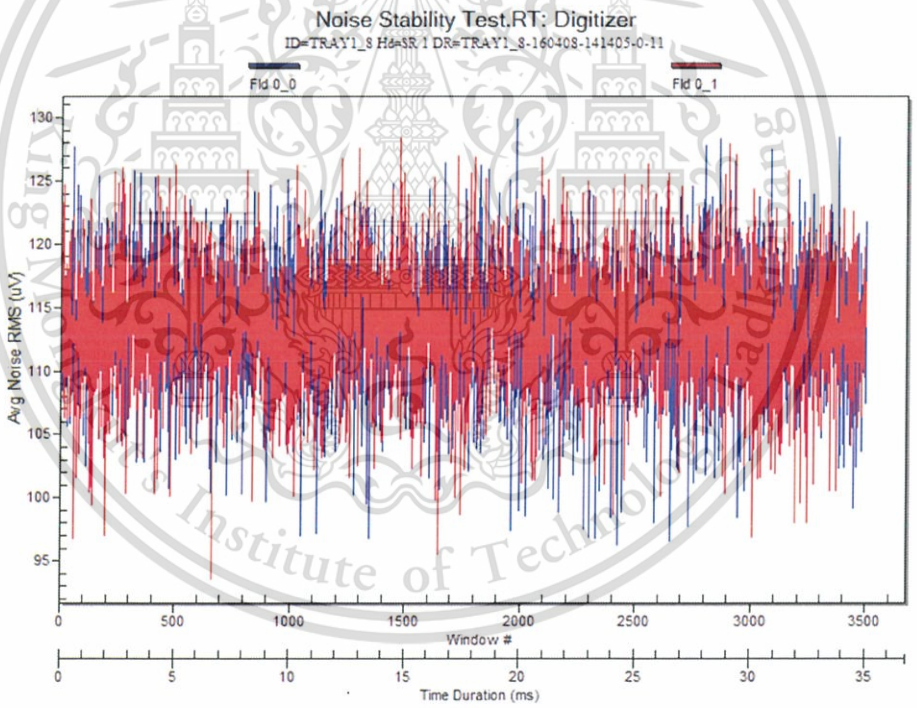

Figure 4.9.3 Example of QST noise stability (μV), source = **walkie-talkie,** D = 100 mm., Ground-Metal-Contact, (a) pre-HGA process (b) post HGA process

(a)

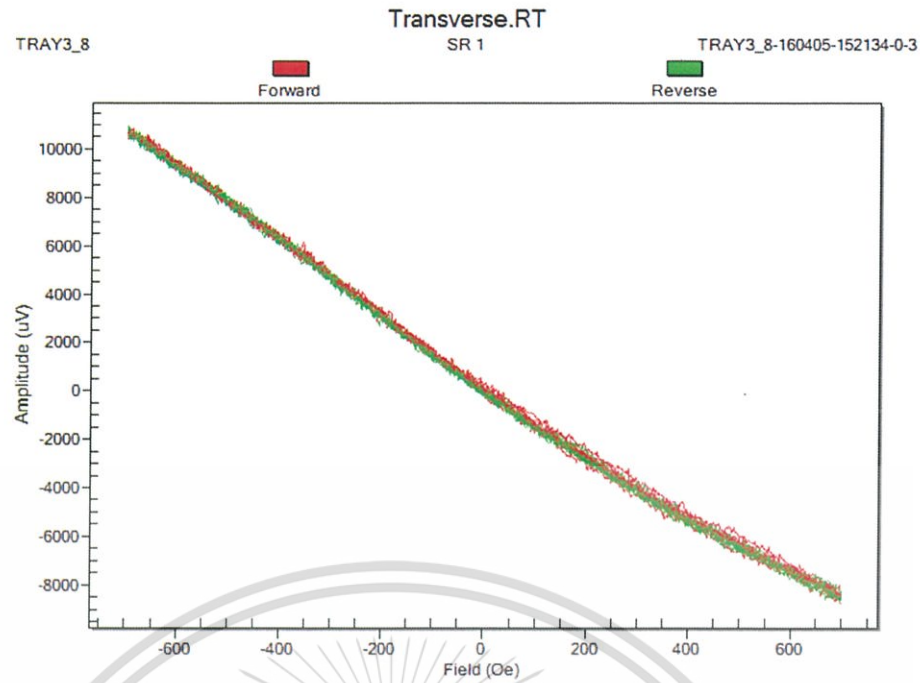

(b)

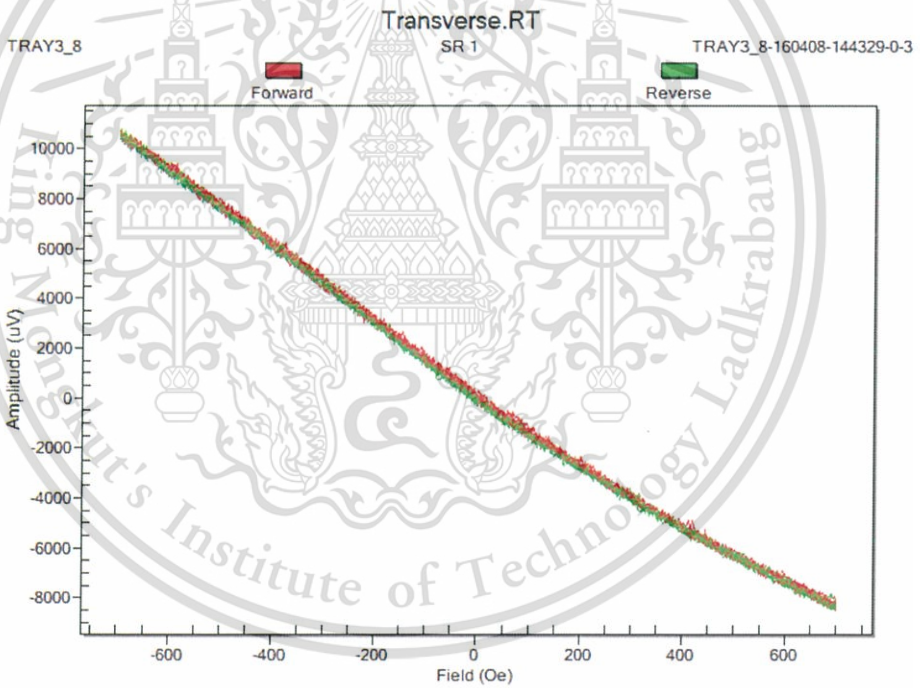

Figure 4.10.1 Example of QST transverse of TGMR amplitude (μV), source = **WiFI router**, D = 100 mm, Ground-Metal-Contact, (a) pre-HGA process (b) post HGA process.

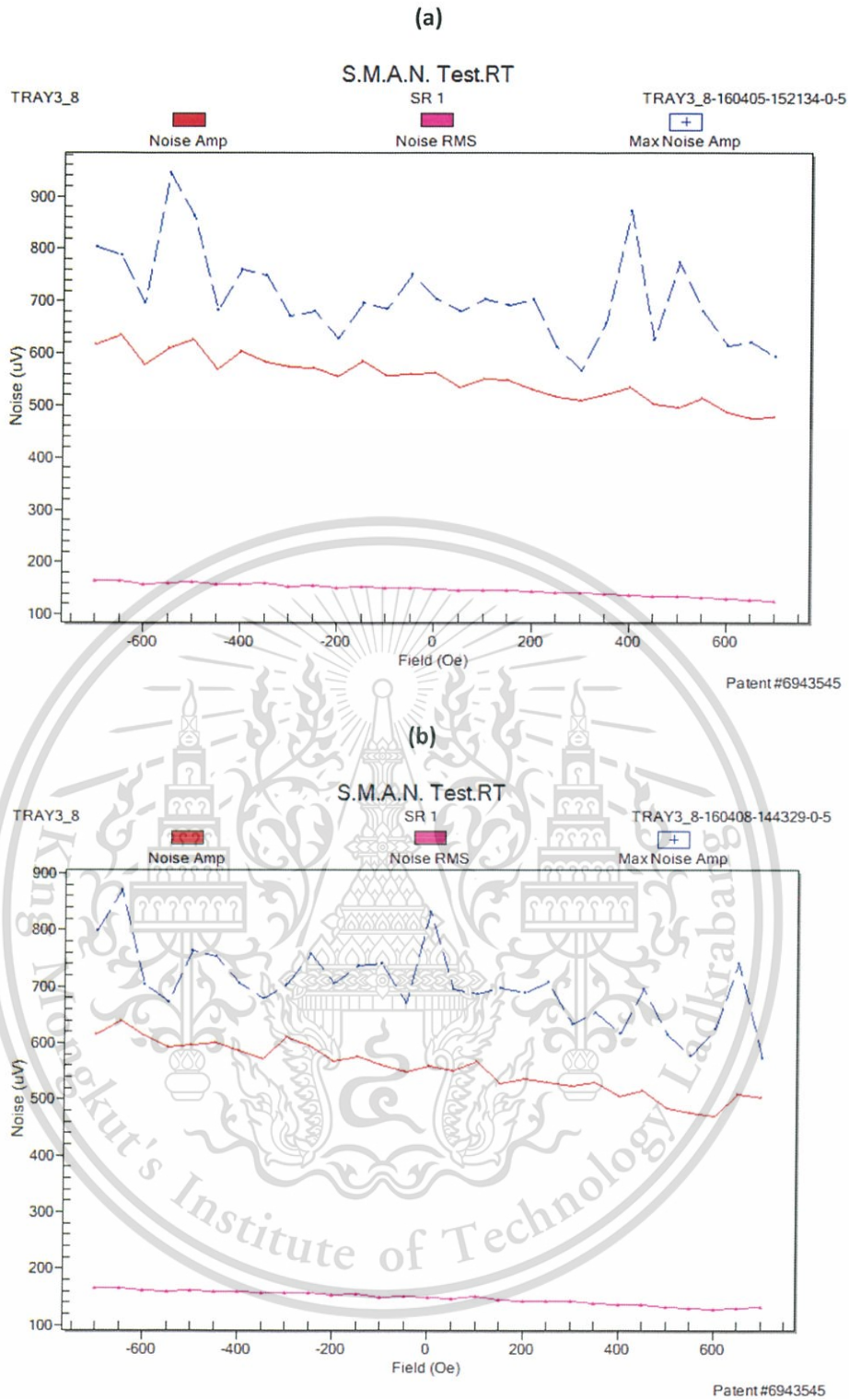

Figure 4.10.2 Example of QST S.M.A.N. (μV), source = WiFI router, D = 100 mm., Ground-Metal-Contact, (a) pre-HGA process (b) post HGA process

(a)

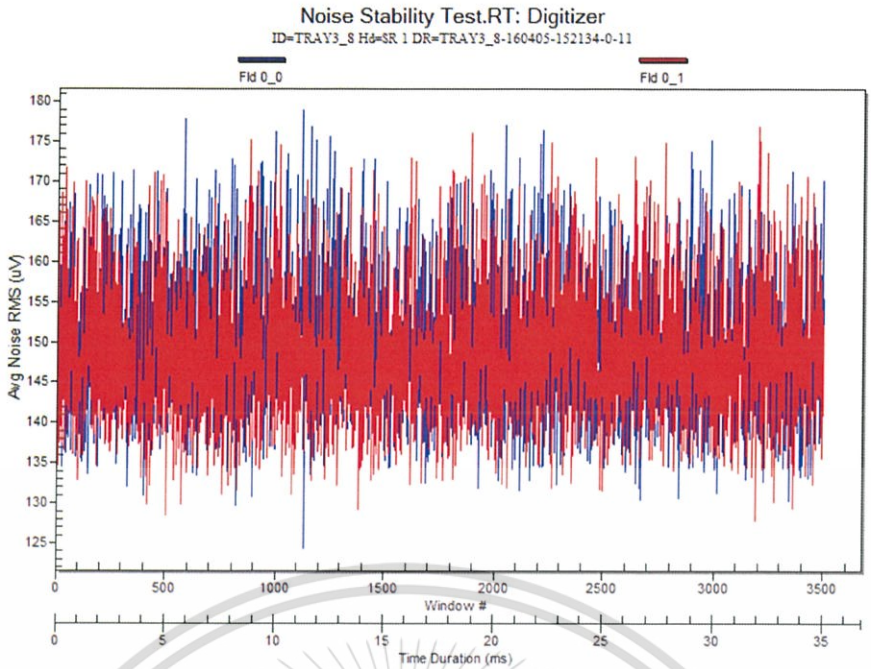

(b)

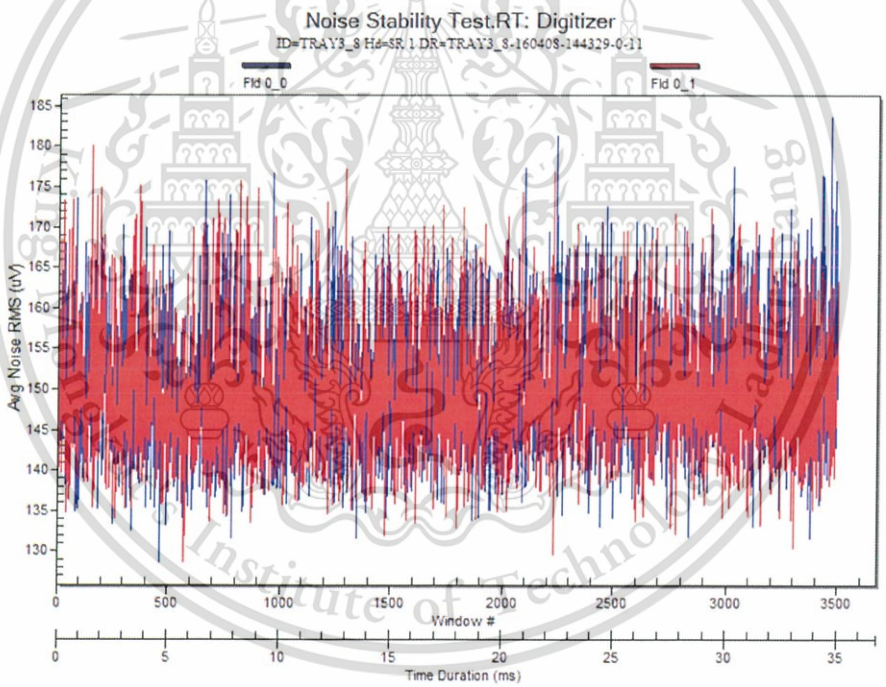

Figure 4.10.3 Example of QST noise stability (μV), source = WiFI router, D = 100 mm, Ground-Metal-Contact, (a) pre-HGA process (b) post HGA process

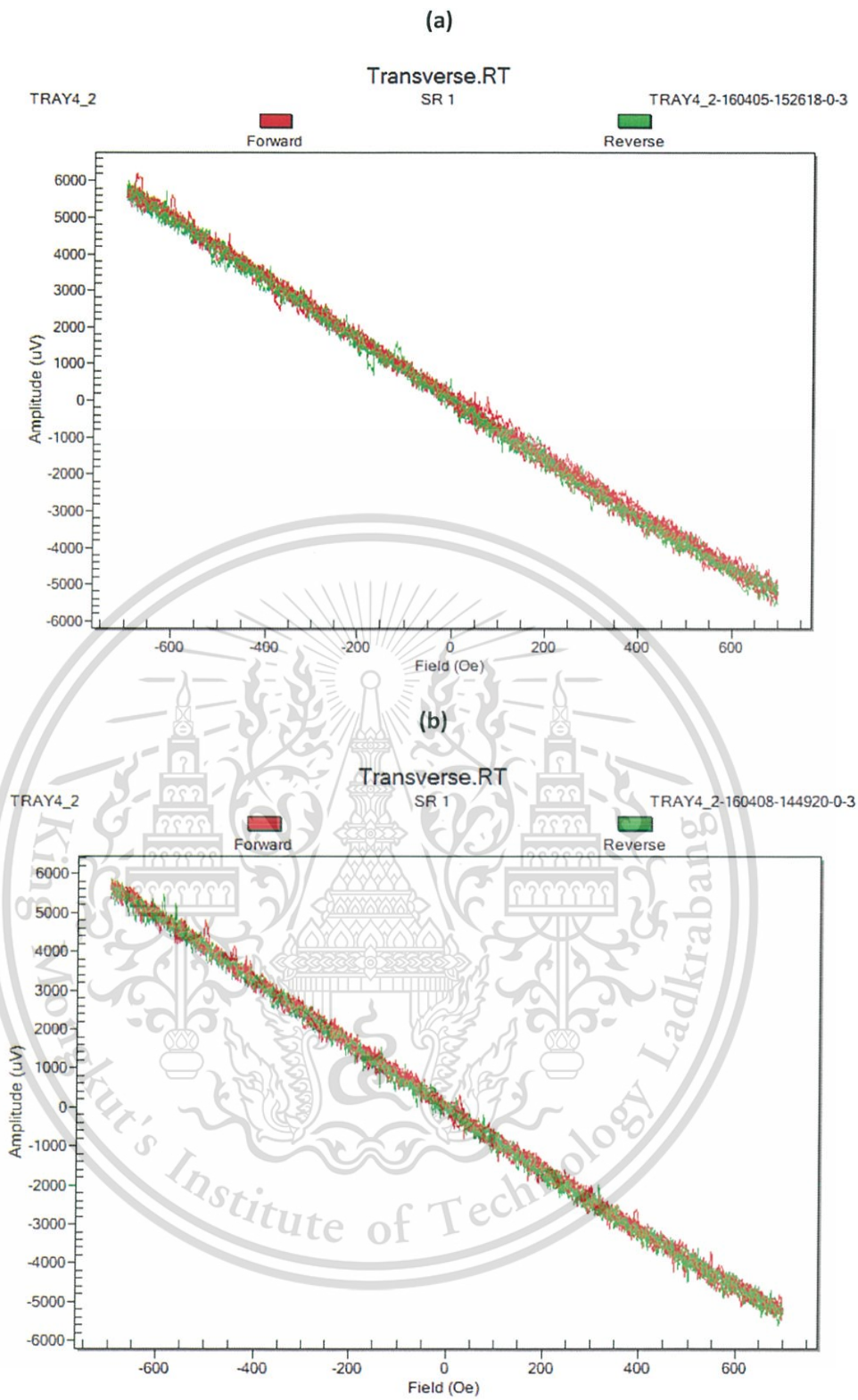

Figure 4.11.1 Example of QST transverse of TGMR amplitude (μV), source = cell phone, D = 100 mm, Ground-Metal-Contact, (a) pre-HGA process (b) post HGA process.

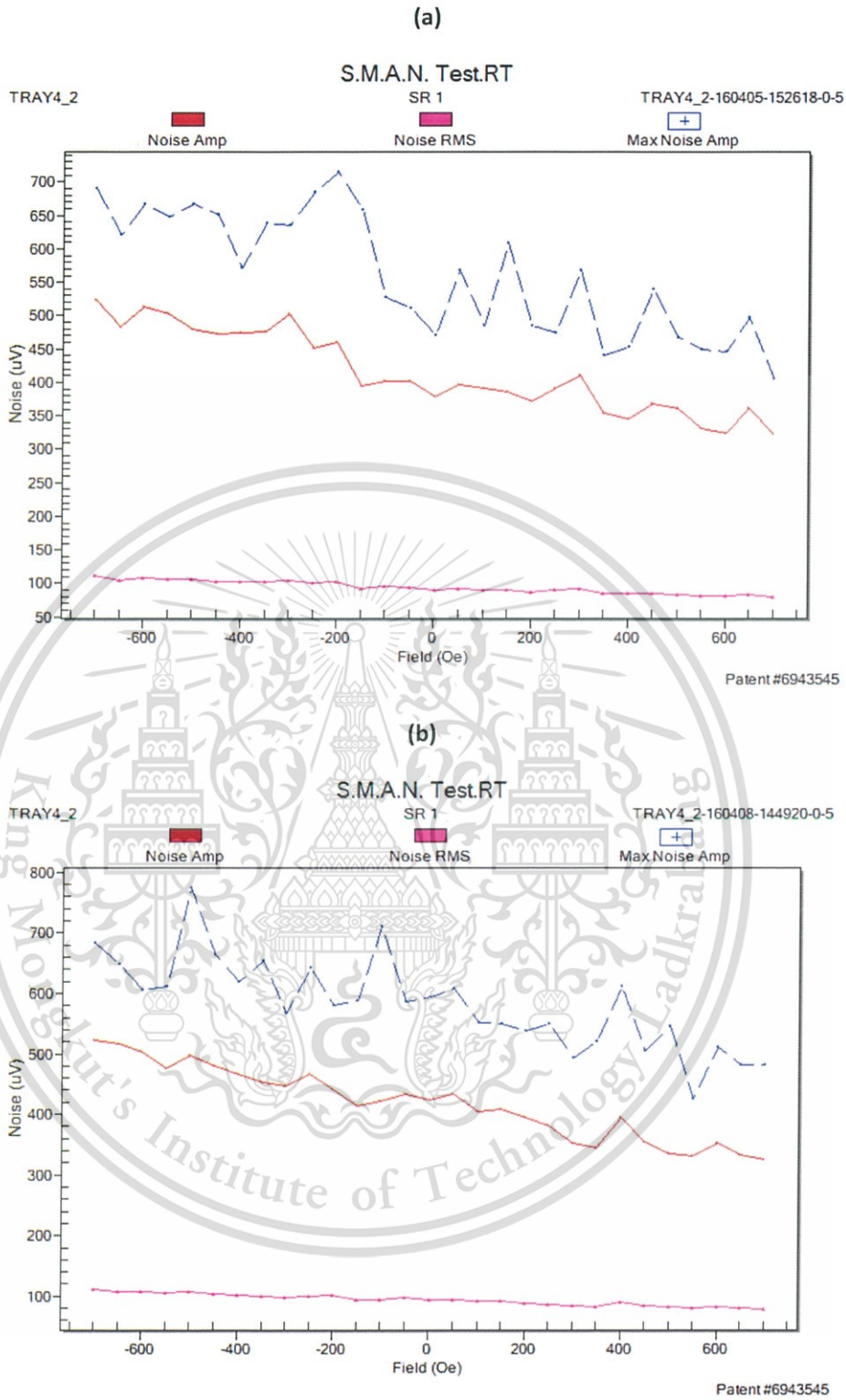

Figure 4.11.2 Example of QST S.M.A.N. (μV), source = cell phone, D = 100 mm, Ground-Metal-Contact, (a) pre-HGA process (b) post HGA process

(a)

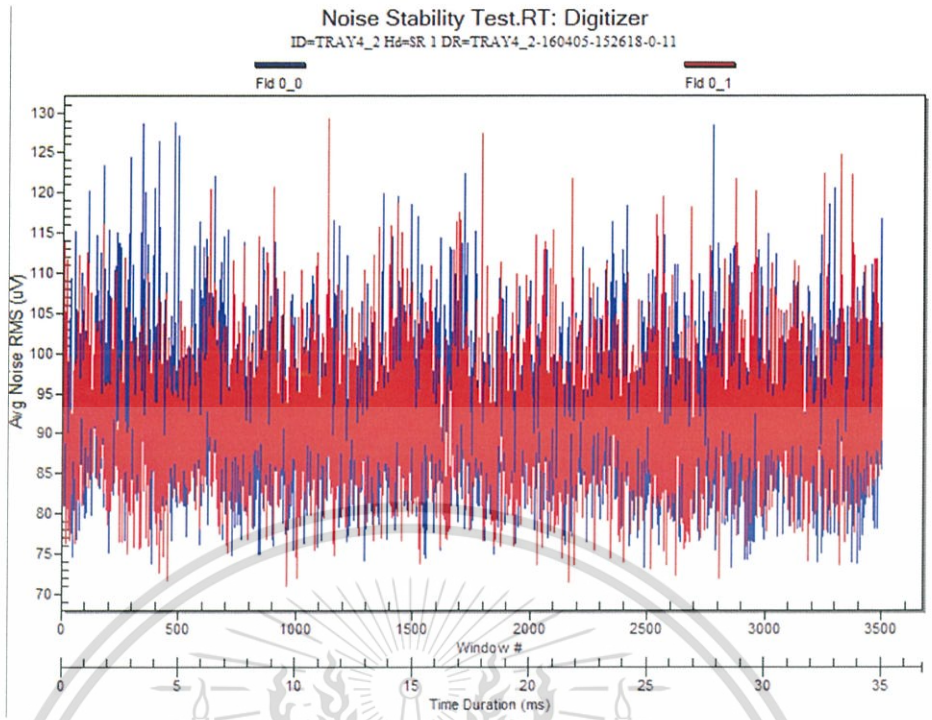

(b)

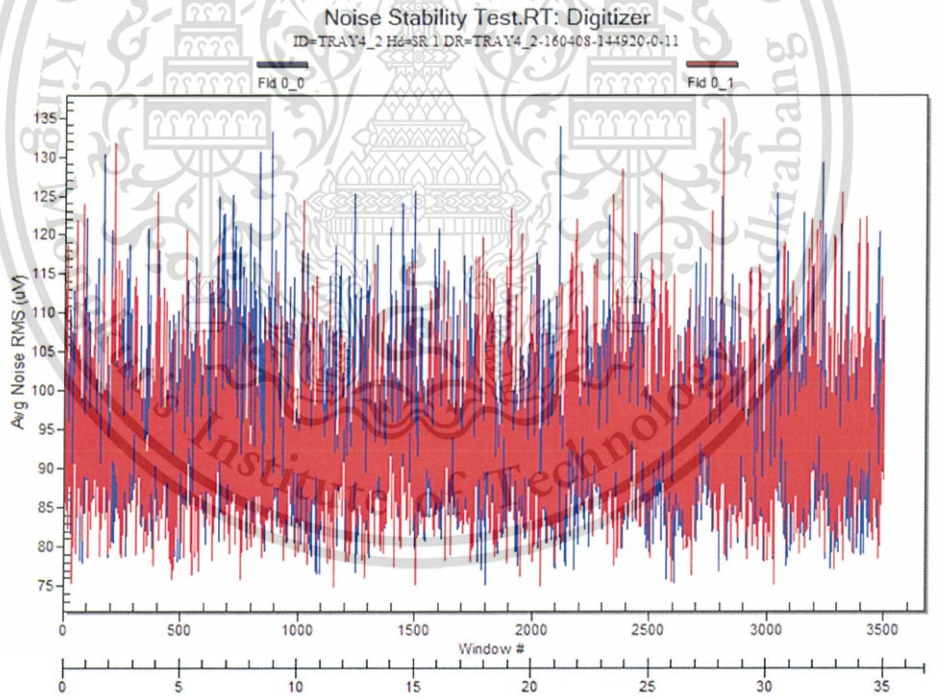

Figure 4.11.3 Example of QST noise stability (μV), source = cell phone, D = 100 mm., Ground-Metal-Contact, (a) pre-HGA process (b) post HGA process

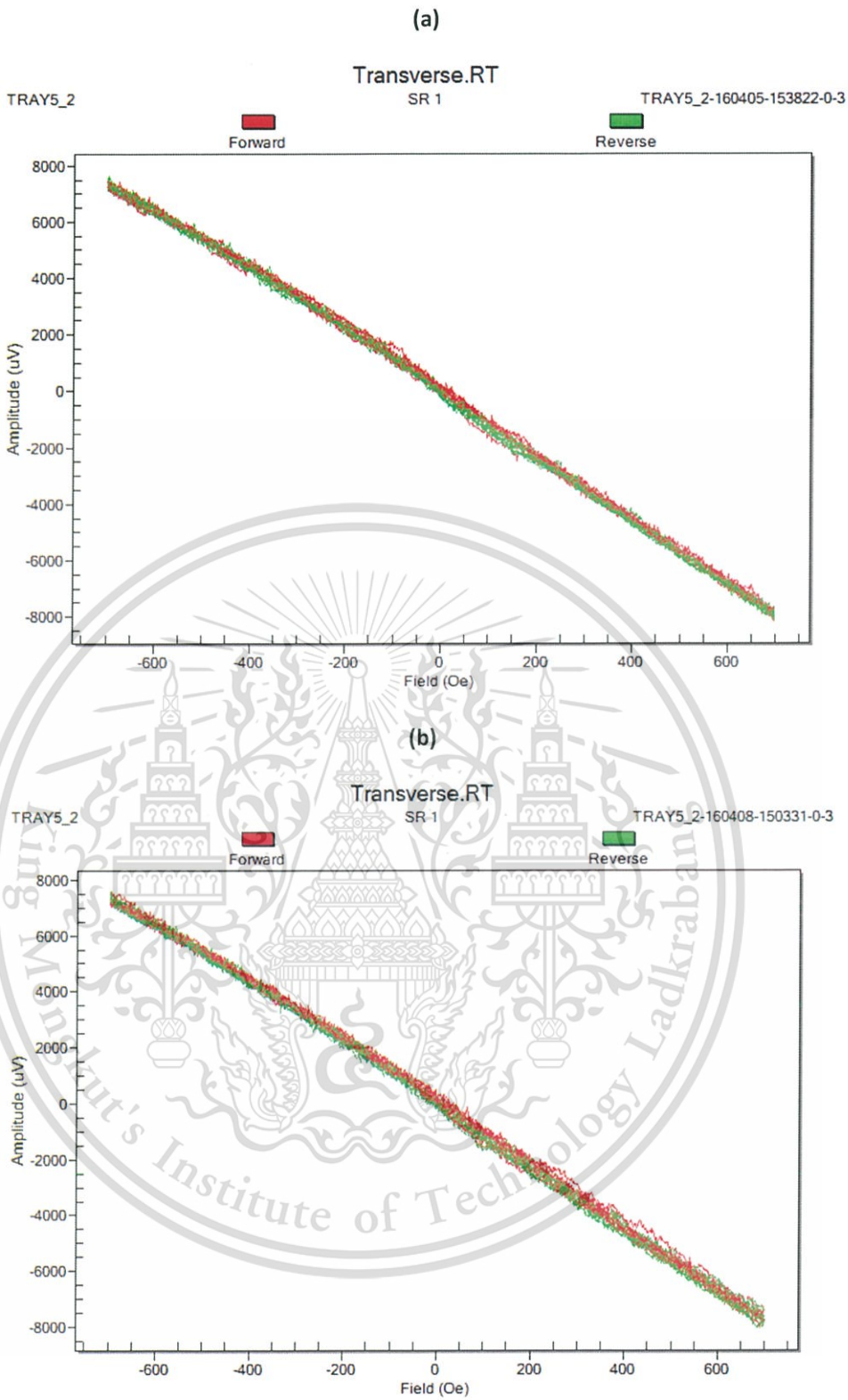

Figure 4.12.1 Example of QST transverse of TGMR amplitude (μV), source = tablet, D = 100 mm, Ground-Metal-Contact, (a) pre-HGA process (b) post HGA process.

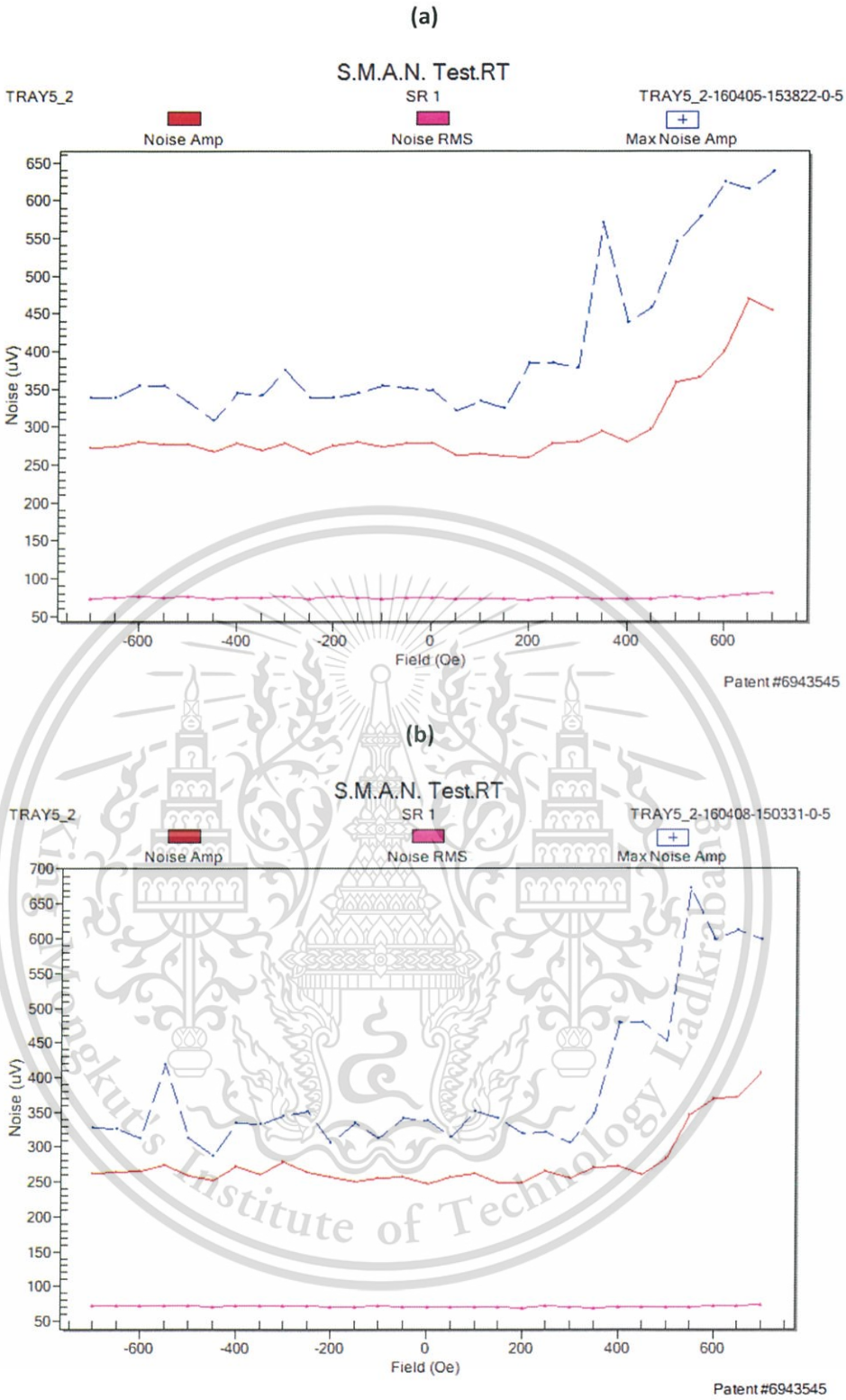

Figure 4.12.2 Example of QST S.M.A.N. (μV), source = tablet, D = 100 mm, Ground-Metal-Contact, (a) pre-HGA process (b) post HGA process

(a)

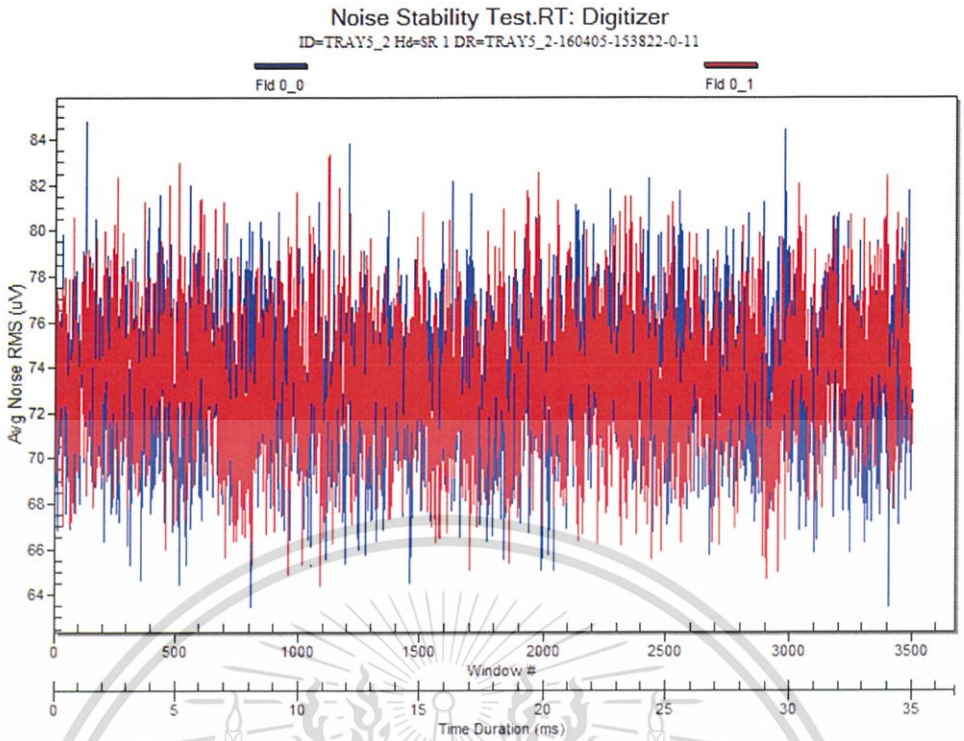

(b)

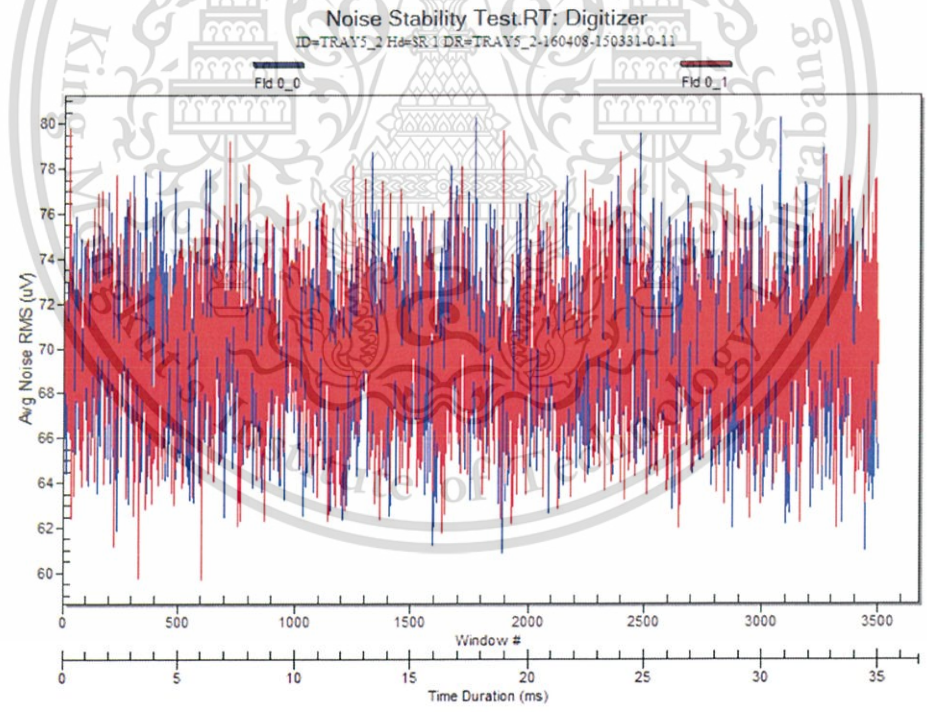

Figure 4.12.3 Example of QST noise stability (μV), source = tablet, D = 100 mm, Ground-Metal-Contact, (a) pre-HGA process (b) post HGA process

(a)

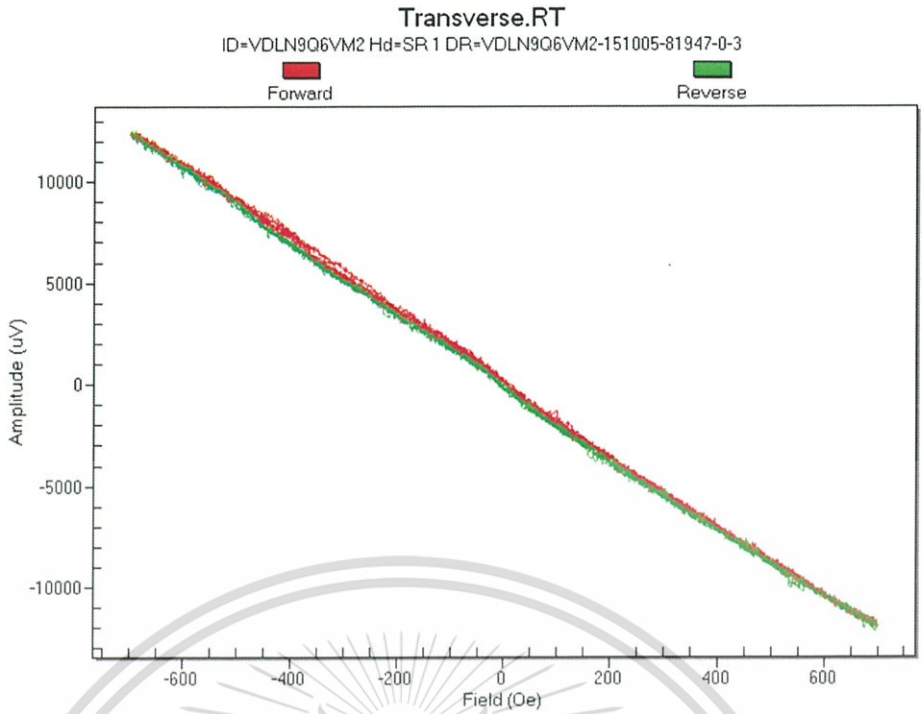

(b)

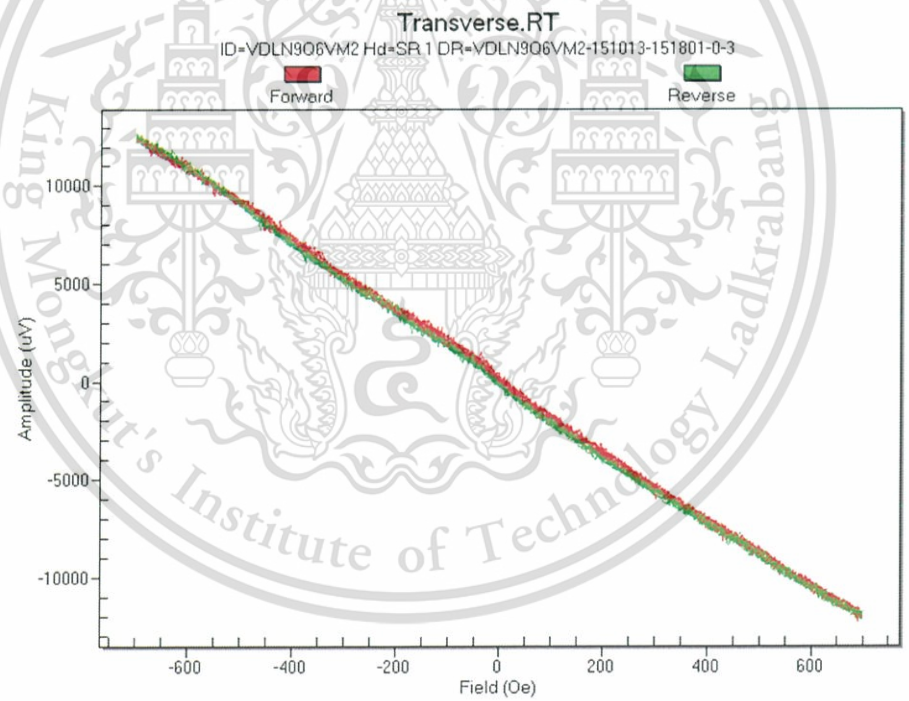

Figure 4.13.1 Example of QST transverse of TGMR amplitude (μV), source = WiFi phone, D = 100 mm., Ground-Metal-Contact, (a) pre-HGA process (b) post HGA process.

(a)

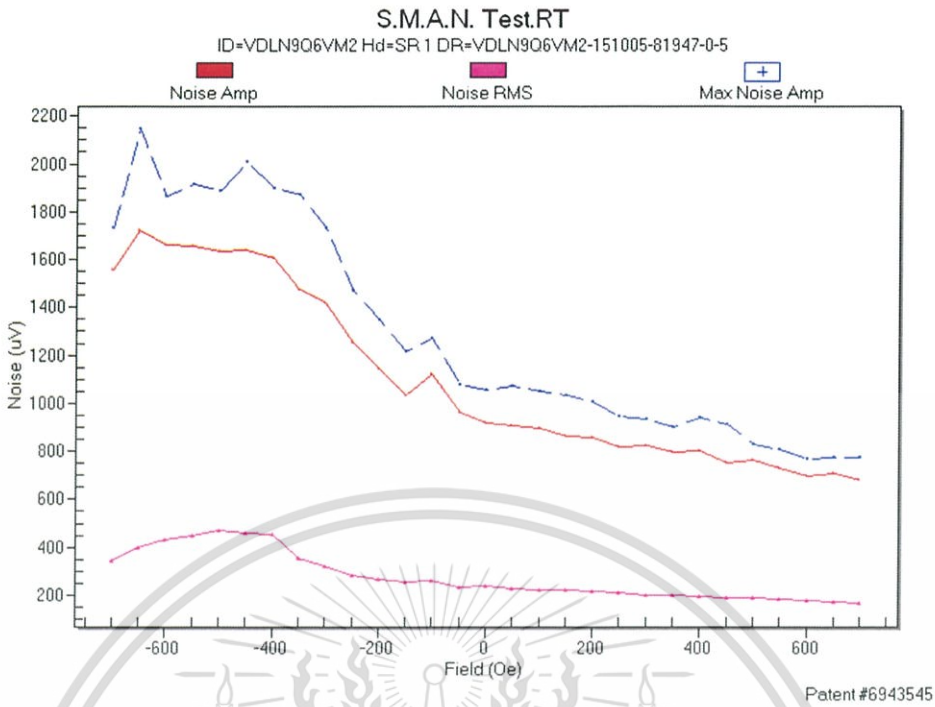

(b)

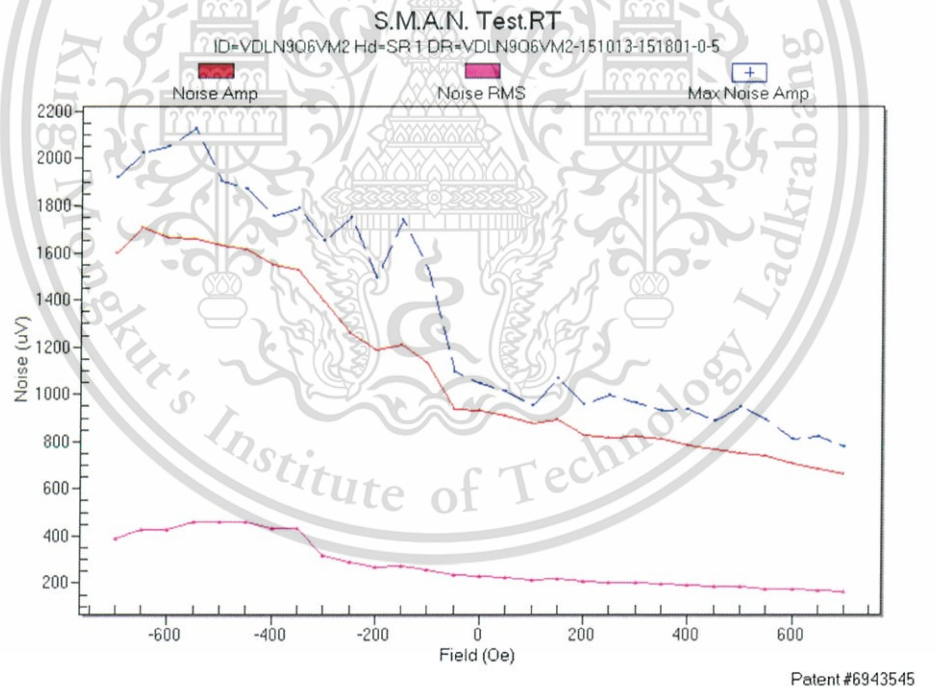

Figure 4.13.2 Example of QST S.M.A.N. (μV), source = WiFi phone, D = 100 mm, Ground-Metal-Contact, (a) pre-HGA process (b) post HGA process

(a)

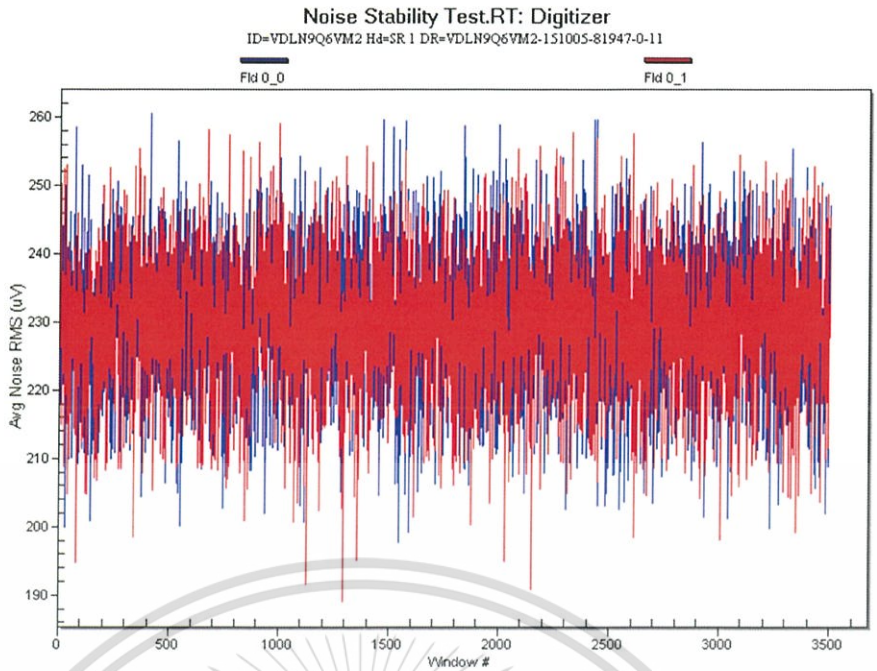

(b)

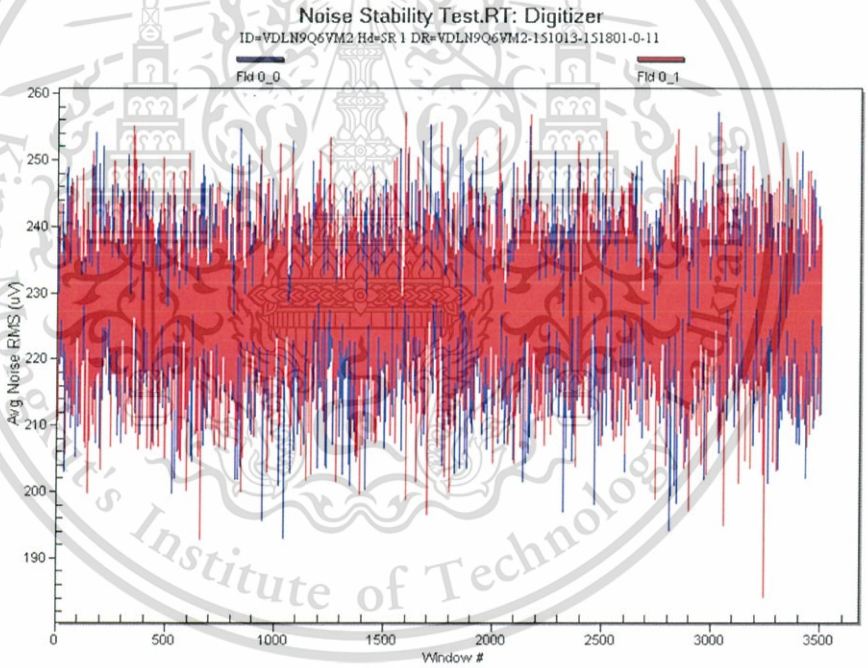

Figure 4.13.3 Example of QST noise stability (μV), source = WiFi phone, D = 100 mm, Ground-Metal-Contact, (a) pre-HGA process (b) post HGA process

CHAPTER 5

CONCLUSION AND SUGGESTION

5.1 Conclusions

The major objectives of this research are to investigate the effect of using wireless communication devices in Head Gimbal Assembly process on the Tunneling Giant Magnetoresistive read head of hard disk drive. Research overview is illustrated in Figure 5.1.

The first objective is to find out what kind of wireless communication devices generate significant electromagnetic interference (EMI), in the form of electric or magnetic fields, than others. And to know the most influence direction of the wireless communication device to its field strength. The measurement results from experiment A showed that,

- ✓ Distance is the main effect to electric field. The maximum electric field strength was found at the closest measurement distance, 25.4 mm, as expected.
- ✓ Direction or orientation of wireless communication devices to the measurement antenna plays important role to the electric field strength as well.
- ✓ Walkie-talkie, WiFi router, cell phone 1, tablet, WiFi phone propagated descending strong electric field of 12, 10, 8.4, 2.7 and 1.8 V/m accordingly.
- ✓ Regression analysis fit to reverse exponential model ($ln\ (Electric\ Field\ (V/m)) = -a_1\ Distance\ (mm) - b_1$), with coefficient of determination (R^2) of about 90%. The coefficient a_1 is specific to a wireless communication device while constant b_1 related to the X Y Z directions.

- ✓ Electric field from cell phone 2, laptop, mouse and keyboard were as weak as background noise of less than 1 V/m. The weak signals result unpredictable electric field versus distance and direction as explained by R^2 of less than 40%.
- ✓ Result of this experiment makes understanding of the 'causes', sources of interference which are the wireless communication devices.

The second objective is to observe actual voltage dropped and estimate temperature of TGMR, which are primary effects, while it exposed to the field of wireless communication device. Then compare actual measurement result with TGMR damage threshold. Result from experiment B,

- ✓ Observed change of voltage drops on TGMR and change of DETCR temperature, while placing HGA in the field of wireless communication.
- ✓ The voltage dropped and temperature of TGMR rank the same way of electric field ranking in experiment A. The highest to lowest field strength are from walkie-talkie, WiFi router, cell phone, tablet, WiFi phone respectively.
- ✓ TGMR experience 3518.96 μV or 4.28×10^{-8} J/s and 140.89 °C when exposing to walkie-talkie at 25.4 mm. This is way higher than the 2nd rank, WiFi router, which gave 4.766 μV or 2.14×10^{-13} J/s and 37.15 °C experiences to TGMR.
- ✓ The 3rd to the 5th rank, cell phone, tablet, WiFi phone made only less than 1.5 °C change on TGMR temperature and Joule heating power of 4.74×10^{-15} to 1.89×10^{-13} J/s in average.
- ✓ Regression to the distance of DC voltage and DETCR temperature can be explained in reverse exponential decay.
- ✓ From calculation, only Walkie-Talkie field can make TGMR reach its damage threshold of power and temperature. The other wireless communication devices are not able to, no matter how close they are to the TGMR

- ✓ Compared with the TGMR damage threshold at 20 nJ/s and 100 °C, using walkie-talkie at closer than 110.80 mm seem to be only possible threat to TGMR damage. But if the TGMR damage threshold changes to be 25 nJ/s and 120 °C, the critical distance is changed to be 79.85 mm.
- ✓ Invention of tools and technique from this experiment is the application of build-in Differential-End Temperature Coefficient Resistance (DETCR), Agilent 34410A DMM with shielded-cables and Modified Gryphic probe to measure TGMR temperature while exposing to the electric field. This technique could be applied to observe TGMR behavior in variety of situation.

The third objective is to confirm actual effect to performance of TGMR in HGA assembly process while exposing to the field of wireless communication device.

- ✓ Actual result of Quasi-Static test Pre-HGA-Process VS Pose-HGA Process came out as expected. It confirmed agreement with Experiment B.
- ✓ There is no change in both catastrophic or hard failure parameters (TGMR resistance, amplitude, slope) and soft failure or instability parameters (asymmetry, Barkhausen-Jump, hysteresis loop, and Spectral Maximum Amplitude Noise) were observed.
- ✓ Individual test data had been compared with total samples of 220 HGAs in all experiment conditions. Final conclusion is that, wireless communication devices in the distance of not less than 100 mm to TGMR, in HGA processes, are harmless to the TGMR.

The forth objective is to provide guideline of methodology to assess risk as well as suggestion of controlling its effect to TGMR heads in HGA assembly process. Table 5.1, summary of the methodology, illustrated design of experiment, output

parameters, tools and technique for each step of thought to assess risk from wireless communication devices to TGMR read head. The steps of thought consist of,

- ✓ Understand sources of interference (wireless communication devices)
- ✓ Understand how TGMR response to interference at the moment of exposure
- ✓ Predict critical distance (mm) of wireless communication devices compared to TGMR failure threshold
- ✓ Confirm the effect of electric field in HGA process to TGMR performance
- ✓ Decision & control of using the wireless communication in HGA process

In conclusion, this research meets all objectives and contributes to the industry to provide methodology to understand effect of wireless communication devices on TMR sensor in Head Gimbal Assembly process. As the technology has never been stopped developing, the knowledge from this research would help understanding how to assess risk from wireless communication devise and make proper control condition. Optimum selection and control of using wireless communication devices in the manufacturing environment will benefit to efficiency, quality, time to market and cost of the manufacturing.

Table 5.1 Methodology to assess risk from wireless communication devices to TGMR read head

STEPS OF THOUGHT	EXPERIEMENT	OUTPUT PARAMETERS	TOOLS & TECHNIQUES
Understand sources of interference (wireless communication devices)	Experiment A. Wireless communication devices – electric Field Survey	Significant Sources (V/m) Significant Direction (X, Y, Z) Significant Distance (mm)	CTM048 EM Field Meter with CTS001 directional antenna and electromagnetic field module.
Understand how TGMR response to the interference at the moment of exposure	Experiment B. TGMR in the field of wireless communication device	Thermal change ($^{\circ}$C) DC voltage dropped (μV) : Calculate to Power (J/s)	Agilent 34410A DMM with shielded-cables Modified Gryphic probe to match with HGA leads to be probed HGA with build-in DETCR.
Predict critical distance (mm) of wireless communication devices		Critical distance (mm) from wireless device to TGMR	Regression analysis and Modeling of power and temperature versus distance. Calculate and compare with TGMR failure threshold
Confirm the effect of electric field in HGA process to TGMR performance	Experiment C. TGMR pre and post HGA assembly process with exposure to wireless device	TGMR: Resistance (ohms), Amplitude (μV), Slope (μV/Oe), Asymmetry (%), Barkhausen-Jump (%), Hysteresis Loop (%), S.M.A.N. (μV)	Simulating HGA in Automation Process, TGMR exposure to EM-Field / Quasi-Static Tester
Decision & control of using the wireless communication in HGA process	Data Analysis	Type (power/freq./electric field) Critical Direction (X, Y, Z) Critical Distance (mm)	Analysis of result and regression model from Experiment A and B

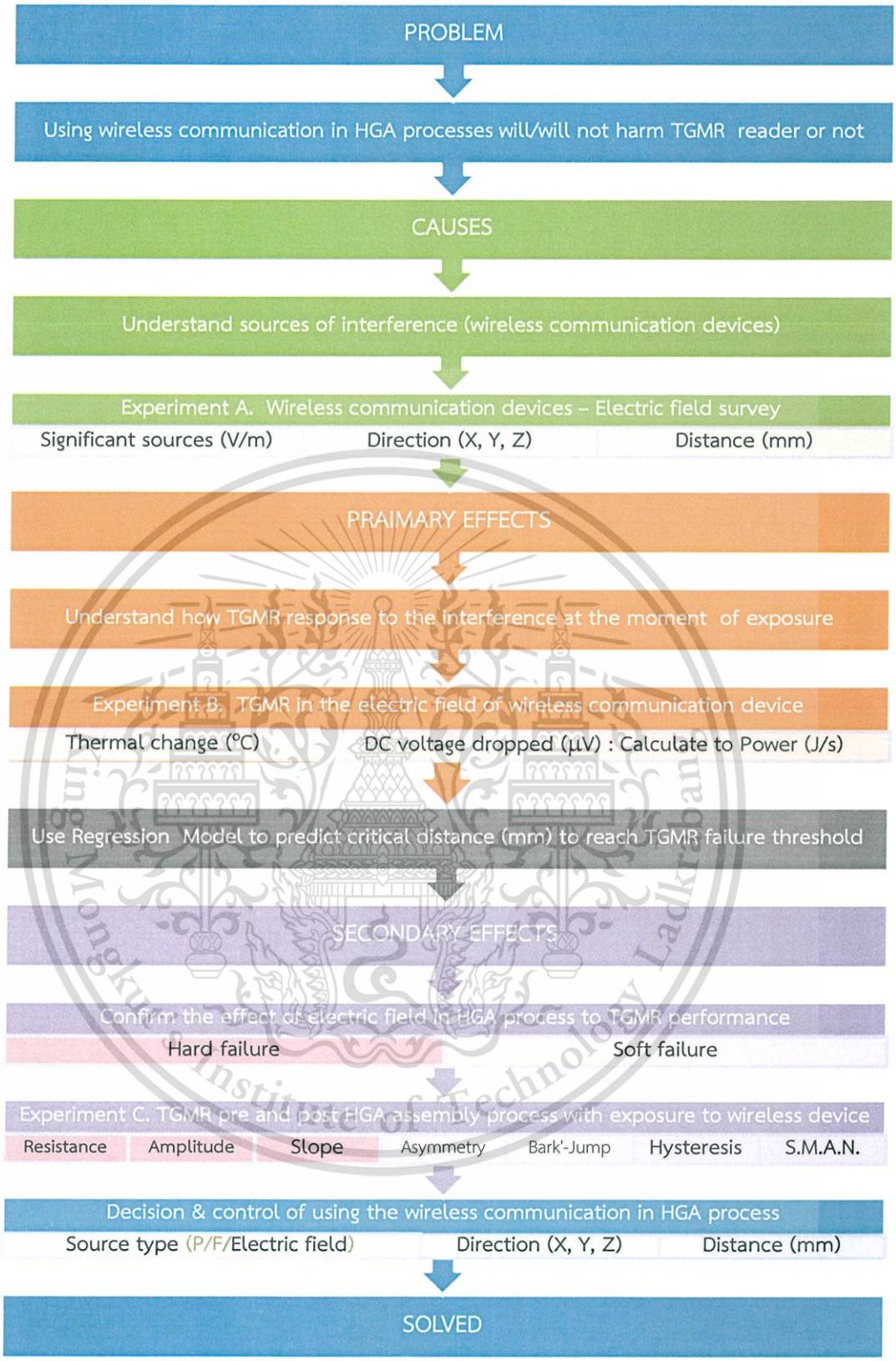

Figure 5.1 Overview of the research

5.2 Suggestions for further work

- This study is limited to specific design of TGMR, HGA, its process, type and specification of wireless communication devices as electric field sources. Same methodology can be applied to study different designs and technologies, whenever it is desired to be used.
- In this study, the cause portion, as shown in Figure 5.1 is only secondary causes, which are electric field, direction and distance. But primary causes such as transmitting frequency and power of wireless communication devices have not been yet measured and controlled in the experiment. The effect from transmitting frequency and power of wireless communication devices shall be studied as well. Since it may help selecting the wireless system from its technical specification.
- Due to limitation of distance setup in real HGA automated process is not to closer than 100 mm, the QST pre and post exposure cannot be done at critical distance to the TGMR damage threshold at 79.8 mm or closer. Further study shall find the way to setup process simulation at closer distance, to confirm the negative effect to the TGMR.
- To prevent victim from radiating coupling not only separate them by distance, but shielding technique could be applied as well.

REFERENCES

[1] Wallash A., Smith D., "EMI Damage to GMR Recording Head", **EOS/ESD Symposium,** 1998, no. 4B.6.1.

[2] Lam C.F., Martinez D., Chang C., "ESD Sensitivity Study of GMR Recording Heads with a FOS Head-Gimbal Assembly", **EOS/ESD Symposium,** 1999, no. 4B.6.2.

[3] Kraz V., Wallash A., "The Effect of EMI from Cell Phone on GMR Recording Heads and Test Equipment", **EOS/ESD Symposium,** 2000, no. 2C.10.1.

[4] Natori S., Wada T., Itou Y., Sakata H., Kataoka K., Tanabe H., Ohtsu T., "Study of EMI pheonomena for GMR/TMR Head", **EOS/ESD Symposium,** 2006, no. 4B.3.1.

[5] Kaengrang S., Kaewrawang A., "EMI Induce Heat on Tunneling Magnetoresistance Read Sensor", **DSTCON 4th,** 2011, pp. 61.

[6] Puapairoj S., Sa-ngiamsak C., "Effect of ESD and EMI on TMR Head during Bonding Process of Gold Ball Bonding Machines", **DSTCON 4th,** 2011, pp. 149.

[7] Kraz V., Tachamaneekorn P., Napombejara D., "EOS Exposure of Magnetic Heads and Assemblies in Automated Manufacturing", **EOS/ESD Symposium,** 2005, no. 4A.4.1.

[8] Zhao T., Zhang K., Wang H. C., Chen Y.H., Li M., Headway Technologies, Inc., "Low resistance tunneling magnetoresistive sensor with natural oxidized double MgO barrier", **US Patents,** US20070111332 A1, May 17, 2007.

[9] Dufresne M.A., Karr B.W., Kunkel G.J., Wei Z., Seagate Technology Llc,, **"Resistive Temperature Sensors for Improved Asperity, Head-Media Spacing, and/or Head-Media Contact Detection"**, US Patents, US20120120982 A1, May 17, 2012.

[10] Liu D., Haapala K., Ryun S.E., Zhou L., Seagate Technology Llc, **"Head-medium contact detection using introduced heat oscillation"**, US Patents, US8638349 B1, Jan 28, 2014.

[11] Patland H., Ogle W.A., Infinitum Solutions, Inc., "**Magnetic head tester**", US Patents, US6943545 B2, Sep 13, 2005.

[12] Patland H., Ogle W.A., "High Frequency Instabilities in GMR Heads Due to Metal-to-Metal Contact ESD Transients", **EOS/ESD Symposium**, 2002, pp. 130.

[13] Kruesubthaworn A., Sivaratana R., Ungvichianc V., Siritaratiwat A., "Testing Parameters of TMR heads affected by dynamic-tester induced EMI", **Journal of Magnetism and Magnetic Materials**, 2007, pp 316, e142-e144.

[14] Kruesubthaworn A., Pratoomthip A., Siritaratiwat A., Ungvichian V., "Anomalous Magnetic Responsiveness of Giant Magnetoresistive Heads Under Specific Electromagnetic Interference Frequencies Using Quasi-static Tester", **Journal of Applied Physics**, 2008, pp 103.

[15] Agarwal T., Electronics Projects Focus, "Different Types of Wireless Communication with Applications". [Online]. Available: https://www.elprocus.com/types-of-wireless-communication-applications/, 15th Nov 2015.

[16] Tikkanen. J., JJT Consulting Group. "Wireless EMI in Healthcare Facilities". [Online]. Available: http://www.blackberry.com/solutions/pdfs/Healthcare/Wireless_EMI_in_Healthcare_Facilities_White_Paper.pdf, 24th Dec 2012.

[17] Kraus. J.D., "**Electromagnetics**", 4th INT.ED, New York, McGraw-Hill, 1991.

[18] Collin. R.E., "**Fundamental for Microwave Engineering**", 2nd INT.ED, New York, McGraw-Hill, 1992.

[19] Dally J.W., Riley W.F, McConnell K.G., "**Instrumentation for Engineering Measurement**", 2nd ED, Singapore, John Wiley & Sons, 1993.

[20] Holman. J. P., "**Heat Transfer**", 10th ED, New York, McGraw-Hill. 2009.

[21] Poole. I., "EMI Electromagnetic Interference Basics". [Online]. Available: http://www.radio-electronics.com/info/circuits/emc-emi/electromagnetic-interference-basics-tutorial.php, 16th Oct 2013.

[22] Remzi H. "**Operating Systems: Three Easy Pieces, Chapter: Hard Disk Drives**". Arpaci-Dusseau Books, 2014.

[23] Wikipedia. "Hard disk drive". [Online]. Available: https://en.wikipedia.org/wiki/Hard_disk_drive, 29th May 2015.

[24] Illustrated by Wongpala. N., Seagate Technology.

[25] Han G. C., Qiu J. J., Wang L., Yeo W. K., Wang. C. C., "Perspectives of Read Head Technology for 10 Tb/in^2 Recording". **IEEE TRANSACTIONS ON MAGNETICS**, vol. 46, no. 3, MARCH 2010.

[26] Re. M., "Tech Talk on HDD Areal Density". Seagate Technology. [Online]. Available: http://www.seagate.com/www-content/investors/_shared/docs/tech-talk-mark-re-20150825.pdf . 2015.

[27] Ashar. K. G., "**Magnetic Disk Drive Technology: heads, medium channel interfaces, and integration**". New Jersey. IEEE Press. 1997.

[28] Seagate Technology PLC.

[29] Butler W.H., Zhang X.-G., Schulthess T.C., and MacLauren J.M., "Spin-dependent tunneling conductance of Fe|MgO|Fe sandwiches", **Phys** Rev. B 63, 054416. 2001.

[30] Childress J., Fontanair R., "Magnetic Recording Read Head Sensor Technology", **Comptes Rendus Physique**, 6(9), 997-1012.

[31] Kittel C., "**Introduction to Solid State Physics**", 8th ED, New York, John Wiley & Sons, 2005.

[32] Rybicki G. B., Lightman A. P., "**Radiative Processes in Astrophysics**", John Wiley and Sons, 1979.

[33] Puapairot S., "**Effect of Electric Field, Magnetic Field and Electromagnetic Radiation on TMR Heads During Gold Ball Bond Process**", A Thesis for the degree of Master of Engineering, Khon Kean University, 2012.

[34] Matsugi J., Nakano T., Mizoh Y., Nakamura K., Sakakima H., "ESD phenomena in GMR heads in the manufacturing process of HDD and GMR heads", **EOS/ESD Symposium**, 2003, p 1-7.

[35] Khan A. A., Schmalhorst J., Thomas A., Schebaum O., Reiss G., "Dielectric breakdown in CoFeB/MgO/CoFeB magnetic tunneling junction". **J.Appl. Phys.**, (103), 123705, 2008.

[36] Surawanitkun C., Kaewrawang A., Siritaratiwat A., Kruesubthaworn A., Sivaratana R., Jutong N., Mewes C. K. A., Mewes T., "Magnetic Instability in Tunneling Magnetoresistive Heads Due to Temperature Increase During Electrostatic Discharge". **IEEE Transactions on Device and Materials Reliability,** Year: 2012, Volume: 12, Issue 3, pp 570 – 575, 2012.

[37] Marongmued K., Sa-Ngiamsak C., "How Does Electrostatic Discharge Event Not Cause Polarity Flip in TMR Read Heads?". **IEEE Transactions on Magnetics**. Year: 2012, Volume: 48, Issue: 11, pp 3555 - 3558, 2012.

[38] Irshad S., "Electromagnetic Interference & Electromagnetic Compatibility". [Online]. Available: http://www.slideshare.net/sabeelirshad/electromagnetic-interference-electromagnetic-compatibility?next_slideshow=1, 7th Oct 2013.

[39] HGST, "Perpendicular Magnetic Recording Technology", [Online]. Available: https://www.hgst.com/sites/default/files/resources/PMR_white_paper_final.pdf, 30th Nov, 2007.

[40] 3M™ , "EM Eye Meter Handheld ESD/EMI Event Detector, EM Field, RF Signal Meter, User's Guide".

[41] Agilent Technologies, "Agilent 34410A/11A, 6 ½ Digit Multimeter, User's Guide".

APPENDIX A

PUBLICATION

Parts of this work has been published and presented in 2016 the 3rd International Conference on Advances in Electronics Engineering (ICAEE 2016) during February 22-23, 2016 in Hong Kong. It had been published in MATEC Web of Conferences vol. 54 (2016), ISSN: 2261-236X, regarding to 2016 7th International Conference on Mechanical, Industrial, and Manufacturing Technologies (MIMT 2016). This study also had been presented and published in The 2nd International Conference on Engineering Science and Innovative Technology (ESIT2016) during April 21-23, 2016 in Phuket, Thailand.

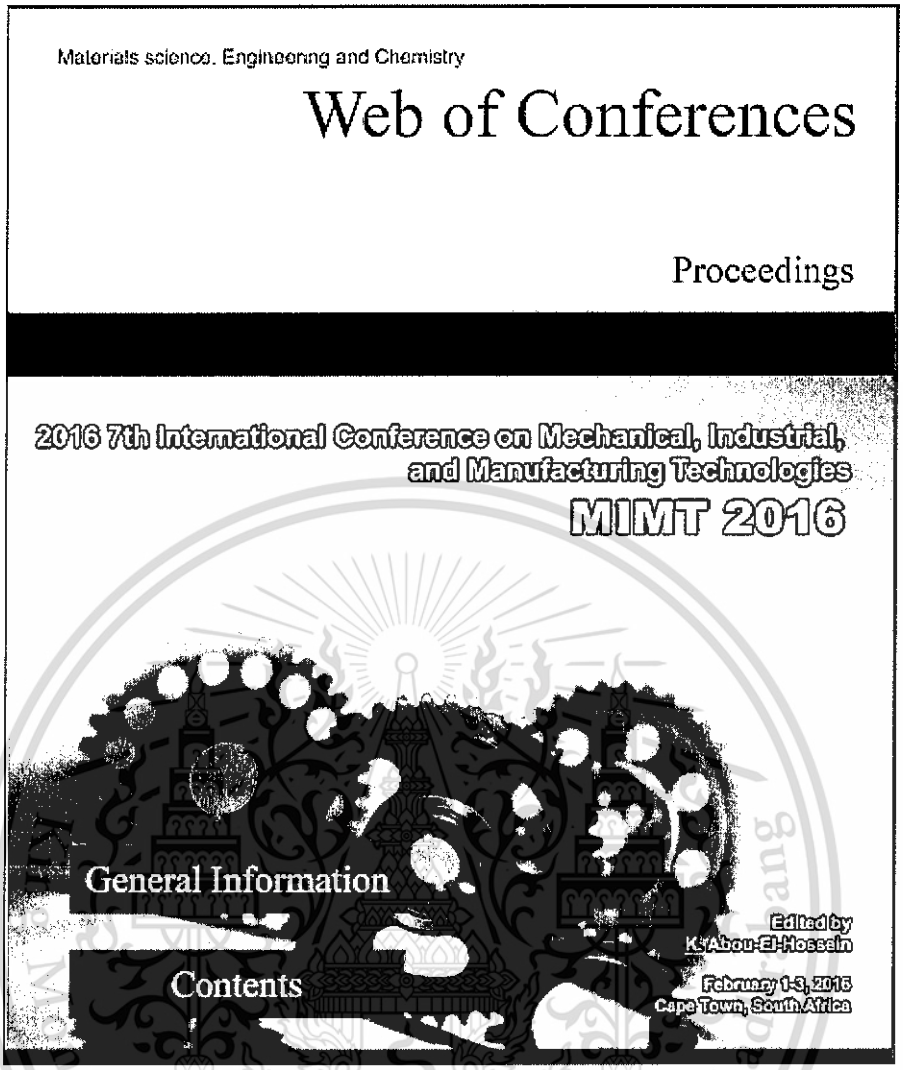

ICAEE 2016

CERTIFICATE
of
PARTICIPATION

Paper Title: *Wireless Communication and Its Effect to Tunneling Giant Magneto-Resistive (TGMR) Reader in Head Gimbal Assembly Process (A203)*

This is to certify *Dutharuthai Na Pombejara* from *King Mongkut's Institute of Technology Ladkrabang, Thailand* has attended and delivered an oral presentation on 2016 the 3rd International Conference on Advances in Electronics Engineering (ICAEE 2016) held during February 22-23, 2016 in Hong Kong.

Conference Committee
ICAEE 2016

Feb. 22-23, 2016 Hong Kong

MATEC Web of Conferences 54, 09004 (2016) DOI: 10.1051/matecconf/20165409004
MIMT 2016

Wireless Communication and Its Effect to Tunneling Giant Magneto-Resistive (TGMR) Reader in Head Gimbal Assembly Process

Dutsarutsai Na Pombejara [1,2], Chaiyan Jettanasen [2], Kraiporn Ritipad [3]

[1]College of Data Storage Innovation, King Mongkut's Institute of Technology Ladkrabang, Thailand
[2]Faculty of Engineering, King Mongkut's Institute of Technology Ladkrabang, Thailand
[3]Seagate Technology (Thailand) Ltd. Nakornratchasima, Thailand

Abstract. TGMR reader is current technology of magnetic recording read sensor which dramatically improves readout amplitude, speed and recording areal density. In advanced manufacturing environment, automated tools are increasingly used and wireless communication device is aimed to be employed to enhance the operation efficiency. However, electromagnetic fields from wireless communication devices could harm or damage the most energy sensitive devices/equipment, such as TGMR reader sensor, in hard gimbal assembly process. This study surveys, therefore, electromagnetic interference from wireless communication devices using GTM04, EM Field Meter with GTN001 directional antenna and electromagnetic field module, then use Agilent 34410A to measure TGMR resistance and thermal charge of TGMR head while placing in the fields of wireless communication device. Built-in Differential Failed Temperature Coefficient of Resistivity sensor is utilized for proximal TGMR temperature. Impact to electrical performance of TGMR pre and post actuators simulating HGA assembly process will be ocntrued using Quasi-static Tester.

1 Introduction

Nowadays wireless communication has been integrated to every activity owing to its convenience. Such interference may cause undesirable effects to sensitive equipment or sensitive devices. There were some studies about Electromagnetic Interference (EMI) effect to magnetic recording head, but nine of them studied on real TGMR head. Previous studies about EMI effect from wireless communication were done on 5 Gb/in^2 PtMn GMR sensors [1] [2] [3], while current technology is up over 500 Gb/in^2 sensor. A study mentioned about TGMR head, but no technical discussion or end result of TGMR sensor impact presented in the paper [4]. Newer studies had simulated TGMR sensor impact in stand-alone stage. The consideration of connection to slider body (Key components of Slider are Reader, Writer and Advance Air Bearing Surface), Trace-Gimbal Assembly (TGA), suspension or other assembly was excluded from simulation scope [5] [6]. A study concludes that magnetic heads in production can be exposed to electrical overstress exposure of different types due to the ultra-sensitive nature of magnetic heads [7]. This study is to confirm if the electromagnetic fields from wireless communication devices will harm the most energy sensitive devices, such as TGMR recording reader sensor, in assembly process.

2 Structures and Process

2.1 The difference between Giant Magneto-Resistive (GMR) and Tunneling Giant Magneto-Resistive (TGMR) head structure

GMR Current-in-Plane (CIP) architecture has been replaced by TGMR Current Perpendicular (CPP) architecture to allow higher data recording density.

Key distinguishing element of TGMR is Magnetic Tunnel Junction (MTJ), which consists of two ferromagnets separated by an angstrom-thin insulator. Electrons can tunnel from one ferromagnet to the other if the barrier is thin enough. With this quantum-mechanical phenomenon, the MTJ can be switched between two states of electrical resistance, high resistance and low resistance, then provides higher MR Ratio ($\Delta R/R_0$: change of TGMR resistance/minimum resistance of TGMR), higher readout amplitude and speed as well as lower areal resistance ($R\cdot A$: Resistance x Area) and head noise [8].

TGMR resistance is ten times higher than GMR resistance. This makes TGMR undergoing ten times higher joule heat than GMR. The angstrom-thin metal oxide barrier makes TGMR more susceptive to external energy. Fortunately, not like GMR, the TGMR head do not have insulator between buffer and shield, so TGMR can dissipate thermal directly through top and bottom

MATEC Web of Conferences **54**, 09004 (2016) DOI: 10.1051/matecconf/20165409004
MIMT 2016

metal shield. Example of simplified structure of GMR and TGMR recording reader head are explained in **Figure1** and **Figure2**. Actual structure and material may be difference base on design and fabrication.

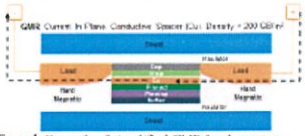

Figure1. Example of simplified GMR head structure.

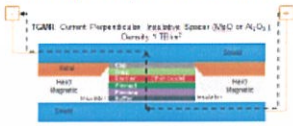

Figure2. Example of simplified TGMR head structure.

2.2 Head-Gimbal Assembly and its process

Head-Gimbal-Assembly (HGA) is an important piece part of Hard Disk Drive in which slider body, which containing read-write head, located and flies above magnetic recording media.

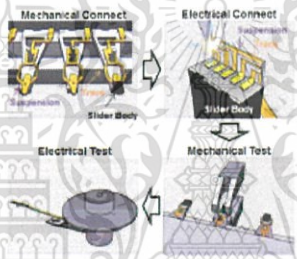

Figure3. Head-Gimbal Assembly process steps

The manufacturing process of Head-Gimbal Assembly is basically in full automation. As shown in Figure 3, robot end-effector pick-and-place each piece part, make mechanical connection and electrical connection between Trace Gimbal Assembly (TGA) and Slider body. Then check performance via mechanical test and electrical test processes. Piece parts of HGA are contacted and uncontacted with grounded metal or static dissipative material many times along the automated process.

3 Experiment and discussion

3.1 Wireless communication devices in factory environment - Electromagnetic Interference

Electric Field from wireless communication devices is measured using CTM048, EM Field Meter with CTS001 directional antenna and electromagnetic field module. This measuring instrument has Peak and Average Measurement Range of 0.001 V/m - 20.00 V/m, Frequency Bandwidth of 1 MHz to 2.5 GHz, Antenna Factor Range of -40.0 to 40.0 dBm-1, Antenna Frequency Response of 10 MHz – 2.5 GHz. The measurement is performed in empty large shield room, at distance of 1 inches (25.4 mm) between CTS001 antenna and wireless communication devices, which are (1) Portable Two-way Radio Transceiver (walkie-talkie), (2) Wireless LAN Access Point (WiFi router), (3) GSM Cellular phone, (4) Cordless phone, (5) Laptop computer, and (6) Wireless mouse & Keyboard set.

In **Figure4**, the result shows that E-Field of higher than 5 V/m is observed from three types of wireless communication devices, Portable Two-way Radio Transceiver, GSM Cellular Phone and Cordless Phone. Whereas the E-Field of higher than 1 V/m is observed

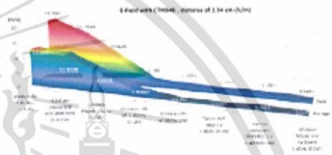

Figure4. Result of Electric field survey of wireless communication devices

3.2 Thermal change and DC voltage of TGMR head while placing in the field of wireless communication device

Build-in Differential-Ended Temperature Coefficient of Resistivity (DETCR) sensor [9] [10] has been used to observe actual thermal change at TGMR head. In this experiment, the build-in DETCR sensor was located inside the slider body, approximately 1 micron ($1x10^{-6}$ m) from TGMR reader.

Agilent 34410A with shielded cables and Gryphic probe was modified to measure DETCR resistance and DC voltage of TGMR while placing TGMR head in the field of wireless communication devices.

The response to local changes in temperature at the DETCR sensor is based on equation (1) and (2). The change of DETCR resistance [$\Delta R_{DETCR} = R_{DETCR} - R_{0\,DETCR}$] is proportional to the change of DETCR

MATEC Web of Conferences **54**, 09004 (2016) DOI: 10.1051/matecconf/20165409004
MIMT 2016

temperature ($\Delta T_{DETCR} = T_{DETCR} - T_{0\ DETCR}$) while $R_{0\ DETCR}$ is original resistance of the DETCR, R_{DETCR} is resistance of the DETCR at the point of time to compare, $T_{0\ DETCR}$ is original temperature of the DETCR, T_{DETCR} is temperature of the DETCR at the point of time to compare, and α is specific to DETCR material.

$$\Delta R_{DETCR} = \alpha \Delta T_{DETCR} \quad (1)$$

$$R_{DETCR} - R_{0\ DETCR} = \alpha * (T_{DETCR} - T_{0\ DETCR}) \quad (2)$$

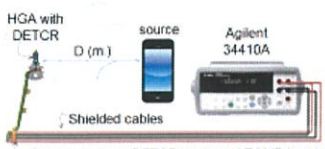

Figure5. Measurement set-up on Thermal change and DC voltage of TGMR head while placing in the field issued from wireless communication device

Result is shown in **Figure6.1**, the temperature changes when placing TGMR in the field of wireless communication device. The original temperature (T_0) is 22 degree Celsius and the change of temperature (ΔT) is less than 3 degree Celsius, so maximum temperature is less than 25 degree Celsius which is needed to be compared whether it is high enough to reach the threshold of soft level of stability failure of TGMR. Typically, the threshold should be more than 100 degree Celsius.

Figure6.2 shows measurement result of DC voltage drops on TGMR, while placing TGMR head in the field of wireless communication device(s). Overall average of DC voltage is 1.2×10^{-4} VDC and overall maximum is 11.78×10^{-4} VDC. As average TGMR resistance is about 300 Ohms, so maximum calculated power on TGMR is 4.8×10^{-11} Watts or 0.48 pico Joule/second. Next, this should be compared with threshold of TGMR failure which is typically susceptible to the energy in nano Joule range.

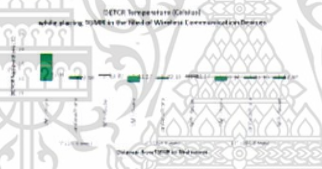

Figure6.1. Temperature of TGMR head while placing in the field of wireless communication device

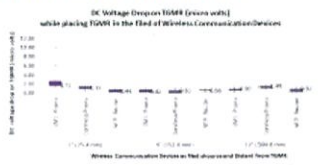

Figure6.2. DC voltage of TGMR head while placing in the field of wireless communication device

3.3 Electrical Performance of TGMR pre and post actions simulating HGA assembly process

Four types of wireless communication devices: GSM Cellular Phone, Cordless Phone, WiFi Router and Tablet Computer have been chosen to be field sources in this experiment because they are mostly used nowadays. HGAs are placed in the field generated from each device at D (cm.) distance far away as set up shown in **Figure5**.

Four actions of HGA process have been simulated during the HGAs are in-field as shown in **Figure7**. There are; (I) No contact to HGA at all (II) Grounded-Metal 10 times contact to open traces of TGMR (III) Grounded-Non-Metal 10 times contact to open traces of TGMR (IV)10 times pick-and-place on base plate with Non-Metal End Effector

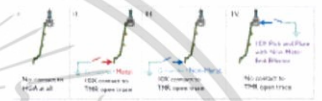

Figure7. Four actions represent HGA process

Electrical performance of HGAs has been tested before and after the actions with Quasi-static Tester (QST) to see how the experiment impacts to electrical performance of HGAs. Both catastrophic failure parameters (TGMR resistance, Amplitude, Slope) and instability parameters (Asymmetry, Barkhausen Jump, Hysteresis Loop, and Spectral Maximum Amplitude Noise S.M.A.N.) were observed and compared with total sample size of 180 HGAs. QST TGMR resistance measurement is static test and quite direct to see obvious physical change of TGMR sensor such as insulator or oxide layer breakdown. The other following parameters are measured and calculated from the Transfer Curve as shown in **Figure8**.

Amplitude is the key performance of reader sensor. The test measures peak amplitude in micro-volt at defined point of magnetic field. Amplitude is directly related to the change of TGMR resistance as shown in (3). While I is the bias current, V is the voltage drop on the

MATEC Web of Conferences **54**, 09004 (2016) DOI: 10.1051/matecconf/20165409004
MIMT 2016

sensor, $\Delta R/R_0$ is the intrinsic TGMR ratio, ε is the efficiency or amount of free layer rotation. External energy such as Thermal, EOS/ESD can cause Pinned Layer reversal in TGMR and Slope test can reveal the magnitude and location of reversal over the sweep test range. Asymmetry test basically shows the symmetry of the transfer curve which can indicate performance of magnetic layers in TGMR. Equation (4) shows calculation of asymmetry from absolute value of the maximum and minimum amplitude. Hysteresis test is measurement area between forward amplitude (Fi) and reverse amplitude (Ri) of the amplitude. Equation (5) shows calculation of hysteresis, in the unit of micro-volt/Oe, from amplitude and magnetic field increment (Inc). Barkhausen-jump (micro-volt) is maximum amplitude jumping between two adjacent measurement points. Percent of Barkhausen jump ($\%BJ$) can be calculated with peak-to-peak amplitude ($Amp_{pk\text{-}pk}$) as shown in (6). Spectral Maximum Amplitude Noise (S.M.A.N.) test measures noise density by sweeping through a range of DC magnetic fields. This parameter is invented to provide capability of high frequency instability identification. [11] [12] Example of S.M.A.N. test is shown in Figure9.

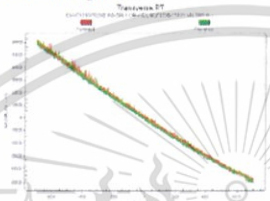

Figure8. Example of Amplitude Test by QST

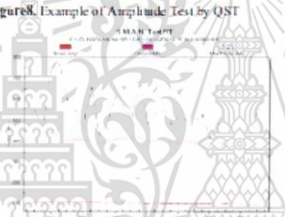

Figure9. Example of SMAN test by QST

$$\text{Amplitude} = I \times \Delta R \times \varepsilon = I \times R_0 \times \frac{\Delta R}{R_0} \times \varepsilon = V \times \frac{\Delta R}{R_0} \times \varepsilon \quad (3)$$

$$\text{Asymmetry}(\%) = \frac{|MAX.amp| - |MIN.amp|}{|MAX.amp| + |MIN.amp|} \times 100 \quad (4)$$

$$Hysteresis(\mu V/Oe) = Inc \times \sum |Fi - Ri| \quad (5)$$

$$\%BJ = [BJ(\mu V)/Amp_{Pk\text{-}Pk}] \times 100 \quad (6)$$

The result from QST shows that, both catastrophic failure and instability failure parameters related to TGMR electrical performance (TGMR resistance, Amplitude, Slope, Asymmetry, Barkhausen Jump, Hysteresis-Loop, and Spectral Maximum Amplitude Noise) are not significantly changed. It is illustrated by correlation plot between pre and post actions simulating HGA assembly processes, in **Figure10.1** to **Figure10.7**. This could confirm with the result of measuring Thermal change and DC voltage of TGMR head while placing in the field of wireless communication device in the section 3.2.

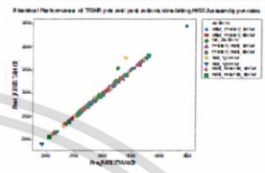

Figure10.1 Correlation of **"TGMR Resistance"**

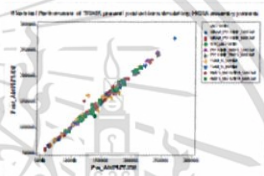

Figure10.2 Correlation of **"TGMR Amplitude"**

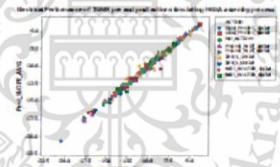

Figure10.3 Correlation of **"TGMR Slope"**

MATEC Web of Conferences 54, 09004 (2016) DOI: 10.1051/matecconf/20165409004
MIMT 2016

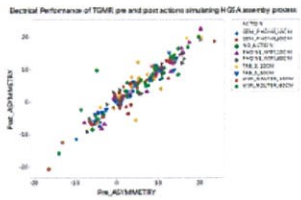

Figure10.4 Correlation of **"Asymmetry"**

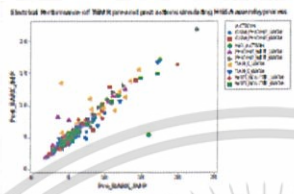

Figure10.5 Correlation of **"Barkhausen Jump"**

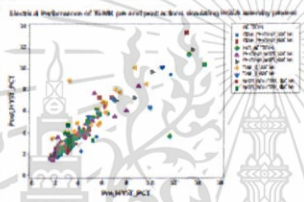

Figure.10.6 Correlation of **"Hysteresis Loop"**

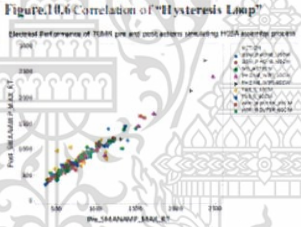

Figure10.7 Correlation of **"S.M.A.N."**

4 Conclusions

In this study, Electromagnetic Interference of 1-16 V/m had been observed from GSM cell phone, Cordless Phone, WiFi Router and Tablet Computer. However, when placing TGMR head in the electromagnetic fields issued from those wireless communication devices, the thermal change of TGMR head and the DC voltage of TGMR are not significant to create instability nor catastrophic failure to TGMR heads.

It had been proved with key QST parameters on 180 HGA samples for pre and post actions simulating HGA assembly process in the field of those wireless communication devices. There is no significant change in TGMR resistance, Amplitude, Slope, Asymmetry, Barkhausen Jump, Hysteresis Loop, and Spectral Maximum Amplitude Noise (S.M.A.N.) in all experiment conditions.

Wireless communication devices may be considered to enhance operation efficiency or operation cost saving. Nevertheless, it should be studied to make sure the effect on energy sensitive devices as well as automated production equipment and testers to be in acceptable level.

Acknowledgements

This work was supported by; [i] Seagate Technology, PLC, [ii] Seagate Technology, Thailand, Ltd, [iii] National Electronics and Computer Technology Center (NECTEC) Thailand, [iv] College of Data Storage Innovation, King Mongkut's Institute of Technology Ladkrabang, [v] Faculty of Engineering, King Mongkut's Institute of Technology Ladkrabang, Thailand.

References

1. Wallash, D. Smith, EOS/ESD Symposium 98, 4B.6.1 (1998).
2. C.F. Lam, D. Martinez, C. Chang, EOS/ESD Symposium 99, 4B.6.2 (1999).
3. V. Kraz, A. Wallash, EOS/ESD Symposium 00, 2C.10.1 (2000).
4. S. Natori, T. Wada, Y. Itou, H. Saikata, K. Katsuka, H. Tanabe, T. Ohtsu, EOS/ESD Symposium 06, 4B.3.1 (2006).
5. S. Kaengning, A. Kaewrawang, DSTCON 4th, pp. 61 (2011).
6. S. Piapairoj, C. Sangtummak, DSTCON 4th, pp. 149 (2011).
7. V. Kraz, P. Tachamaneekoth, D. Napombejara, EOS/ESD Symposium 05, 4A.4.1 (2005).
8. T. Zhao, K. Zhang, H. C. Wang, Y.H. Chen, M. Li, US Patents, US20070111332 A1 (2007).
9. M.A. Dufresne, R.W. Karr, G.J. Kunkel, Z. Wei, US Patents, US20120209582 A1 (2012).
10. D. Liu, K. Harpale, S.E. Ryun, L. Zhou, US Patents, US8638849 B1(2014).
11. H.Parland, W.A. Ogle, US6948545 B2 (2005).
12. H.Parland, W.A. Ogle, EOS/ESD Symposium 02, pp. 130 (2002).

KMUTNB

International Conference on ESIT 2016

Certificate to Participation

This is to certify that

Dutharuthai Na Pombejara,
Chaiyan Jettanasen, Kraisorn Rittipad

have participated

The 2nd International Conference on
Engineering Science and Innovative Technology

April 21-23, 2016, Angsana Laguna Phuket, Phuket, THAILAND

P. Ong-aree
Asst. Prof. Preecha Ong-aree
Dean of College of Industrial Technology
King Mongkut's University of Technology North Bangkok

T. Boonyasopon
Prof. Dr. Teravuti Boonyasopon
President
King Mongkut's University of Technology North Bangkok

Asst. Prof. Dr. Rattanakorn Phadungthin
Chair and Program Coordinator
ESIT Conference 2016

Paper ID 106

The 2nd International Conference on Engineering Science and Innovative Technology (ESIT 2016), Phuket, Thailand, April 21 - 23 2016

Effect of Wireless Local Area Network Devices in Head Gimbal Assembly Process to the properties of Tunneling Giant Magneto Resistive Reader

Dutharuthai Na Pombejara [1,2, a *], Chaiyan Jettanasen [3,b*], Kraisorn Rittipad [2,c*]

Abstract

Nowadays wireless local area network (WLAN) application is growing in manufacturing and business facility because it helps improving operation efficiency. While, Tunneling Giant Magneto Resistive (TGMR) Reader, current and future technology of magnetic recording read sensor, is one of the most sensitive devices to external energy. This study is to understand actual effect of Electromagnetic Interference (EMI) from Wireless Local Area Network (WLAN) devices in Head Gimbal Assembly (HGA) process to the properties of Tunneling Giant Magneto Resistive (TGMR) reader in the process by measuring temperature at proximity of TGMR and voltage drops at the TGMR while in the field of WLAN using Build-in Differential-Ended Temperature Coefficient of Resistivity (DETCR) sensor and Agilent 34410A. Impact to electrical performance of TGMR pre and post actions simulating HGA assembly process will be confirmed using Quasi-static tester to see change in key process output variables of TGMR which are TGMR resistance, Amplitude, Slope, Asymmetry, Barkhausen Jump, Hysteresis Loop, and Spectral Maximum Amplitude Noise (S.M.A.N.), compared with controlled samples.

Keywords : Local Area Network, Tunneling Giant Magneto Resistive, Head Gimbal Assembly, Differential-Ended Temperature Coefficient of Resistivity, TGMR, WLAN, WiFi, HGA, DETCR

[1]College of Data Storage Innovation, King Mongkut's Institute of Technology Ladkrabang, Thailand
[2]Seagate Technology (Thailand) Ltd, Nakornratchasima, Thailand
[3]Faculty of Engineering, King Mongkut's Institute of Technology Ladkrabang, Thailand
[a]dutharuthai.napombejara@seagate.com, [b]chaiyan@kmitl.ac.th, [c]kraisorn.rittipad@seagate.com

1. Introduction

TGMR reader is current technology of magnetic recording read sensor which dramatically improves readout amplitude, speed and recording areal density. In advanced manufacturing environment, automated tools are increasingly used and wireless local area network (WLAN) device is aimed to be employed to enhance the operation efficiency. However, electromagnetic fields from WLAN devices might harm the most energy sensitive devices such as TGMR reader sensor. There were some studies about Electromagnetic Interference (EMI) effect to magnetic recording head [1 – 7], but not yet any study on effect to actual TGMR in HGA process and WLAN had not been included.

This study is to confirm if the electromagnetic fields from wireless local area network devices will harm the most energy sensitive devices, life-like TGMR recording reader sensor, in actual assembly process.

2. Structure and Process

2.1 Tunneling Giant Magneto Resistive

Key distinguishing element of TGMR is Magnetic Tunnel Junction (MTJ), which consists of two ferromagnets separated by an angstrom-thin insulator. Electrons can tunnel from one ferromagnet to the other if the barrier is thin enough. With this quantum mechanical phenomenon, the MTJ can be switched between two states of electrical resistance, high resistance and low resistance, then provides higher MR Ratio (ΔR/R0; change of TGMR resistance/minimum resistance of TGMR), higher readout amplitude and speed as well as lower areal resistance (RA; Resistance x Area) and head noise [8].

The angstrom-thin metal oxide barrier makes TGMR more susceptive to external energy. Fortunately, the TGMR head does not have insulator between buffer and shield, so TGMR can dissipate thermal directly through top and bottom metal shield.

2.2 Head Gimbal Assembly Process

Head-Gimbal Assembly (HGA) is an important piece part of Hard Disk Drive in which slider body, containing read-write head, is located and flies above magnetic recording media. As its functional is to provide mechanical and electrical connection from read-write head to pre-amplifier and Head Stack Assembly (HAS), so it has copper trace along the length of reaching the very inner tract of recording media. HGA typically has a length of around 3-5 cm., which is perfectly matched to the size of 2.4 GHz frequency dipole antenna; one of the most utilized frequency in WLAN network.

Currently, the assembly process of Head-Gimbal Assembly is in full automation. The processes basically consist of robotic pick-and-place, making mechanical connection and electrical connection between Trace-Gimbal Assembly (TGA) and Slider body, and following with performance checking via mechanical test and electrical test processes.

Piece parts of HGA are contacted and in-contacted with grounded metal or static dissipative material many times along the automated process.

3. Experiment and Discussion

3.1 Wireless Local Area Network devices in factory environment

In this experiment, electric field from WLAN devices was measured using CTM048, EM Field Meter with CTS001 directional antenna and electromagnetic field module. This measuring instrument has peak and average measurement range of 0.001 V/m to 20.00 V/m, frequency bandwidth of 1 MHz to 2.5 GHz, antenna factor range of -40.0 to 40.0 dBm-1

and antenna frequency response of 10 MHz – 2.5 GHz. The measurement is performed in empty large room, at distance of 1 inch, 3 inches, 6 inches and 12 inches between CTS001 antenna and WLAN devices during transmitting, which are various samples of (1) WiFi phone (2) Wireless LAN Access Point (WiFi router) (3) Tablet Computer (4) Laptop computer, and (5) Wireless mouse & Keyboard set.

The result in Fig.1 shows that E-Field at 1 inch distance from the WLAN devices used in this study is higher than 5 V/m. for WiFi phone. Whereas the E-Field of more than 1 V/m were observed from WiFi router and tablet computer whereas the E-field of less than 1 V/m was found from lap top computer, wireless mouse and wireless keyboard. The field strength gradually decreased at the distance of 3 inches, 6 inches and 12 inches. So the WiFi phone, WiFi router and tablet computer were selected to be E-field sources for the next two experiments.

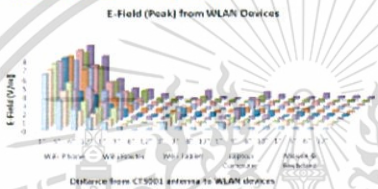

Fig.1 E-Field from WLAN Device (V/m)

3.2 Temperature and DC voltage of TGMR head while placing in the field of WLAN

From the result of pervious experiment, CISCO 7926G WiFi phone and Cisco Aironet 3500 WiFi router, set at 2.4 GHz transmit mode, have been selected to be E-field source of this experiment. HGA is placed at distance of 1 inch, 6 inches and 12 inches from the E-field source. Agilent 34410A with shielded-cables and Gryphic probe were modified to measure DETCR resistance and DC voltage of TGMR while placing HGA with TGMR head in the E-field and without E-filed (turn off) as shown in Fig.2.

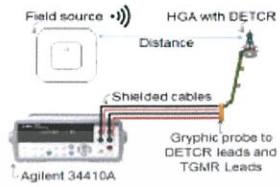

Fig.2 TGMR Temperature and DC Voltage measurement setup

The build-in DETCR sensor [9, 10] was located inside the slider body, approximately 1 micron ($1x10^{-6}$ m) from TGMR reader, to observe actual thermal change at TGMR head. Equation (1) and (2) explain response to local changes in temperature at the DETCR sensor. The change of DETCR resistance ($\Delta R_{DETCR} = R_{DETCR} - R_{0,DETCR}$) is proportional to the change of DETCR temperature ($\Delta T_{DETCR} = T_{DETCR} - T_{0,DETCR}$) while $R_{0,DETCR}$ is original resistance of the DETCR, R_{DETCR} is resistance of the DETCR at the point of time to compare, $T_{0,DETCR}$ is original temperature of the DETCR, T_{DETCR} is temperature of the DETCR at the point of time to compare, and α is specific to DETCR material.

$$\Delta R_{DETCR} = \alpha \, \Delta T_{DETCR} \quad (1)$$

$$R_{DETCR} - R_{0,DETCR} = \alpha^* (T_{DETCR} - T_{0,DETCR}) \quad (2)$$

Result in Fig.3 (a) shows that the temperature changes when placing TGMR in the field of WLAN device. The original temperature (T_0) is 22 degree Celsius and the change of temperature (ΔT) is less than 1 degree Celsius, so maximum temperature is less than 23 degree Celsius which is needed to be compared whether it is high enough to reach

the threshold of soft level of stability failure of TGMR. Typically, the threshold should be more than 100 degree Celsius.

Measurement result of DC voltage drops on TGMR, while placing TGMR head in the field of WLAN device(s) as shown in Fig.3 (b). Overall maximum is 1.49×10^{-6} VDC. As average TGMR resistance is about 300 Ohms, so calculated power on TGMR is 7.4×10^{-15} Watts (Joule/second). This should be compared with threshold of TGMR failure which is typically susceptible to the energy in nano Joule range.

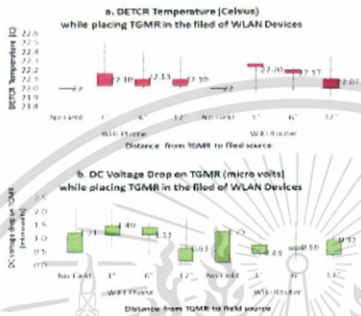

Fig.3 Result of Temperature and DC voltage of TGMR head while placing in the field of Wireless Local Area Network

3.3 Electrical Performance of TGMR in the field of WLAN during HGA Process

Four actions of HGA process have been simulated during the HGAs are in field of WLAN. There are: (I) No contact to HGA at all. (II) Grounded-Metal 10 times contact to open traces of TGMR. (III) Grounded-Non-Metal 10 times contact to open traces of TGMR, and (IV)10 times pick-and-place on base plate with Non-Metal End-Effector.

Electrical performance of HGAs has been tested before and after the actions with Quasi-static Tester (QST) to see how the simulation impacts to electrical performance of HGAs. Both catastrophic failure parameters and instability parameters were observed and compared with total sample size of 140 HGAs.

QST **TGMR resistance** measurement is static test and quite direct to see obvious physical change of TGMR sensor such as insulator or oxide layer breakdown.

Amplitude is the key performance of reader sensor. The test measures peak amplitude in micro-volt at defined point of magnetic field. Amplitude is directly related to the change of TGMR resistance as shown in (3). While I is the bias current, V is the voltage drop on the sensor, $\Delta R/R_0$ is the intrinsic TGMR ratio, ε is the efficiency or amount of free layer rotation.

$$\text{Amplitude} = I \times \Delta R \times \varepsilon = I \times R_0 \times \frac{\Delta R}{R_0} \times \varepsilon = V \times \frac{\Delta R}{R_0} \times \varepsilon \quad (3)$$

External energy such as Thermal, EOS/ESD can cause Pinned Layer reversal in TGMR and **Slope** test can reveal the magnitude and location of reversal over the sweep test range.

Asymmetry test basically shows the symmetry of the transfer curve which can indicate performance of magnetic layers in TGMR. Equation (4) shows calculation of asymmetry from absolute value of the maximum and minimum amplitude.

$$\text{Asymmetry}(\%) = \frac{|MAX\ amp| - |MIN\ amp|}{|MAX\ amp| + |MIN\ amp|} \times 100 \quad (4)$$

Hysteresis test is measurement area between forward amplitude (Fi) and reverse amplitude (Ri) of the amplitude. Equation (5) shows calculation of hysteresis, in the unit of micro-volt/Oe, from amplitude and magnetic field increment (Inc).

$$Hysteresis(\mu V/Oe) = Inc \times \sum |Fi - Ri| \quad (5)$$

Barkhausen-jump (micro-volt) is maximum amplitude jumping between two adjacent measurement points. Percent of Barkhausen jump ($\%Bj$) can be calculated with peak-to-peak amplitude (Amp_{pk-pk}) as shown in (6).

$$\%\Delta BJ = [\Delta BJ(\mu T)/Amp_{Pre-PS}] \times 100 \quad (6)$$

Spectral Maximum Amplitude Noise test measures noise density by sweeping through a range of DC magnetic fields. This parameter is invented to provide capability of high frequency instability identification. [11] [12].

Fig.4 illustrates the QST result of this experiment.

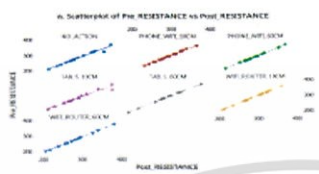

Fig.4 a. "TGMR Resistance" pre-post HGA process

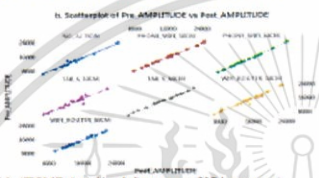

Fig.4 b. "TGMR Amplitude" pre-post HGA process

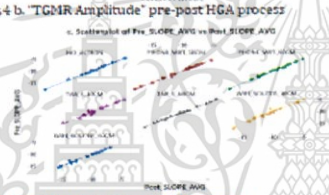

Fig.4 c. "TGMR Slope" pre-post HGA process

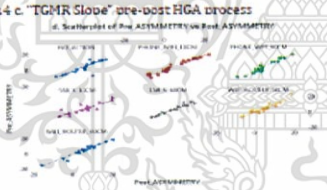

Fig.4 d. "TGMR Asymmetry" pre-post HGA process

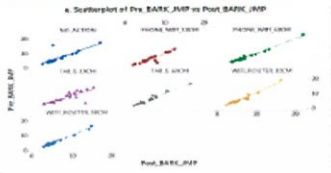

Fig.4 e. "Barkhuasen-Jump" pre-post simulated HGA Process

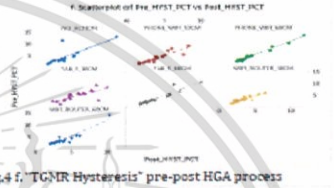

Fig.4 f. "TGMR Hysteresis" pre-post HGA process

Fig.4 g. "TGMR S.M.A.N." pre-post HGA process

The results from QST show that, both catastrophic failure and instability failure parameters related to TGMR electrical

performance (TGMR resistance, Amplitude, Slope, Asymmetry, Barkhausen Jump, Hysteresis-Loop, and Spectral Maximum Amplitude Noise) are not significantly changed. It is illustrated by correlation plot between pre and post actions simulating HGA assembly processes, in Fig.4. This is corresponded with the result of section 3.2, measuring Thermal change and DC voltage of TGMR head while placing in the field of wireless communication device

4. Conclusions

In this study, thermal change of TGMR head and the DC voltage of TGMR in HGA Process in the electromagnetic fields issued from WLAN devices are existed but not significant enough to create neither instability nor catastrophic failure to TGMR heads. It had been proved with key QST parameters on 140 HGA samples for pre and post actions simulating HGA assembly process in the field of WLAN. There is no significant change in TGMR resistance, Amplitude, Slope, Asymmetry, Barkhausen Jump, Hysteresis Loop, and Spectral Maximum Amplitude Noise in all experiment conditions.

Before introducing new wireless communication system or network, organization shall consider and study to understand the effect on performance of energy sensitive devices using in its process to make sure there is no unacceptable negative impact to its outcome.

5. Acknowledgements

This work was supported by (i) Seagate Technology, Thailand, Ltd., (ii) National Electronics and Computer Technology Center (NECTEC) Thailand, (iii) College of Data Storage Innovation, King Mongkut's Institute of Technology Ladkrabang, and (iv) Faculty of Engineering, King Mongkut's Institute of Technology Ladkrabang.

REFERENCES

[1] A. Wallash, D. Smith, "EMI Damage to GMR Recording Head", EOS/ESD Symposium 98, 4B.6.1 (1998).

[2] C.F. Lam, D. Martinez, C. Chang, "ESD Sensitivity Study of GMR Recording Heads with a FOS Head-Gimbal Assembly", EOS/ESD Symposium 99, 4B.6.2 (1999).

[3] V. Kraz, A. Wallash, "The Effect of EMI from Cell Phone on GMR Recording Heads and Test Equipment", EOS/ESD Symposium 00, 2C.10.1 (2000).

[4] S. Natori, T. Wada, Y. Itou, H. Sakata, K. Kataoka, H. Tanabe, T. Ohtsu, "Study of EMI pheonomena for GMR/TMR Head", EOS/ESD Symposium 06, 4B.3.1 (2006).

[5] S. Kaengrang, A. Kaewrawang, "EMI Induce Heat on TMR Read Sensor", DSTCON 4th, pp. 61 (2011).

[6] S. Puapairoj, C. Sa-ngiamsak, "Effect of ESD and EMI on TMR Head during Bonding Process of Gold Ball Bonding Machines", DSTCON 4th, pp. 149 (2011).

[7] V. Kraz, P. Tachamaneekorn, D. Napombejara, EOS Exposure of Magnetic Heads and Assemblies in Automated Manufacturing", EOS/ESD Symposium 05, 4A.4.1 (2005).

[8] T. Zhao, K. Zhang, H. C. Wang, Y.H. Chen, M. Li, "Low resistance TMR sensor with natural oxidized double MgO barrier", US Patents, US20070111332 A1 (2007).

[9] M.A. Dufresne, B.W. Karr, G.J. Kunkel, Z. Wei, "Resistive Temperature Sensors for Improved Asperity, Head-Media Spacing, and/or Head-Media Contact Detection", US Patents, US20120120982 A1 (2012).

[10] D. Liu, K. Haapala, S.E. Ryun, L. Zhou, "Head-medium contact detection using introduced heat oscillation", US Patents, US8638349 B1(2014).

[11] H.Patland, W.A. Ogle, "Magnetic head tester" ", US Patents, US6943545 B2 (2005)

AUTHOR BIOGRAPHY

Name-Surname:	Ms. Dutharuthai Na Pombejara
Date of Birth:	May 15th, 1973
Present Address:	1 Soi Ngamwongwan 1/1, Amphure Muang, Nonthaburee THAILAND 11000
Education:	1995: Bachelor of Engineering (Electrical), King Monkut's Institute of Technology, North Bangkok 2002: Master of Business and Administration (MBA), Ramkhamkhang University
Scholarships:	2011 Scholarship for study in Master of Engineering in Data Storage Technology (English program) by NSTDA, KMITL and Seagate Technology (Thailand) Ltd.
Publications:	V. Kraz, P.Tachamaneekorn, D. Napombejara, "EOS Exposure of Magnetic Heads and Assemblies in Automated Manufacturing", EOS/ESD Symposium 2005, Anaheim, California, USA, September 11-15, 2005 D. Na Pombejara , C. Jettanasen , K. Rittipad, "Wireless Communication and Its Effect to Tunneling Giant Magneto-Resistive (TGMR) Reader in Head Gimbal Assembly Process", 2016 the 3rd International Conference on Advances in Electronics Engineering (), 2016. D. Na Pombejara , C. Jettanasen , K. Rittipad, "Effect of Wireless Local Area Network Devices in Head Gimbal Assembly Process to the properties of Tunneling Giant Magneto Resistive Reader", The 2nd International Conference on Engineering Science and Innovative Technology (ESIT), 2016.

Special Qualifications: 1996-Management Problem Solving and Decision Making, Kepner-Tregoe International, Princeton, New Jersey, USA.

1998- ESD Symposium and Tutorial, Official member of ESD Association (Member ID#98242), Santa Clara, CA, USA

2003-ISO9001 Lead Auditor, IRCA Certificated, (certification ID#02/S/QMS1/1242), AJA Registration, Thailand

2007- ESD Symposium and Tutorial, Anaheim, CA, USA

2007- International Association for Radio, Telecommunications and Electromagnetics (iNARTE), Electrostatic Discharge Control Certified Engineer (ID#ESD-00482-NE), Anaheim, CA, USA

2010-ANSI/ESD S20.20 Auditor Training, John T. Kinnear, ESD Association Standard Working Group Chairman, Malaysia

2011-Leadership Development Program-Manager, Harvard Business School Publishing, Thailand

2012-Situation Leadership II, Ken Blanchard Companies, Thailand

2013-Working Globally, Apiarian Global, Inc., Thailand

2013-Internal Energy Audit, Ministry of Energy, Thailand

2014-ISO22301 Business Continuity Management System Lead Auditor, The British Standard Institute in Corporated by Royal Charter, (certification ID#THL-141206), Thailand

2015- ANSI/ESD S20.20 certified auditor, ESD Association, NY, USA

Experience: 1995-Present Seagate Technology (Thailand) Ltd.,

Senior Engineering Manager of ESD Engineering,

Drive Process Engineering, Business Continuity Management.